Microscale Electroporation for Transfection of Genetic Constructs into Adherent Secondary Cells and Primary Neurons in Culture

by

Chetan Patel

A Dissertation Presented in Partial Fulfillment
of the Requirements for the Degree
Doctor of Philosophy

Approved November 2012 by the
Graduate Supervisory Committee:

Jitendran Muthuswamy, Chair
Stephen Helms Tillery
Tilak Jain
Michael Caplan
Brent Vernon

ARIZONA STATE UNIVERSITY

December 2012

ABSTRACT

Gene manipulation techniques, such as RNA interference (RNAi), offer a powerful method for elucidating gene function and discovery of novel therapeutic targets in a high-throughput fashion. In addition, RNAi is rapidly being adopted for treatment of neurological disorders, such as Alzheimer's disease (AD), Parkinson's disease, etc. However, a major challenge in both of the aforementioned applications is the efficient delivery of siRNA molecules, plasmids or transcription factors to primary cells such as neurons. A majority of the current non-viral techniques, including chemical transfection, bulk electroporation and sonoporation fail to deliver with adequate efficiencies and the required spatial and temporal control. In this study, a novel optically transparent biochip is presented that can (a) transfect populations of primary and secondary cells in 2D culture (b) readily scale to realize high-throughput transfections using microscale electroporation and (c) transfect targeted cells in culture with spatial and temporal control. In this study, delivery of genetic payloads of different sizes and molecular characteristics, such as GFP plasmids and siRNA molecules, to precisely targeted locations in primary hippocampal and HeLa cell cultures is demonstrated. In addition to spatio-temporally controlled transfection, the biochip also allowed simultaneous assessment of a) electrical activity of neurons, b) specific proteins using fluorescent immunohistochemistry, and c) sub-cellular structures. Functional silencing of GAPDH in HeLa cells using siRNA

demonstrated a 52% reduction in the GAPDH levels. In situ assessment of actin filaments post electroporation indicated a sustained disruption in actin filaments in electroporated cells for up to two hours. Assessment of neural spike activity pre- and post-electroporation indicated a varying response to electroporation. The microarray based nature of the biochip enables multiple independent experiments on the same culture, thereby decreasing culture-to-culture variability, increasing experimental throughput and allowing cell-cell interaction studies. Further development of this technology will provide a cost-effective platform for performing high-throughput genetic screens.

DEDICATION

To my parents, Lalit & Varsha Patel

To my sister, Swetha Patel

&

To the love of my life, Hanin H. Bearat

ACKNOWLEDGMENTS

I would like to sincerely thank the many individuals who played a significant role in the completion of this work. First and foremost, I would like to thank Dr. Muthuswamy for his exceptional guidance, support and patience throughout my doctoral work. I truly appreciate the many in-depth discussions about both science and life. I am grateful for his teachings that have helped me become a better scientist and a better person.

I would like to thank my PhD committee members, Dr. Caplan, Dr. Jain, Dr. Tillery and Dr. Vernon for their insight and feedback about my doctoral work. I would like to acknowledge the faculty at the Harrington bioengineering department ASU for the exceptional courses they offered which inspired me, widened my knowledge base and enhanced my critical thinking. I am indebted to the several labs at ASU for allowing me access to their resources that made this work possible. I would like to thank the staff at CSSER at ASU for training me in the clean room and for always being there to assist me with the fabrication process. I am grateful to my colleagues in lab Sindhu Anand, Arati Sridharan, Massoud Kraiche and Jemmy Sutanto for the many insightful discussions and collaborations.

I thank my parents and my sister for believing in me and providing me moral support throughout my life. I am incredibly fortunate to have parents who invested all their life savings to get me and my sister through college. I am grateful to them for making me realize the importance of

education early in life and always inspiring me to become a selfless person. I would like to thank Hanin Bearat, my partner in life, for the tremendous support and love during both good and bad times. I am touched by her utmost patience with me during frustrating times and always being there to provide me a soothing comfort. I am grateful to her for motivating me and giving me the confidence to accomplish this work. I would like to thank my second parents, Hamdallah and Nadia Bearat, for providing me love and support that helped me tremendously. I thank my two new sisters Hayat and Lina Bearat for their support and love. I am grateful to my family in US and INDIA for their patience with me during the last five years. I am would like to thanks my cousins and friends for putting up with me at my worst, their friendship and support.

I would like to acknowledge the administrative staff the Harrington bioengineering department for their help at numerous occasions and making the process easier. I am forever indebted to the ASU community for providing an excellent place to learn and grow. I owe it to ASU for giving me some of the best experiences in my life.

TABLE OF CONTENTS

Page

CHAPTER Page

CHAPTER Page

CHAPTER Page

LIST OF FIGURES

Figure Page

CHAPTER 1

INTRODUCTION

1.1 Introduction

A recent report released by the World Health Organization estimates that around 1 billion people globally are affected by neurological disorders, ranging from migraines to epilepsy and dementia. A great number of these disorders, such as Alzheimer's disease (AD), Parkinson's disease (PD) and multiple sclerosis, severely impact the quality of life of the patients, rendering them incapable of doing most basic tasks, and ultimately costing patients their lives. To this day, the treatment options for central nervous system (CNS) disorders are very limited; therapies are mostly symptomatic and do not offer much improvement. Thus there is a critical need for novel therapeutic strategies that can target the CNS disorders at their root cause to offer a complete cure.

A major challenge in developing successful therapies for neurological disorders is the sheer complexity of the nervous system in terms of its structure and function. The nervous system comprises of complex neural circuits that operate synergistically to perform the most basic and high level functions of life. Within each of the neurons that form the neural circuits, there are complex molecular pathways that control the functioning of neurons. Any disruption in the molecular pathways by environmental cues or genetic mutation(s) leads to disease manifestation.

A therapy that aims to completely cure a neurological disorder needs to intervene at the molecular level and/or the neural circuit level (Jain, 2007). The ultimate goal of the research here is to deliver a technology that will enable such a therapy.

1.2 Genetic underpinnings in CNS disorders

In many disorders of the CNS, genetic components have been implicated in underlying pathogenic mechanisms. In certain neurological disorders, mutation(s) in a specific gene(s) has been identified as the fundamental cause of disease pathology. For instance, in Huntington's disease, a mutation in the Huntington gene leads to gradual damage to specific areas of the brain (Boudreau et al., 2009). Another example of an inherent brain disorder is spinocerebellar ataxia (SCA) which is characterized by progressive loss in coordination of limb movement and speech. There are more than 7 types of SCA (type 1, 2, 3 6, 7, 12 and 17) caused by CAG repeat expansions occurring within a gene and thus disrupting the normal functioning of the protein (Manto, 2005).

In neurological disorders with complex etiology such as Alzheimer's disease (AD), several genes including amyloid precursor protein gene (APP), presenilin 1 and 2 genes (PS1, PS2), beta secretase (BACE1), apolipoprotein E (APOPE), and SORL-1 have been implicated and many more are currently being investigated for their role in the pathology and as potential therapeutic targets (Citron et al., 1997; Y. Luo et al., 2001;

Rogaeva et al., 2007; Strittmatter & Roses, 1995). Another example is Parkinson's disease (PD), where point mutation in α-synuclein, a phosphoprotein enriched in presyanptic terminals, has been linked to pathogenesis of the disease (Sapru et al., 2006). Apart from the neurodegenerative disorders mentioned above, gene therapy is also amenable to brain tumors, brain trauma, and neurogenic diseases (During & Ashenden, 1998).

Thus, there is a critical need for therapeutic strategies that can intervene at the genetic level in CNS disorders. *The long term goal of this project is to develop novel technology that will enable gene modulation in targeted neurons to restore function.*

1.3 Genetic Intervention in CNS disorders

Gene manipulation offers a precise approach for elucidating gene function and is also a powerful tool in the discovery of therapeutic targets. For instance, in neurological disorders, where one or more mutations in a gene(s) are responsible for the disease manifestation, the mutated gene(s) can be silenced to offer relief from diseased-proteins (During & Ashenden, 1998). Alternatively, therapeutic-genes can be expressed to compensate for diseased or ineffective genes. In non-monogenetic neurological disorders with complex etiology, the cellular pathways that contribute to disease manifestation can be silenced while therapeutic genes encoding neuro-protective and pro-survival factors can be employed to prevent cell

loss (During & Ashenden, 1998). A specific example where the above mentioned therapeutic strategies can be applied is in PD (Figure 1).

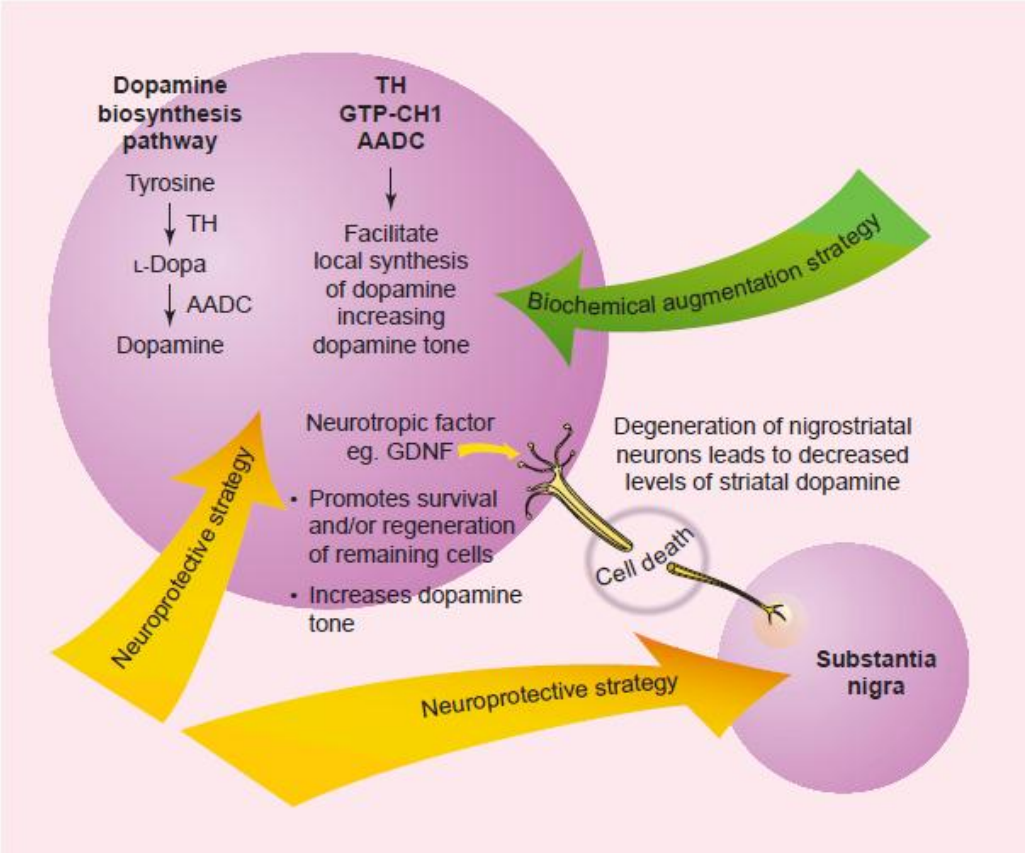

Figure 1. Strategies for gene intervention in Parkinson's disease. Image adapted by permission from Elsevier Ltd: Molecular Medicine Today (During & Ashenden, 1998) , copyright (2006).

Parkinson's disease is one of the most debilitating neurodegenerative disorders, which is primarily characterized by the loss of dopaminergic neurons that project from the substantia nigra pars compacta to the corpus striatum (Dauer & Przedborski, 2003). One of the current pharmacological approaches for the treatment of Parkinson's relies on compensating for the loss of dopamine by administering levodopa (L-dopa), a dopamine precursor that is converted to dopamine by action of aromatic amino acid decarboxylase (AADC) (During & Ashenden, 1998). However, the efficacy of L-dopa treatments decreases over time and fails to prevent the disease progression. In a gene therapy based approach, the aforementioned limitation can be overcome by manipulating genes involved in the diseased pathway to maintain a continuous and regulated production of dopamine. For instance, rate limiting enzymes in the biosynthesis of dopamine, such as tyrosine hydroxylase (TH) and AADC, can be over expressed within striatal cells (During & Leone, 1997). In addition, the loss of neurons can be prevented by augmenting the expression of neurotrophic factors. Further advancements in the understanding of the etiology of Parkinson's disease will help identify novel therapeutic genetic targets.

The primary requirement for the implementation of gene therapy for treatment of neurological disorders is the identification of therapeutic genetic targets and the identification of target regions in the CNS for gene manipulation. *The goal of this project is to develop a scalable technology*

that will enable rapid discovery of therapeutic genetic targets for CNS disorders using a gene manipulation technique in a high-throughput fashion. The current strategies employed for gene manipulation are discussed in the following sub-section.

1.3.1 Gene manipulation in CNS

Two strategies currently employed for gene manipulation include gene expression and gene silencing. In gene expression, the gene of interest is packaged in a plasmid vector and delivered to desired cells to induce expression of the gene. On the contrary, gene silencing involves inhibition of a target gene expression. RNA interference (RNAi) is one of the most powerful approaches for suppressing genetic activity of targeted genes. RNAi technique involves the use of synthetically designed 20-25 base pair long nucleotide sequences, known as small interfering RNA (siRNA), to suppress the translational activity of mRNA with complementary strand. Once introduced inside the cell, siRNA sequences bind to complementary sequences on target mRNA strand and initiate mRNA cleavage (H. Xia, Mao, Paulson, & Davidson, 2002), as seen in Figure 2.

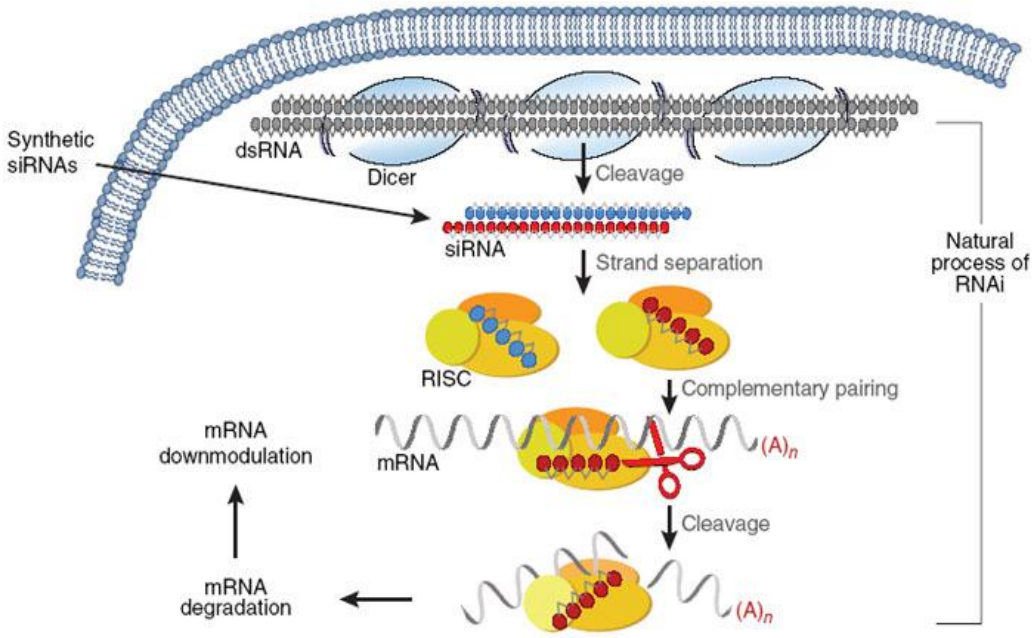

Figure 2. Mechanism of RNAi based gene silencing. Image adapted by permission from Macmillan Publishers Ltd: Nature Chemical Biology (Bumcrot, Manoharan, Koteliansky, & Sah, 2006) , copyright (2006).

The technique of siRNA based gene silencing offers very high target specificity and potent target inhibition. Several recent studies have demonstrated the applicability of siRNA as a therapeutic tool by silencing genes that contribute to disease manifestation (Boudreau & Davidson, 2010). For instance, Xia et al. have demonstrated that RNAi targeting of mutant ataxin-1 in a mouse model of spinocerebellar ataxia type-1 improved disease phenotype (H. Xia, Mao, Eliason, Harper, Martins, Orr, Paulson, Yang, Kotin, & Davidson, 2004). In another proof of concept study, Singer et al. demonstrated a decrease in neurodegenerative and behavioral deficits in a transgenic mouse model of Alzheimer's by targeting BACE-1 (Singer et al., 2005). RNAi based gene silencing can also be used to modulate electrical activity of specific pathways in CNS. For instance, Pan et al. showed that silencing of SNAP-29, a synaptic receptor associated protein, led to an increase in synaptic strength (Pan et al., 2005). There are many neuronal pathways, excitatory and inhibitory, involved in neurological diseases. By silencing specific genes in a selected group of neurons, functioning of the entire diseased pathway can be modulated.

A key requirement for gene therapy is precise spatial control over delivery of genetic constructs. This is particularly important in CNS because of its complexity in both structure and function. In CNS, siRNA delivered to non-targeted neurons can risk provoking unwanted responses (Jackson & Linsley, 2010; Mahato, Cheng, & Guntaka, 2005). In addition,

spatial control over delivery is highly desirable in high-throughput genomic studies (Pepperkok & Ellenberg, 2006; Wheeler, Carpenter, & Sabatini, 2005).

1.4 Current approaches for delivery of genetic constructs to neurons

A major limitation in successful realization of gene manipulation in CNS is efficient, non-toxic and spatially restricted delivery of genetic payload and other molecules, such as drugs and proteins, to cells. Numerous strategies have been developed over the years to enable delivery of genetic material to cells. The current delivery strategies can be grouped in viral and non-viral delivery technologies.

1.4.1 Viral delivery

Viral vectors are recombinant viruses , such as retroviruses, lentiviruses, adenovirus, and herpes simplex virus (HSV), packaged with genes to be delivered without the toxic genetic components of the viruses , as shown in Figure 3 (Walther & Stein, 2000).

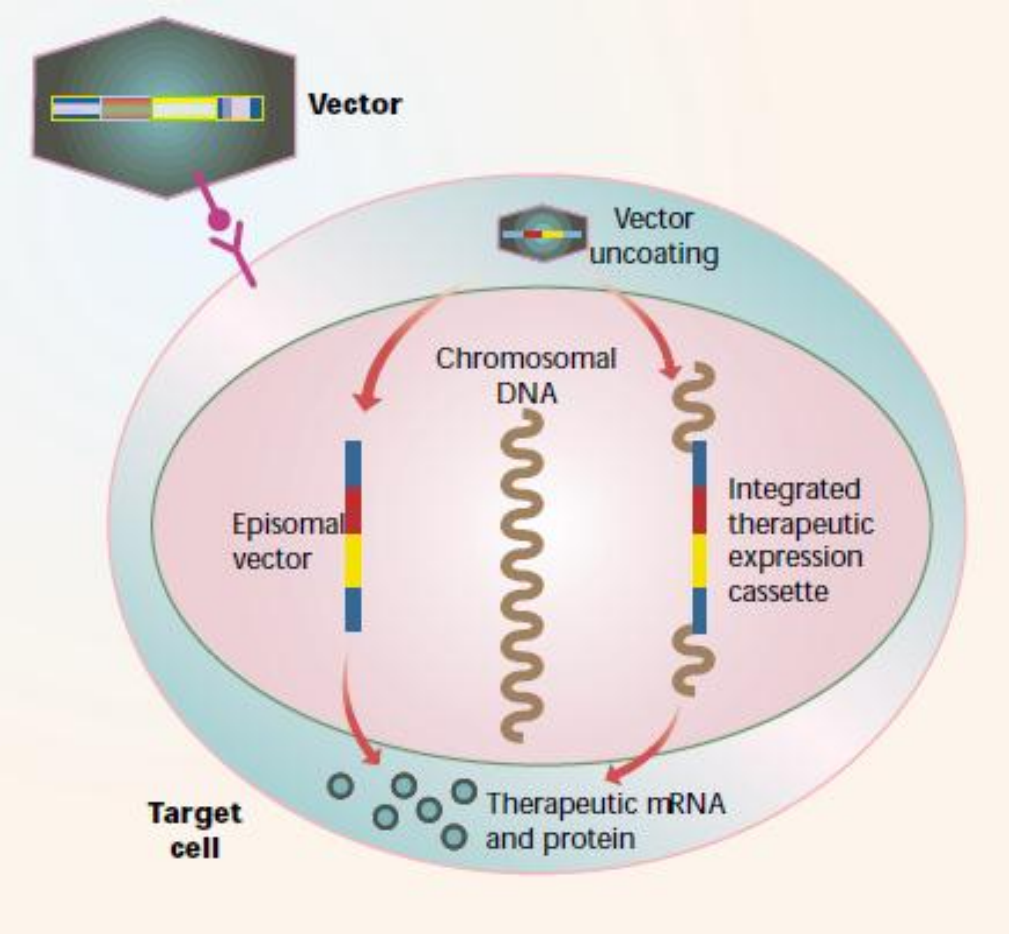

Figure 3. Viral vector mediated transduction. Image adapted by permission from Macmillan Publishers Ltd: Nature Medicine (Naldini, 2001), copyright (2001).

Virus vectors offer one of the most efficient methods for gene transduction particularly in hard-to-transfect cell lines such as primary neurons (Washbourne & McAllister, 2002). In addition, the viral vectors can be designed to target specific cell-types for transduction. Typically, the viral vectors can either be delivered locally by injecting them into the target site or globally by injecting them in ventricular system or by systemic delivery (Davidson & Breakefield, 2003). Local delivery of viral vectors is beneficial in applications that require spatially controlled transfection. The use of viral vectors has been demonstrated for gene expression as well as RNAi based gene silencing both in vivo and in vitro (H. Xia, Mao, Paulson, & Davidson, 2002). For example, in a study Xia et al. (2004) demonstrated the therapeutic potential of viral vector mediated RNAi in a transgenic mouse model (SCA1-82Q) of spinocerebellar ataxia (H. Xia, Mao, Eliason, Harper, Martins, Orr, Paulson, Yang, Kotin, & Davidson, 2004). In this study, AAV1 viruses packed with shRNAs against human ataxia-1 were directly injected in the cerebellum of the SCA1-82Q mouse. The SCA1-82Q mice treated with RNAi demonstrated significant improvement in motor coordination and neuropathology highlighting the potential of viral delivery of genetic constructs. However, major disadvantages with viral vectors include cytotoxicity, immunogenicity, and insertional mutagenesis (During & Ashenden, 1998). In addition, the viral delivery techniques are complex, time consuming, expensive and always carry a risk of infection. In contrast to viral techniques for transfection, non-viral techniques have a

lower risk of immune response and a higher chance of approval by the FDA for use in clinical trials.

1.4.2 Non-viral delivery

Non-viral delivery techniques offer cost-effective and less toxic alternatives to viral methods. Non-viral methods for transfection can be categorized into two groups, chemical and physical methods. Chemical methods of transfection include cationic lipids, cationic polymers and nanoparticles. Unlike the viral transfection, chemical transfection is not limited by the size of the genetic payload. Physical methods involve creation of transient pores in cell membrane using physical forces. The major current physical methods are magnetofection, sonoporation, and electroporation.

1.4.2.1 Cationic lipids and polymers

The cationic lipids and polymers facilitate DNA/siRNA uptake by encapsulating them in unique condensed complexes by electrostatic interactions (Al-Dosari & Gao, 2009). Owing to the high positive charge density, the DNA-lipid (lipoplexes) or DNA-polymer (polyplexes) complexes electrostatically interact with the negatively charged molecules on the cell membrane and subsequently internalize them through endosomes (Figure 4). The encapsulation of the DNA/siRNA also protects the nucleic acids from degradation agents such as nucleases.

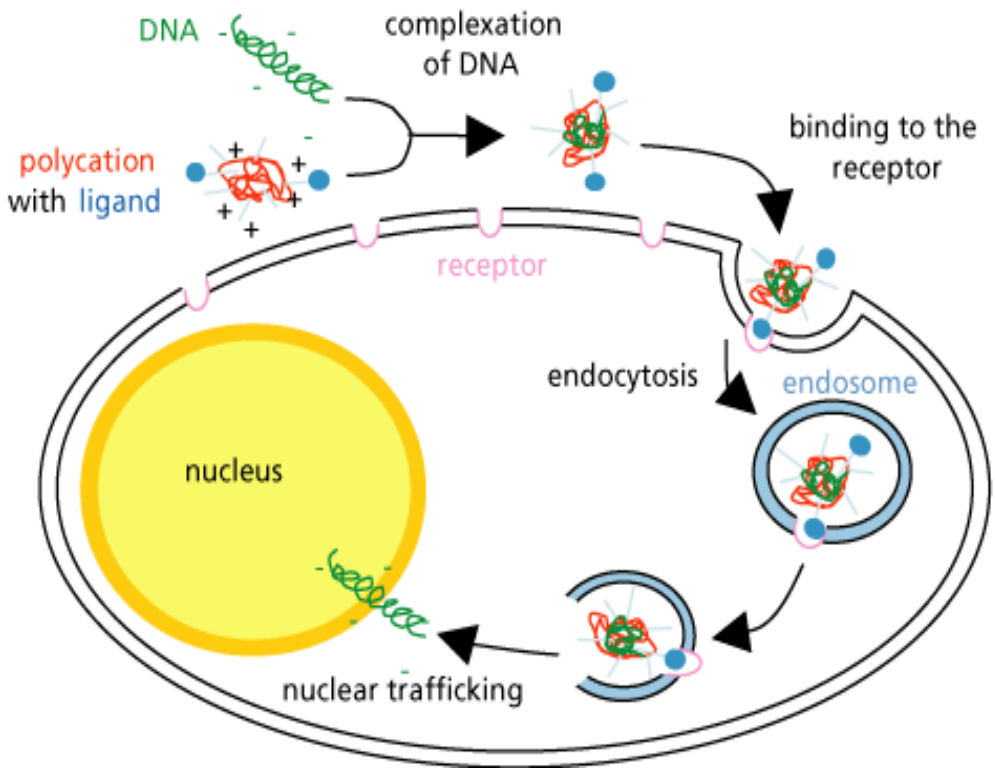

Figure 4. Cationic lipid based transfection: Lipoplex formation and endosomal escape of DNA. Image adapted from http://www.nano-lifescience.com/research/gene-delivery.html

The cationic lipids typically consist of a positively charged hydrophilic head connected to a carbon based hydrophobic tail via a linker (Wasungu & Hoekstra, 2006). Over the years, hundreds of cationic lipids have been developed and validated, all of which share the common structure of hydrophilic head and hydrophobic tail (Al-Dosari & Gao, 2009). In the lipoplex structure, the DNA/siRNA molecules are surrounded by the cationic lipids forming compact structures with a net positive charge. Once inside the cell, the lipoplex escape from the endosomes and DNA/siRNA molecules disassociate from the cationic lipids in the cytoplasm (Al-Dosari & Gao, 2009). A major disadvantage of the lipoplex-mediated delivery of nucleic material is the low transfection efficiency in primary cell lines (Al-Dosari & Gao, 2009).

Cationic polymer mediated-transfection involves the use of branched or linear polymers such as polyethylenimine (PEI) to form nanosized complexes with DNA/siRNA (Matsumoto, Itaka, Yamasoba, & Kataoka, 2009; Pérez-Martínez, Guerra, Posadas, & Ceña, 2011). PEI is the most extensively used polymer as a transfection agent. The presence of amine groups in the PEI backbone provides it with a high cationic charge density. Unlike the cationic lipids, the polyplexes dissociate from the DNA after entry into the nucleus (Matsumoto, Itaka, Yamasoba, & Kataoka, 2009). The dissociation of the DNA from the polymer in the nucleus is the most critical step; it is a bottleneck for transfection efficiency in polymer-based transfection as incomplete dissociation can interfere with

transcription activity (Pérez-Martínez, Guerra, Posadas, & Ceña, 2011). However, a major advantage of PEI over the cationic lipids, apart from the relatively small size of polyplexes, is the ability of PEI to retain a significant buffering capacity thereby protecting the DNA/siRNA from the acidic environment of the lysosomes (Al-Dosari & Gao, 2009).

Major drawbacks of cationic lipid and cationic polymer based-transfection include low transfection efficiency in post-mitotic cell lines and toxicity at high concentrations. In addition, both of these techniques are bulk in nature and provide limited or no spatial-temporal control over transfection region.

1.4.2.2 Inorganic nanoparticles

Nanoparticle-mediated gene transfection is amongst the latest and most promising technique for high efficiency transfection in all cell types. A typical strategy for use of inorganic nanoparticles (gold, silicon, carbon nanotubes and silver) involves modification of the nanoparticle surface with positive charge to facilitate electrostatic binding with DNA (Z. P. Xu, Zeng, Lu, & Yu, 2006). The major advantage with the use of nanoparticles is the small size of the particles that can bypass most cellular and physiological barriers and result in gene silencing or expression (Z. P. Xu, Zeng, Lu, & Yu, 2006). The nanoparticles can also be modified to be transported through specific receptors enabling target specificity (Gupta & Curtis, 2004). Nanoparticles-mediated gene delivery has demonstrated

high transfection efficiency both in vivo and in vitro as well as low cell cytotoxicity in neurons. However, a major limitation of the use of nanoparticles in neuronal studies is the lack of spatial control over the transfection region.

1.4.2.3 Magnetofection

Magnetofection involves delivery of genetic material associated with magnetic particles to cells in the presence of magnetic fields (Buerli et al., 2007). In this approach, plasmid vectors associated with magnetic particles are incubated with cells in the presence of a magnetic field which drives the magnetic vectors towards the cells resulting in transfection (Figure 5). The use of magnetofection has been demonstrated both in vivo and in vitro (Scherer et al., 2002). Magnetofection offers an easy to use method for transfection (Buerli et al., 2007). However, transfection efficiency for neurons is low and spatial control over deliver with magnetofection remains to be demonstrated and would require complex experimental setup (Buerli et al., 2007).

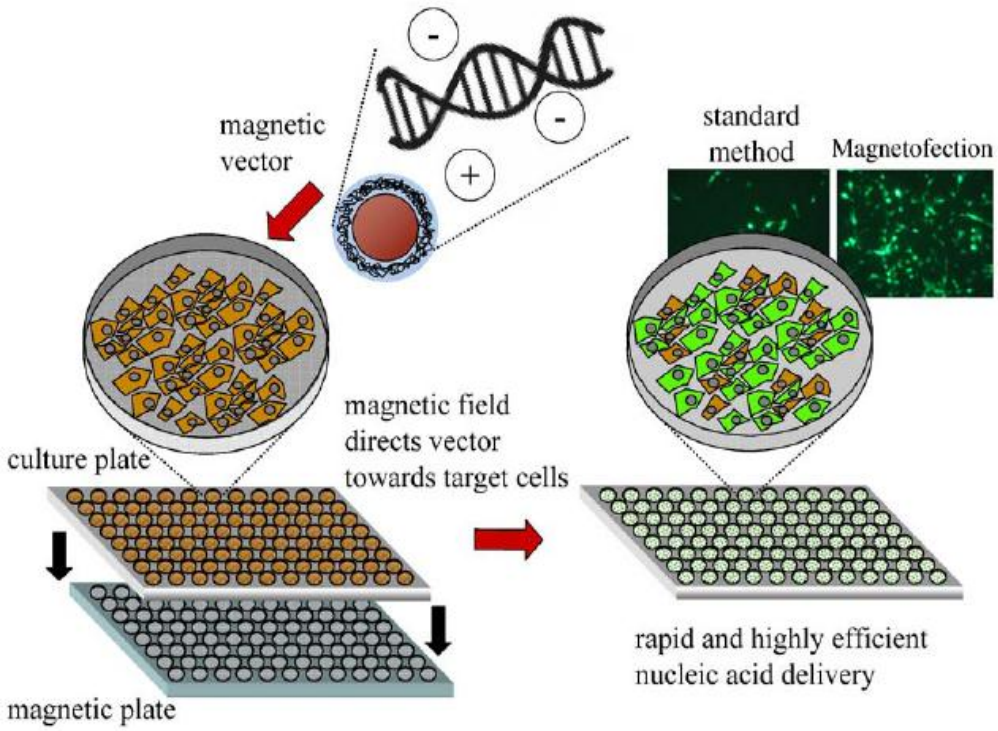

Figure 5. Magnetofection: DNA-lipid complexes associated with magnetic vectors are driven towards the cells surface under the influence of magnetic fields. Image adapted by permission from Elsevier Ltd: Journal of Magentism and Magnetic Materials (Schillinger et al., 2005), copyright (2005).

1.4.2.4 Sonoporation

Sonoporation involves the application of ultrasound waves to target cells/tissue to create transient defects in the cell membrane by acoustic cavitation, and thus allow the entry of exogenous molecules into the cell (ter Haar, 2007). In sonoporation, ultrasound irradiation is applied to cells in the presence of air-filled microbubbles, which are used as gene delivery vehicles. In the presence of an acoustic field, the microbubbles undergo forceful oscillations and breakup, resulting in high-velocity shock waves that disrupt and cause pore formation in the nearby membrane (Endoh et al., 2002). Several studies have been successful in demonstrating ultrasound enhanced gene delivery in vitro and in vivo (ter Haar, 2007). The main advantage of sonoporation is non-toxicity and noninvasiveness. In addition, ultrasound can be focused on a desired region to achieve targeted transfection (Tsunoda et al., 2005). However, a major limitation of sonoporation has been relatively low transfection efficiency, especially in primary neurons.

1.4.2.5 Electroporation

Electroporation-assisted gene delivery was first demonstrated by Neumann et al. in mouse lyoma cells. Since then, electroporation has been widely adopted as a technique for gene delivery both in vitro and in vivo. In electroporation, gene delivery is accomplished by exposing cells to brief pulses of high intensity electric field which leads to a temporary change in

the permeability of the membrane. It is the transient change in the permeability of the membrane that allows entry of exogenous molecules into the cells (Figure 6).

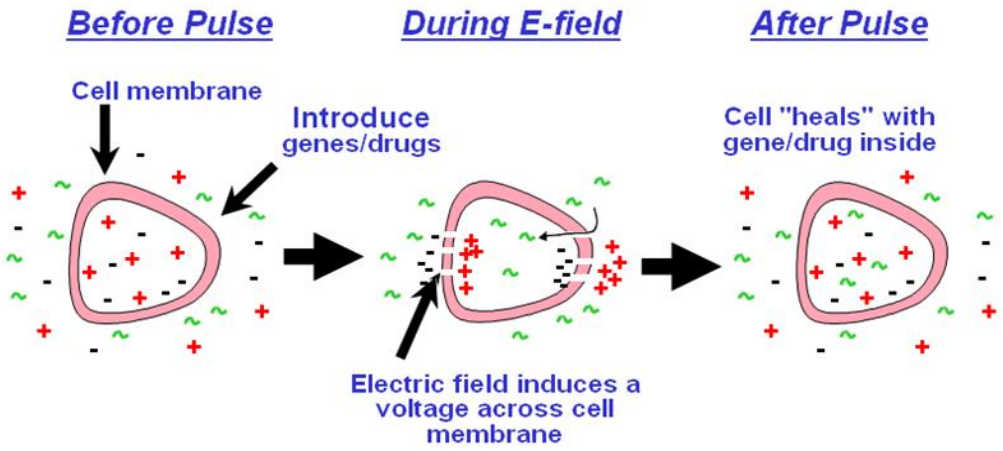

Figure 6. Electroporation: Application of a high intensity electric field leads to formation of pores in the membrane thereby increasing molecular uptake. Image adapted from http://www.btxonline.com/

Unlike chemical methods for transfection, electroporation allows delivery of naked siRNA and plasmid DNA molecules directly inside the cell, thereby averting the critical limiting step of liposomal escape associated with chemical transfection. In addition, the use of electroporation can be extended for delivery of various molecules including drugs, dyes, plasmid DNA, siRNA, and shRNA. Moreover, electroporation has shown to offer transfection efficiencies comparable to that of viral transfection without the risk of provoking an immune response. Traditionally, electroporation is performed by applying an electric field to a suspension of cells in electroporation buffer containing probe molecules placed between two parallel plate metal electrodes. The traditional system is limited to cells in suspension; however, recent studies have demonstrated the implementation of electroporation at a microscale level, enabling delivery of macromolecules to cells in vitro and in vivo with precise spatial and temporal control over the region of transfection.

1.5 Theory of electroporation

Electroporation is a biophysical phenomenon in which the permeability of the cell/bilayer membrane increases transiently in the presence of a high intensity electric field, allowing the transport of ions, polar and non-polar molecules across the membrane (Neumann, Schaefer-Ridder, Wang, & Hofschneider, 1982; Neumann, 1992). The key steps involved in electroporation are the following (Weaver, 2000):

1. Exposure of cell(s)/tissue(s) to high intensity electric field on a microsecond to millisecond time scale.
2. Electric field-induced charging of the cell membrane.
3. Rapid and localized rearrangement of molecular structures, such as proteins and lipids, within the membrane.
4. Localized formation of aqueous pores which span through the thickness of the membrane.
5. A several fold increase in ionic and molecular transport across the membrane via the aqueous pores.
6. Membrane recovery and pore resealing upon the removal of an externally applied electric field.

The cell membrane is a semi-permeable lipid bilayer that permits transport of small water and lipid soluble low-molecular-weight molecules freely while remaining impermeable to macromolecules, such as nucleic acids. The cell membrane can be considered as a dielectric separating the conductive intracellular and extracellular solutions. In the presence of an externally applied electric field, the membrane acts as a dielectric in a capacitor and becomes charged. The transmembrane potential $\Delta V_m(t)$ induced across the membrane of a cell by an externally applied electric field E_{ext} can be described by the equation:

$$\Delta V_m(\mathrm{t}) = -f E_{ext} r \cos\varphi \left[1 - \mathrm{e}^{-\frac{\mathrm{t}}{\tau}}\right] \quad (1)$$

Where φ is the angle between the membrane site and the direction of the applied field, r represents the radius of the cell, t is the time after the

electric pulse onset, τ is the membrane charging time constant and f represents the form factor of the cell (Bernhardt & Pauly, 1973; J. M. Escoffre et al., 2009; Neumann, 1992). The form factor of the cell describes the impact of the cell on the electric field distribution. It is dependent on the conductivities of the external solution σ_o, cell interior σ_i and the cell membrane σ_m. For $\sigma_m << \sigma_i, \sigma_o$ the form factor f for spherical cells is given by:

$$f = \left[1 + \frac{\sigma_m\left(2 + \frac{\sigma_i}{\sigma_o}\right)}{\frac{2\sigma_i d}{r}}\right]^{-1} \quad (2)$$

Where d is the thickness of the membrane (Neumann, 1992). The transmembrane potential at any site on the cell membrane is the sum of the induced potential due to the applied electric field at that site and resting membrane potential ΔV_{res} (Mehrle, Hampp, & Zimmermann, 1989; Neumann, 1992) and can be described by the equation:

$$\Delta V_c = f E_c r \cos\varphi \left[1 - e^{-\frac{t}{\tau}}\right] + \Delta V_{res} \quad (3)$$

Electroporation of a cell is achieved when the superimposed transmembrane potential of the cell exceeds a certain threshold ΔV_c (equation 3). Experimental studies have demonstrated the value of ΔV_c to be in the range of 0.2 – 0.3 V (Gabriel & Teissie, 1997; Teissié & Rols, 1993). It is believed that at the critical value of the transmembrane potential, a dielectric breakdown of the membrane occurs, which results in the formation of aqueous pores (Hibino, Shigemori, Itoh, Nagayama, &

Kinosita, 1991; Weaver, 2003; Zimmermann, Pilwat, & Riemann, 1974). The critical electric field necessary of electroporation derived from equation 3 is given by:

$$E_c = \frac{\Delta V_c - \Delta V_{res}}{fr\cos\varphi\,[1 - \mathrm{e}^{-\frac{t}{\tau}}]} \tag{4}$$

For a spherically shaped cell, when an electric field of amplitude equal to E_c is applied, electroporation occurs only for φ values close to 0 or π (equation 4). In this situation, only the section of the membrane facing the electrodes is electroporated as shown in Figure 7.

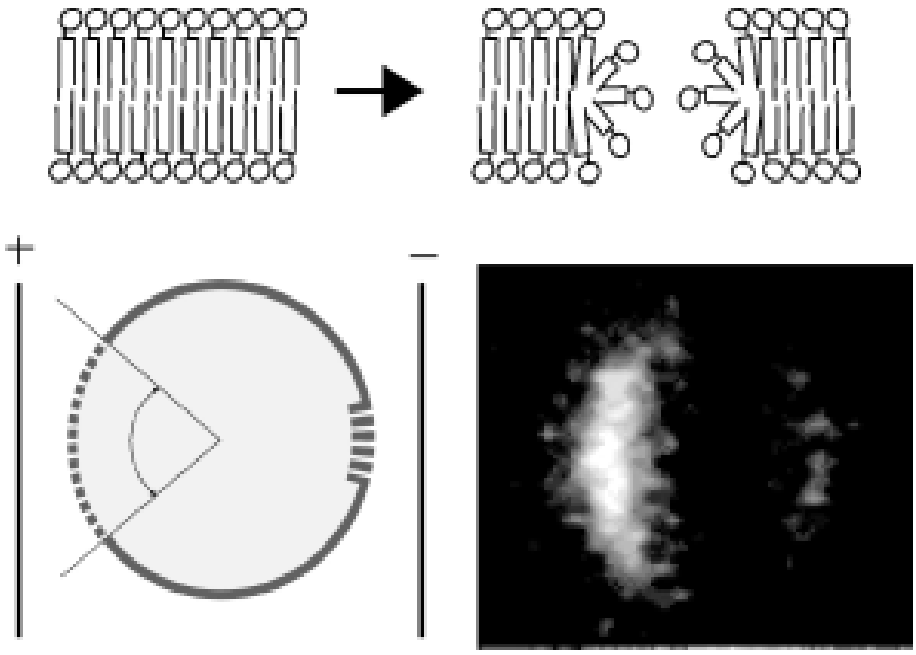

Figure 7. Electroporation observed at poles facing the electrodes. Top: Electroporation leads to the formation of aqueous pores. Bottom right: Entry of a dye into the cell after electroporation is observed only at the sides facing the electrodes. Image adapted by permission from John Wiley and Sons: Acta Physiologica (Gehl, 2003), copyright (2003).

The strength of the electric field controls the area of the cell membrane that undergoes electroporation (Schwister & Deuticke, 1985). Another observation that can be made from equation 1.4 is that the strength of the critical electric field is inversely related to the radius of the cells. Thus for electroporation, larger cells (i.e. mammalian cells) require an electric field with lower strength when compared to smaller cells (i.e. bacteria) (Teissié & Rols, 1993). The nature of permeabilization is dependent on the strength of the applied electric field. At electric field strengths equal to or slightly higher than E_c, the poration of the membrane is temporary and reversible. However, at field strengths much higher than E_c, the cell membrane is irreversibly damaged, ultimately leading to cell death. The underlying phenomenon that allows the cell membrane to reseal after electroporation is not very well understood (Weaver, 2003).

Studies investigating the kinetics of pore formation have reported that the process of resealing happens over a range of minutes (M. P. Rols & Teissié, 1990). One of the methods to characterize the dynamics of pore resealing, apart from fluorescence microscopy (Neumann, 1992), is by measuring the transmembrane potential and current during and after electroporation (Abidor et al., 1979; Krassen, Pliquett, & Neumann, 2007; Ryttsén et al., 2000). The aqueous pores formed in the membrane due to an externally applied electric field behave as conductive channels and as a result lead to an increase in the conductance of the cell membrane. The change in the conductance of the membrane can be captured by measuring

the current flow through the membrane. Ryttesen et al. used a patch clamp with NG108-15 cells to demonstrate that pore resealing is a two-step process (Ryttsén et al., 2000); wherein cells display a high conductance state within 100 msec after electric pulse application and typically recover from the high conductance state within 500 msec. Following recovery from the high-conductance state, the cell membranes remain in a low conductance state in the range of minutes to hours. The recovery time also depends on the strength of the applied electric pulse; longer recovery times are observed for higher strength of electric pulse.

The manner of entry of probe molecules into the cell cytoplasm via electroporation largely depends on the size and charge of the molecules (Gehl, 2003). Small molecules (such as dyes and anticancer drugs) have been shown to enter cells by free and rapid diffusion regardless of charge during the life time of the pores (Gehl, 2003; Neumann, Tönsing, Kakorin, Budde, & Frey, 1998). However, entry of macromolecules such as plasmid DNA into the cytoplasm is a complex multistep process (Figure 8), which includes the following (J. M. Escoffre et al., 2009):

1. Pore formation in the membrane. The process occurs on a microsecond time scale
2. Electrophoretic migration of the plasmid DNA towards the membrane surface facing the cathode. The process occurs in a millisecond time scale.

3. DNA-membrane interaction and complex formation. The process occurs in a second time scale.
4. Translocation of the DNA to the cytoplasm. It takes upto 30 mins for DNA translocation to the cytoplasm.
5. DNA entry into the nucleus. It can take upto an hour after pulse application for DNA to enter the nucleus.

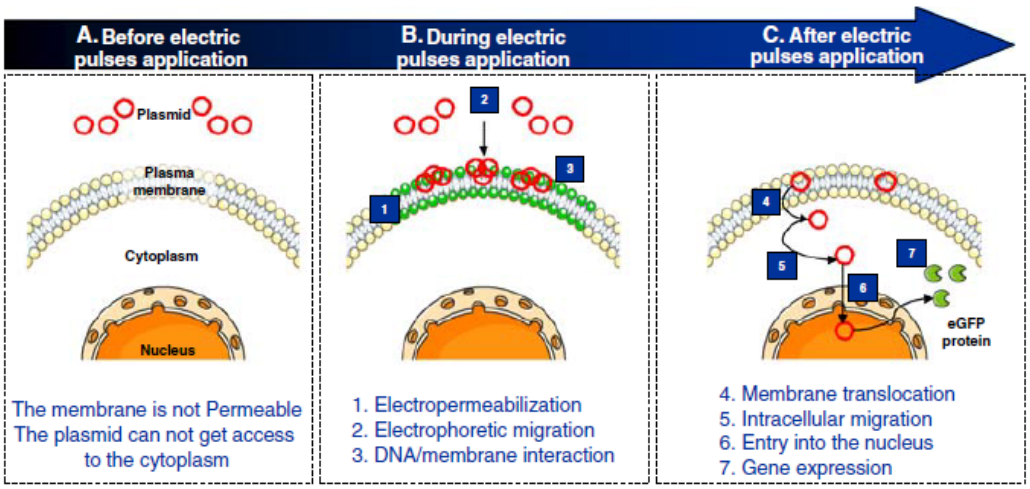

Figure 8. Mechanism of electroporation assisted plasmid entry into cell. Image adapted by permission from Springer: Molecular Biotechnology, (J. M. Escoffre et al., 2009), copyright (2009).

The exact mechanism involved in the DNA-membrane interaction, complex formation and subsequent translocation to cytoplasm is not fully understood (J. M. Escoffre et al., 2009). Recent evidence from studies suggests that an important role is played by the cytoskeleton (actin filaments) by actively participating in DNA uptake following electric pulse application (Rosazza, Escoffre, Zumbusch, & Rols, 2011; Teissie & ROLS, 1994). The formation of DNA-membrane complexes undergoes a two stage process (Golzio, Teissié, & Rols, 2002). First, metastable DNA-membrane complexes are formed, from which plasmid DNA can leave the membrane and return to the extracellular medium under the influence of a reverse direction electric field. Second, within 1 second following pulse application, the metastable DNA-membrane complexes convert to highly stable complexes. Next, the plasmid DNA is translocated to the cytoplasm. Another key aspect of DNA delivery via electroporation is that plasmid DNA enters cells on the side facing the cathode (Golzio, Teissié, & Rols, 2002). This phenomenon is primarily caused by the electrophoretic migration of DNA towards the side of the cell facing the cathode due to its negative charge.

1.6 Microscale electroporation assisted gene manipulation

In the conventional form of electroporation, a large volume biological sample (in the range of a few cubic centimeters) is typically placed in a cuvette between two parallel metallic plate conductors and a

high intensity electric field is applied to the sample to achieve electroporation. In contrast, microscale electroporation involves controlled application of electric field to a targeted region of the biological sample (in the order of microns) using microelectrodes to achieve electroporation. There are many advantages to microscale electroporation over the conventional form of electroporation, which include (W. G. Lee, Demirci, & Khademhosseini, 2009) (1) symmetric and uniform electric fields, (2) precise spatial control over the transfection area, up to single cells, (3) high transfection efficiency in hard-to-transfect cell lines, (4) rapid optimization of electroporation parameters, (5) in situ assessment of cellular response to electric field, (6) applicable for in vivo, in vitro and in utero setting (S. Li, 2004; Pacary et al., 2012).

Microscale electroporation has proven capability to transfect spatially restricted neurons, up to single cells, with high transfection efficiency of up to 30% (using micropipette based approach). For instance, Haas et al. (2001) demonstrated single cell electroporation in a tadpole by positioning a micropipette close to the cell. A microelectrode placed inside the micropipette was used to generate and apply the electric field to a target neuron for electroporation. The technique developed by Hass et al. (2001) and similar approaches by others has shown high transfection efficiency in single neurons and localized transfection in the brain (Åberg et al., 2001; Akaneya, Jiang, & Tsumoto, 2005; Kitamura, Judkewitz,

Kano, Denk, & Häusser, 2007; Matsuda & Cepko, 2004; Nevian & Helmchen, 2007; Tanaka, Yanagawa, & Hirashima, 2009).

In addition, microscale electroporation has been demonstrated in high-throughput applications and offers many advantages over conventional high-throughput systems. For instance, current high-throughput systems for gene screening involve use of microwell plates (96 or 384 wells) and rely on chemical transfection, which is known to be inefficient in primary neuron transfection (Vanhecke & Janitz, 2005). The microwell based screening is a time consuming and expensive process (due to the large amount of reagent needed). For example, a pooled siRNA based genome wide screen would require 267 96-well plates (M. Jiang, Instrell, Saunders, Berven, & Howell, 2011). If three replicates were to be performed (total 801 plates) at a well manipulation time of 1 min/well, it would require 13 hours to process all the wells. On the contrary, microscale electroporation enables miniaturization of the high-throughput system, thereby increasing the speed and reducing the cost. For instance, Tilak et al. (2012) demonstrated a miniaturized electroporation ready microwell system. In this approach, microfabrication techniques were used to create a micro-pattern of wells on a conductive substrate. The conductive substrate allowed parallel electroporation of cells in all the wells immediately after seeding. siRNAs were spotted individually in each of the wells prior to seeding. Similar approaches have been demonstrated by several other groups (Z. Li, Wei, Li, Du, & Liang, 2011); however, some major

limitations with these approaches have been 1) limited temporal control over transfection, due to siRNA spotting, which is a key requirement in studies involving primary neurons and 2) studies involving primary neuronal cultures can greatly benefit from technology that integrates the capability to record electrical activity of targeted neurons and the entire neuronal network in real time. *It is hypothesized that a novel optically transparent microelectrode array (MEA) based biochip can be fabricated to spatially target and transfect a population of primary neuronal cells in vitro in a high throughput fashion using electroporation. In addition, the MEA can be used for simultaneous electrophysiological assessment of neurons.*

1.7 Preface to the following chapters

Chapter 2 describes a detailed protocol and experimental setup for targeted transfection in adherent cells using a custom made or commercially available microelectrode array (MEA). The protocol describes strategies for rapid optimization of electroporation parameters for transfection with siRNA and GFP. The protocol was designed to make this technique accessible to most research labs with basic cell culture equipment.

Chapter 3 presents the development of an optically transparent platform for spatially and temporally controlled transfection in adherent cells in a high-throughput fashion. In this chapter, targeted transfection

using the developed MEA based biochip is demonstrated in a secondary cell line (HeLa cells). Electroporation parameters were optimized for three different electrode sizes. Finite element method was used to simulate electric field intensities associated with the three electrode sizes. The electric field simulation predicted the regions of cell death on the three electrode sizes. Biomolecules such as functional siRNA and GFP were delivered to targeted cells and phenotypical changes were measured. The impact of microscale electroporation on cells was measured by monitoring dynamic changes in sub-cellular structures (Actin). Chapter 3 shows successful demonstration of the initial hypothesis in a secondary cell line.

Chapter 4 reports for the first time, targeted transfection of genetic payloads of different sizes and molecular characteristics such as GFP plasmids and fluorescently tagged siRNA molecules (Alexa 488-siRNA) in a primary culture of hippocampal neurons using the MEA based biochip. In addition, the MEA was used to measure the electrical activity of neurons and assess the impact of the electroporation on neural activity. Finally, is reported for the first time delivery of GFP plasmids to neurons through electroporation of neuronal processes. Chapter 4 shows further validation of the initial hypothesis.

Chapter 5 reports the use of nano-porous alumina membrane in tandem with MEA for achieving targeted nanochannel based electroporation in adherent cells. In chapter 5, it is hypothesized that integration of MEA with nanochannels will provide a high-throughput

method for transfecting cells with similar efficiency and consistency offered by single cell nanochannel electroporation. Proof-of-concept of the integrated approach was demonstrated by electroporating HeLa cells cultured on alumina membrane with an MEA placed underneath the alumina membrane. Electric field intensity at the opening of the nanochannel integrated with MEA was performed to predict region of electroporation. Electrical characterization of the MEA nanoporous membrane assembly was performed to assess the suitability of the platform in measuring neural activity.

Chapter 6 presents the conclusion of the results obtained in this dissertation work and identifies potential future work directions. Critical limitations are addressed and strategies for further development of the technology reported in this work are suggested.

CHAPTER 2

HIGH EFFICIENCY, SITE-SPECIFIC TRANSFECTION OF ADHERENT CELLS WITH SIRNA USING MICROELECTRODE ARRAYS (MEA)

2.1 Introduction

The discovery of RNAi pathway in eukaryotes and the subsequent development of RNAi agents, such as siRNA and shRNA, have achieved a potent method for silencing specific genes (Brummelkamp, Bernards, & Agami, 2002; Caplen, Parrish, Imani, Fire, & Morgan, 2001; Elbashir et al., 2001; Fire et al., 1998; N. S. Lee et al., 2002; Miyagishi & Taira, 2002; Paul, Good, Winer, & Engelke, 2002; H. Xia, Mao, Paulson, & Davidson, 2002) for functional genomics and therapeutics. A major challenge involved in RNAi based studies is the delivery of RNAi agents to targeted cells. Traditional non-viral delivery techniques, such as bulk electroporation and chemical transfection methods often lack the necessary spatial control over delivery and afford poor transfection efficiencies (Chu, Hayakawa, & Berg, 1987; Felgner et al., 1987; Jordan, Schallhorn, & Wurm, 1996; Raptis et al., 1995). Recent advances in chemical transfection methods, such as cationic lipids, cationic polymers and nanoparticles, have resulted in highly enhanced transfection efficiencies (Y. Gao, Liu, & Li, 2011). However, these techniques still fail to offer precise spatial control over delivery that can immensely benefit miniaturized high-throughput technologies, single cell studies and

investigation of cell-cell interactions (Wheeler, Carpenter, & Sabatini, 2005).

Recent technological advances in gene delivery techniques have enabled high-throughput transfection of adherent cells (H. Huang et al., 2010; Jain & Muthuswamy, 2007a; Jain & Muthuswamy, 2007b; Jain & Muthuswamy, 2008; Jain, McBride, Head, & Saez, 2009; Jain, Papas, Jadhav, McBride, & Saez, 2012; Z. Li, Wei, Li, Du, & Liang, 2011; Yamauchi, Kato, & Iwata, 2004; Yamauchi, Kato, & Iwata, 2005; Ziauddin & Sabatini, 2001), a majority of which use microscale electroporation. Microscale electroporation offers precise spatio-temporal control over delivery (up to single cells) and has been shown to achieve high efficiencies (Akaneya, Jiang, & Tsumoto, 2005; K. Haas, Sin, Javaherian, Li, & Cline, 2001; Jain & Muthuswamy, 2008; W. G. Lee, Demirci, & Khademhosseini, 2009). Additionally, electroporation based approaches do not require a prolonged period of incubation (typically 4 hours) with siRNA and DNA complexes as necessary in chemical based transfection methods and lead to direct entry of naked siRNA and DNA molecules into the cell cytoplasm. As a consequence, gene expression can be achieved as early as six hours after transfection (Boukany et al., 2011). The use of microelectrode arrays (MEA) for site-specific transfection in adherent mammalian cell cultures has been previously demonstrated (Jain & Muthuswamy, 2007a; Jain & Muthuswamy, 2007b; Jain & Muthuswamy, 2008). In the MEA based approach, delivery of genetic payload is achieved via localized micro-scale

electroporation of cells. An application of electric pulse to selected electrodes generates local electric field that leads to electroporation of cells present in the region of the stimulated electrodes. The independent control of the micro-electrodes provides spatial and temporal control over transfection and also enables multiple transfection based experiments to be performed on the same culture increasing the experimental throughput and reducing culture-to-culture variability.

Here, detailed protocol and experimental setup for targeted transfection of HeLa cells with a fluorescently tagged scrambled sequence siRNA using electroporation is described. The same protocol can also be used for transfection of plasmid vectors. Additionally, the protocol described here can be easily extended to a variety of mammalian cell lines with minor modifications. Commercial availability of MEAs with both pre-defined and custom electrode patterns make this technique accessible to most research labs with basic cell culture equipment.

2.2 Protocol

2.2.1 MEA preparation

1) MEAs for use in electroporation experiments can either be fabricated using standard photolithography technique as described in the following chapter or purchased directly from vendors of MEA manufacturers such as Multi Channel Systems

(http:/www.multichannelsystems.com/) and Alpha MED Scientific, Inc. (http://www.MED64.com). The MEAs used in the experiments were fabricated in-house at the clean room facility in Arizona State University, which is administered by the Center for Solid State Electronics Research (CSSER). The MEAs used for these experiments had 32 indium tin oxide electrodes in an 8 by 4 array with electrode diameter sizes from 50-200 μm within a 1 cm inner diameter glass well. The glass well was bonded on the MEA using polydimethylsiloxane (PDMS).

2) Sterilize the MEA in an autoclave prior to cell seeding. Other methods of sterilization such as a soaking in 70% ethanol, UV treatment and hot water treatment as described elsewhere can also be used as long they do not compromise the integrity of the MEA.

3) Transfer the autoclaved MEA to a laminar flow hood and place it in a standard sterile polystyrene Petri dish. Prior to seeding cells on the MEA sterilize the laminar flow hood by turning on the UV light for 20 minutes. If the MEA is sensitive to UV light cover the Petri dish containing the MEA with sterile aluminum foil while the flow hood is under UV illumination.

2.2.2 Seeding cells on the MEA

1) Harvest cells from a running cell line of adherent mammalian cells using Trypsin/EDTA and raise them to a concentration of 100-200

cells/μl in 1 ml cell media for plating. In these experiments, NIH 3T3 fibroblasts cell line, HeLa cell line and primary cortical and hippocampal neurons were successfully cultured on the MEA.

2) Place a 20-30 μl drop of media with cells on the MEA. Transfer the Petri dish with the MEA to the incubator. It is important to ensure that the cell drop size is large enough to cover all the electrodes on the MEA.

3) 2 hours after seeding the cells transfer the Petri dish with the MEA from the incubator to laminar flow hood and gently add 400-500 μl of pre warmed media (37°C) to the MEA well. Check under the microscope to ensure that cells are still attached and evenly spread on the MEA surface. Transfer the MEA back to the incubator. The 2 hour wait period before the addition of media ensures enough time for the cells to adhere with the MEA surface. Addition of cell media too soon after seeding the cells can wash away the cells. If cells do not adhere well on the MEA, its surface can be treated with cell attachment factors such as polylysine, fibronectin, and laminin to improve cell adhesion. In the HeLa cell experiments, the MEA surface was treated with fibronectin (10 μg/ml) for 1-2 hours.

4) 8-12 hours after seeding the cells, perform 1-2 washes with PBS to remove any dead cells. Cell medium can replaced every 24-48 hours as needed. In a typical experiment, the cells are usually ready for transfection 24-48 hours after seeding. To maintain consistency in

electroporation efficiencies it is recommended to wait until the culture is at least 80% confluent before electroporation.

2.2.3 Site-specific transfection of siRNA

1) Prepare nucleic acid solution. For siRNA transfection, prepare a 1-2 μM siRNA electroporation solution in ice cold electroporation buffer to attain a final volume of 200-400 μl. This protocol demonstrates the procedure for successful transfection of HeLa cells with Alexa 488 conjugated scrambled sequence of siRNA.
2) Transfer the MEA with cells from the incubator to sterile laminar flow hood. Remove the cell media from the MEA and perform a wash with PBS. Thereafter, add 200-400 μl of the ice cold 1μM siRNA electroporation solution to the well.
3) Apply anodic square electric pulses to the targeted electrodes (Refer to step 4 for determining optimal parameters of the electric pulse. A Pragmatic Instruments 2414A waveform generator can be used to generate electric pulses and a dual-inline-package (DIP) 16 pin clip to make contact with the MEA bond pads. The waveform generator can be connected to the DIP clip via a demultiplexor printed circuit board to provide selectivity of individual electrodes. For the reference electrode, place a steel cathode in the cell media. While lowering the steel reference electrode in the media it is extremely important to ensure that it does not make contact with the MEA surface. Upon

contact, it can cause damage to the cells and the MEA. It is recommended to lower the reference electrode to a position of 1 mm above the cells. A spacer with a height of 1 mm can be placed in the well to assist in placement of the reference electrode. An alternate approach to using an external reference electrode is to use neighboring electrodes as cathode-anode pairs.

4) Immediately after applying the electric pulses to the targeted electrodes on the MEA, transfer the MEA back to the incubator. After an incubation period of 5 min, gently replace 75% of the electroporation buffer with pre-warmed (37°C) cell media. Later, fluorescent imaging can be done to confirm the delivery of fluorescently tagged siRNA to the cells.

2.2.4 Electroporation parameter optimization

1) To determine the optimal electric pulse parameters for electroporation, design electroporation experiments for a range of values of pulse amplitude, pulse duration, and number of pulses. In experiments with HeLa cells, it was observed that a single voltage pulse of amplitude from 3 V to 9 V, and duration from 1 msec to 10 msec for an electrode size of 100 μm led to successful electroporation with minimal cell death. It is recommended that one parameter be varied at a time and others are kept constant. To quantitate the electroporation efficiency for each of the pulse parameters, use

propidium iodide (PI), a cell impermeant dye that stains nucleic material, and live assay based methodology, as described in steps 4.2-4.5.

2) Establish a cell culture on the MEA following the directions outlined in steps 1 and 2.

3) Prior to electroporation prepare a 300-500 µl of 30 µg/ml PI solution in ice cold electroporation buffer and 400 µl of 4 µM calcien AM solution in PBS.

4) Transfer the MEA from the incubator to the laminar flow hood. Remove the cell media from the MEA and perform a wash with PBS. Thereafter, add 300-500 µl of the ice cold electroporation buffer with PI.

5) Apply electric pulses with desired pulse amplitude and duration to the targeted electrodes (The equipment used for generating and applying the electric pulse to the MEA is described in step 3.3). For the reference electrode either lower a steel electrode into the electroporation buffer in the MEA well or use the neighboring electrode as reference. By selectively applying pulses of varying amplitudes or durations to different electrodes multiple experiments can be performed on the same device. For example, on a 32 electrode MEA, 8 experiments can be performed by splitting the 32 electrodes in 8 groups, each consisting of 4 electrodes. Each of the 8 groups can then be stimulated by a single rectangular voltage pulse of duration 5

msec with amplitudes varying in 3 V-6 V range in 0.5 V increments and one group can be used as a control.

6) Immediately after applying the voltage pulses transfer the MEA to the incubator for 5 min. Afterwards, gently remove 75% of the electroporation buffer from the MEA well and replace it with warm cell media. Transfer the MEA back to the incubator.

7) After an incubation period of 2-4 hours replace the cell media in the MEA well with 300-500 µl of 4 µM Calcein AM solution in PBS. Transfer the MEA back to incubator for another 30 min.

8) Following the incubation of the cells with Calcein AM replace the Calcein AM solution in the MEA well with PBS after two washes with PBS. Obtain fluorescent images of cells using with an optical microscope with filters for PI (Excitation/Emission - 535 nm/617 nm) and Calcein AM (Excitation/Emission – 490 nm/520 nm). The uptake of PI, due to electroporation, causes cells to fluoresce red and the Calcein AM causes cells that are alive to fluoresce green. Three possible scenarios that can be observed are 1) cell electroporated and alive (will fluoresce both red and green) 2) Cells alive but not electroporated (will fluoresce just green) 3) Cells dead due to electroporation (will fluoresce just red). The cell viability was calculated as a percent of the total number of cells alive on the electrode and the electroporation efficiency was calculated as percent of the total number of cells loaded with PI/siRNA.

2.3 Results

Figure 9 shows the site-specific loading of HeLA cells with PI. It can be observed that only cells on the electrode demonstrate an uptake of PI (Figure 9(a)). A live assay performed post electroporation was used to assess the viability of cells (Figure 9(a)). The electroporation efficiency and cell viability for the example shown in Figure 9 are 81.8 % and 96.1 % respectively. High cell viability and electroporation efficiency can be achieved by optimizing the electroporation pulse parameters.

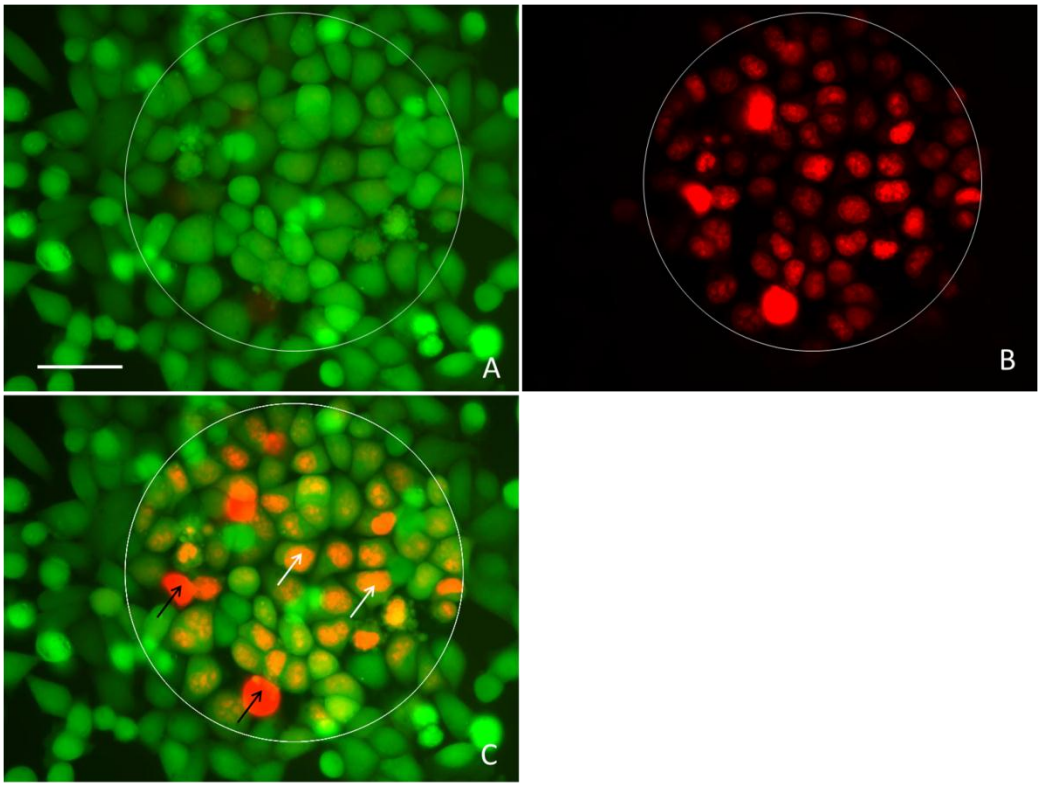

Figure 9. Site-specific delivery of PI in HeLa cells on a 200 μm electrode (6 V, 5 msec). (a) Calcein based live assay performed 2 hours post electroporation. Alive cells are indicated by green fluorescence. (b) Red fluorescence demonstrates the uptake of PI by cells on the electrode. (c) A superimposed image of (a) and (b). The white arrows indicates cells that are electroporated and alive. The black arrows indicate cells that are dead. The white circle in (a), (b) and (c) indicates the outline of the electrode. Scale bar is 50 μm.

2.4 Discussion and Conclusion

In this work, the use of MEA for site-specific transfection of HeLa cells with scrambled sequence of siRNA was demonstrated. One of the advantages of this technology is its applicability to different cell lines including primary cell lines. The use of this technology for site-specific transfection of primary hippocampal neuronal culture from E18 day old rat and NIH-3T3 cells with scrambled siRNA sequences and GFP plasmid has been previously demonstrated (Jain & Muthuswamy, 2007a; Jain & Muthuswamy, 2008). Successful delivery of functional siRNA against an endogenous target was also demonstrated in HeLa cells (please refer to Chapter 2). A typical commercially available MEA is compatible with optical imaging (upright microscope), enabling quantitative assessment of functional impact of gene silencing, using fluorescent immunostaining techniques. Additionally, the microelectrodes in MEA can be used to monitor electrical activity of cells, such as primary neurons, in response to genetic perturbation. Currently a major limitation with the MEA based system is the large amount of siRNA needed for transfection (400 μl of 1μM siRNA), which is high compared to conventional chemical transfection based approaches and thus limits the cost effectiveness of the system. This can potentially be overcome by incorporating microfluidics with the MEA based system to decrease the total volume of siRNA electroporation solution to less than a few microliters. Further

development of this technology offers a novel high-throughput, efficient and low cost method for gene manipulation studies.

CHAPTER 3

A NOVEL OPTICALLY TRANSPARENT BIOCHIP FOR SITE-SPECIFIC TRANSFECTION OF BIOMOLECULES IN ADHERENT CELLS

3.1 Introduction

Recent advances in genomics and the advent of genome sequencing have created a need for technologies that can systematically and efficiently determine gene function. RNA interference (RNAi) offers one of the most powerful and practical approaches for decoding gene function in a high-throughput fashion (Mohr, Bakal, & Perrimon, 2010). In RNAi, synthetically designed silencer RNA (siRNA) molecules, with a sequence that is complementary and unique to target mRNA, is commonly used to silence the activity of a target gene by preventing the translation process (Elbashir et al., 2001). The most significant obstacle between RNAi technology and its implementation in high-throughput studies is efficient, non-toxic and spatially targeted delivery of siRNA molecules to cells in culture (Whitehead, Langer, & Anderson, 2009). Spatial control over delivery of siRNA molecules to cells in a culture is highly desirable in high-throughput gene screening and cell-cell interaction studies (Wheeler, Carpenter, & Sabatini, 2005). In addition, spatial control over delivery of genetic material enables multiple experiments to be performed on a cell culture thereby reducing culture-to-culture variability. Current approaches

for siRNA transfection, such as physical methods (electroporation (Prasanna & Panda, 1997), magnetofection (Scherer et al., 2002), sonoporation(Miller, Pislaru, & Greenleaf, 2002)) and chemical methods (cationic lipids (Lonez, Vandenbranden, & Ruysschaert, 2008), cationic polymers (Park, Jeong, & Kim, 2006) and nanoparticles (Ghosh, Han, De, Kim, & Rotello, 2008)) fail to deliver the desired spatial control over delivery. Advances in nanoparticle based transfection have allowed receptor mediated targeted delivery of siRNA to cells (S. D. Li & Huang, 2006); nonetheless, lack spatial control over delivery.

Microscale electroporation has demonstrated precise spatial and temporal control over transfection both in vivo and in vitro (W. G. Lee, Demirci, & Khademhosseini, 2009; Olofsson et al., 2003). In microscale electroporation, strong localized electric fields are generated to selectively transfect the region of interest. Micropipettes (K. Haas, Sin, Javaherian, Li, & Cline, 2001; Tanaka, Yanagawa, & Hirashima, 2009), electrolyte filled capillaries (Nolkrantz et al., 2001), AFM tips (Nawarathna, Unal, & Wickramasinghe, 2008) and nanochannels (Boukany et al., 2011) have been established for their utility in electroporation. These methods provide a very high level of spatial control allowing selective electroporation of single cells and subcellular structures; however, they are low throughput in nature due to the skilled and precise manipulation required for positioning of the electroporation probes either in the vicinity or in contact with the cell membrane. Recently, standard MEMS based

fabrication techniques have been increasingly employed to develop platforms that allow microscale electroporation (W. C. Chang & Sretavan, 2009; Hai & Spira, 2012; K. S. Huang, Lin, Su, & Fang, 2006; Y. Huang & Rubinsky, 2001; Inoue, Fujimoto, Ogino, & Iwata, 2008; Ishibashi, Takoh, Kaji, Abe, & Nishizawa, 2007; Jain & Muthuswamy, 2007a; Jain, Papas, Jadhav, McBride, & Saez, 2012; Y. C. Lin, Jen, Huang, Wu, & Lin, 2001; Y. C. Lin, Li, Fan, & Wu, 2003; Olbrich, Rebollar, Heitz, Frischauf, & Romanin, 2008; Valero et al., 2008; Valley et al., 2009; C. Xie, Lin, Hanson, Cui, & Cui, 2012; Y. Xu, Yao, Wang, Xing, & Cheng, 2011; Zhan, Wang, Bao, & Lu, 2009). Microfabrication of lab-on-chip style device provides the unique ability to integrate tools for cell manipulation, transformation and phenotype detection in a single platform. For instance, Xu et. al demonstrated a device that allowed microscale electroporation of adherent cells cultured within microwells (Y. Xu, Yao, Wang, Xing, & Cheng, 2011). The electroporation in each well was carried out by applying an electric pulse to a microelectrode present at the bottom of each well directly beneath the adherent cells. In addition to electroporation, the same microelectrodes were also used for patterning cells in microwells at seeding using dielectrophoresis. Several similar microwell based approaches have been developed for high-throughput studies (H. Huang et al., 2010; Jain, Papas, Jadhav, McBride, & Saez, 2012; Y. Xu, Yao, Wang, Xing, & Cheng, 2011); however, a major limitation with such approaches is their inapplicability in cell-cell interaction studies.

The use of a microelectrode array (MEA) for delivery of nucleic acids to pre-determined locations in an adherent cell culture using microscale electroporation has been previously demonstrated (Jain & Muthuswamy, 2007a; Jain & Muthuswamy, 2007b; Jain & Muthuswamy, 2008). In the above mentioned MEA based approach, application of small electric pulses to the independently controllable microelectrodes allowed targeted electroporation of cells adhered directly on top of the patterned microelectrodes. The MEA based approach offers a novel scalable platform for delivery of nucleic material with precise spatial and temporal control to cells in culture with integrated capability to monitor electrical activity of cells such as primary neurons. A major limitation of the MEA based device was its optical opaqueness, due to silicon substrate, that impeded imaging based assays. Compatibility with standard imaging equipment is critical for most biological experiments. In this study, the fabrication of indium tin oxide (ITO) based fully optically transparent MEA for site-specific transfection is reported. More specifically, the use of patterned ITO MEA for endogenous gene silencing in targeted cells using siRNA was demonstrated for the first time. Additionally, microelectrodes of three different sizes were patterned to investigate the impact of electrode size on electroporation efficiency. Furthermore, the applicability of the biochip for assessing subcellular phenotypes was showns by investigating the impact of microscale electroporation on actin, its disruption and reorganization post electroporation.

3.2 Materials and Methods

3.2.1 MEA fabrication

The MEA was fabricated using a standard photolithography technique in a clean room facility. A schematic for the photolithography steps is shown in Figure 10(a). First, the ITO wafers were cleaned with isopropanol and then coated with 50nm thick layer of chromium using a thermal evaporator. After chromium deposition, the first photolithography step was carried out using a positive photoresist, AZ 3310, to pattern bond pads and alignment marks. The bond pads and alignment marks were patterned in chromium. Since ITO is optically transparent, patterning the bond pads and alignment marks in chromium ensured that they remained visible throughout the fabrication process; visible alignment marks were necessary for subsequent photolithography steps and visible bond pads were assistive in making an electrical interface to access the electrodes. Prior to the second photolithography step, ITO wafers were heated at 175°C for 45 min to remove moisture from the surface. The moisture removal from the ITO surface facilitated better photoresist adherence. A second photolithography step was then carried out to pattern the electrodes, bond pads and traces in ITO. ITO was etched using ITO etchant, TE-100, purchased from Transene, Inc. (MA, USA). Following the second photolithography step, a 1.0 μm thick parylene layer was deposited using chemical vapor deposition as an insulation layer on the ITO wafer.

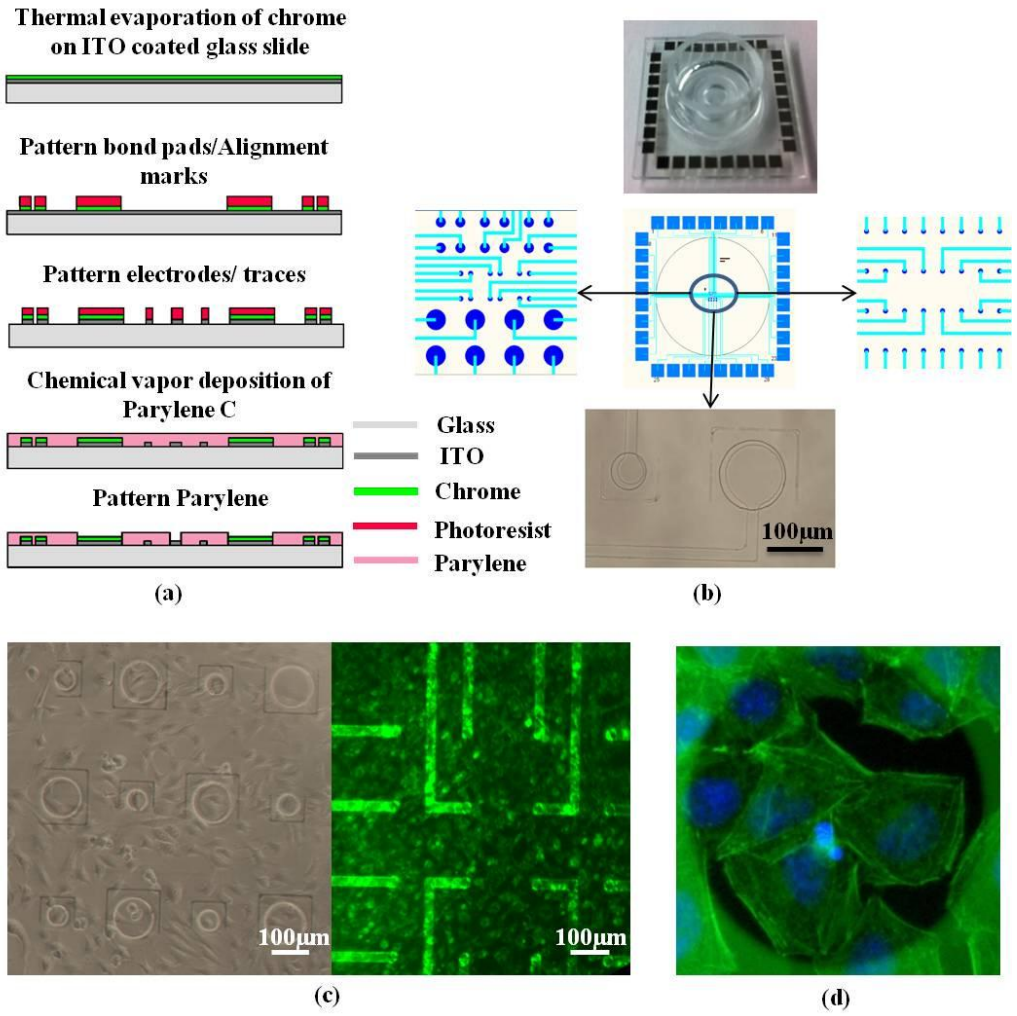

Figure 10. (a) Fabrication steps for the ITO based MEA. (b) An image of the biochip and schematic of two different MEA patterns and electrodes sizes. (c) Comparison of brightfield imaging of cells on ITO based MEA (left) and silicon based MEA (right) (d) Image of cells stained for actin filaments (green) and nucleus (blue) on a 100 µm ITO electrode.

A final photolithography step was then carried out to expose the bond pads and electrodes. Parylene etching was done using oxygen plasma. A glass well with 1.5 cm diameter and 1 cm height was bonded on the MEA using polydimethylsiloxane (PDMS) as an adhesive. PDMS was cured in a conventional dry oven at a temperature of 80°C for 45mins. Using the above described approach, two different MEA patterns were fabricated, each with 32 total electrodes, as shown in Figure 10(b). One of the patterns had electrodes of three different sizes (50 μm, 100 μm and 200 μm diameters) while the other had all electrodes of the same size (100 μm diameter).

3.2.2 Cell culture

HeLa cells were grown in DMEM supplemented with 1% FBS, 1% penicillin-penstrep and 1% glutamate. The HeLa cell culture was maintained in a humidified incubator at 37°C and 5% CO_2. The MEA was sterilized by autoclaving at 122°C for 30 mins. Post sterilization, the MEA surface was treated with fibronectin (10 μg/ml) for two hours at room temperature to improve adhesion, followed with DI water washes. Thereafter, cells were harvested using Trypsin/EDTA and raised to a concentration of 200 cells/μL in fresh media. Subsequently, 30-35 μl of cells were pipetted on the MEA surface and the device was transferred to an incubator. Following a 2 hr incubation period that was allowed for the cells to adhere on the MEA surface, 500-600μl of pre-warmed and CO_2

equilibrated cell media was added to the MEA well. The MEA was then quickly transferred back to the incubator.

3.2.3 Experimental setup and imaging

A 16 pin dual-inline-package (DIP) clip was used to electrically interface with the MEA bond pads. Electric pulses for electroporation were generated using a waveform function generator (Pragmatic 2414A, Pragmatic Instruments) and was connected to the DIP clip via an 8 channel custom made demultiplexor circuit board. A flat steel electrode covered in sterilized aluminum foil was used as a ground in the electroporation experiments and was positioned 1 mm directly above the cells using a metallic spacer. The cells were imaged using either an inverted or upright fluorescent microscope. Fluorescent images were captured on an inverted microscope and were processed in ImageJ.

3.2.4 Experimental protocol

The experimental protocol is described in detail in Chapter 2(Patel & Muthuswamy, 2012). Electroporation experiments were generally carried out when the cells reached 80-100% confluency. Prior to electroporation, a solution of probe molecule (propidium iodide, siRNA or GFP) in electroporation buffer was prepared (cat. no. #165-2677, Biorad laboratories, CA, US) and maintained at 4°C. Thereafter, cell media was replaced with electroporation buffer containing biomolecules and single

electric pulses, with predetermined pulse amplitudes and pulse widths, were applied to targeted electrodes. Immediately afterwards, the MEA was transferred to the incubator. Following a 10 min incubation period, 70-80% of the electroporation buffer in the MEA well was replaced with pre-warmed and CO_2 equilibrated cell media and the MEA was placed back in the incubator.

3.2.5 Immunofluorescence

Cells were fixed in either 4% formaldehyde (for actin staining) for 15 min or ice-cold 100% methanol (for GAPDH staining) for 5 min. Post fixation, the cells were incubated in blocking buffer (1% bovine serum albumin(BSA)/10% normal goat serum/0.3M glycine in 0.1% PBS-tween) for 1 hour. For GAPDH staining, the cells were then incubated with GAPDH antibody (cat. no. #ab9484, Abcam, MA, US) prepared at 10 µg/ml in blocking buffer for 12 hours at 4°C. Subsequently, the cells were washed and incubated with a solution of secondary antibody (cat. no. #ab96789, Abcam) and DAPI (for staining the nuclei) in 1% BSA-0.1% PBS-tween for 1 hour. Thereafter, the cells were washed with PBS and imaged using a fluorescent microscope. For actin staining, the cells were incubated with phalloidin (cat. no. #A12379, Invitrogen) and DAPI for 1 hour in blocking buffer. Afterwards, the cells were imaged using the fluorescent microscope.

3.2.6 Finite element (FEM) simulations of electric field intensity

FEM simulations were performed in COMSOL Multiphysics V3.4 (COMSOL, CA) to simulate the electric field intensities generated around the microelectrodes in response to voltage application. To accomplish this, a 3D model of the microelectrodes (three sizes 200 μm, 100 μm and 50 μm in diameter) and the surrounding buffer (conductivity of 1.6 S/m) was generated in COMSOL. The model was solved after the application of a fine mesh and the appropriate boundary conditions. The electric field intensities were plotted for the top view of microelectrodes.

3.2.7 Statistical analysis

The mean and standard deviations of the GAPDH silencing data were analyzed using a two-sided t-test, with a level of significance set at $P < 0.05$.

3.3 Results

3.3.1 ITO based MEA and site-specific electroporation

The micro-patterning of the conductive ITO layer on glass substrate and the use of parylene as an insulation layer provided the MEA with a transparent biocompatible substrate for cell growth and site-specific electroporation (Figure 10(b)), which is highly desirable in cell culture based experiments. As seen in Figure 10(c), the bright-field image of HeLa

cell culture on an ITO MEA provides greater detail about the cell morphology when compared to a cell culture on a silicon-based MEA. Images in Figure 10(c) were captured using a standard upright microscope and in both MEAs (ITO and silicon), magnifications higher than 100X (10X objective) could not be achieved due to the presence of 1 cm high well on the MEAs. However, the compatibility of the ITO MEA with the inverted microscope enabled imaging at higher magnifications upto 400X (Figure 10(d)). In the case of inverted microscopes, the working distance was limited by the thickness of the glass substrate (0.8 mm).

To evaluate the site-specific control over delivery of biomolecules and to determine the optimal pulse parameters for microscale electroporation, a series of experiments were performed with propidium iodide (PI), a cell impermeant nuclear stain, as a probe molecule. Figure 11(a) shows a view of cells on a MEA both pre- and post-electroporation.

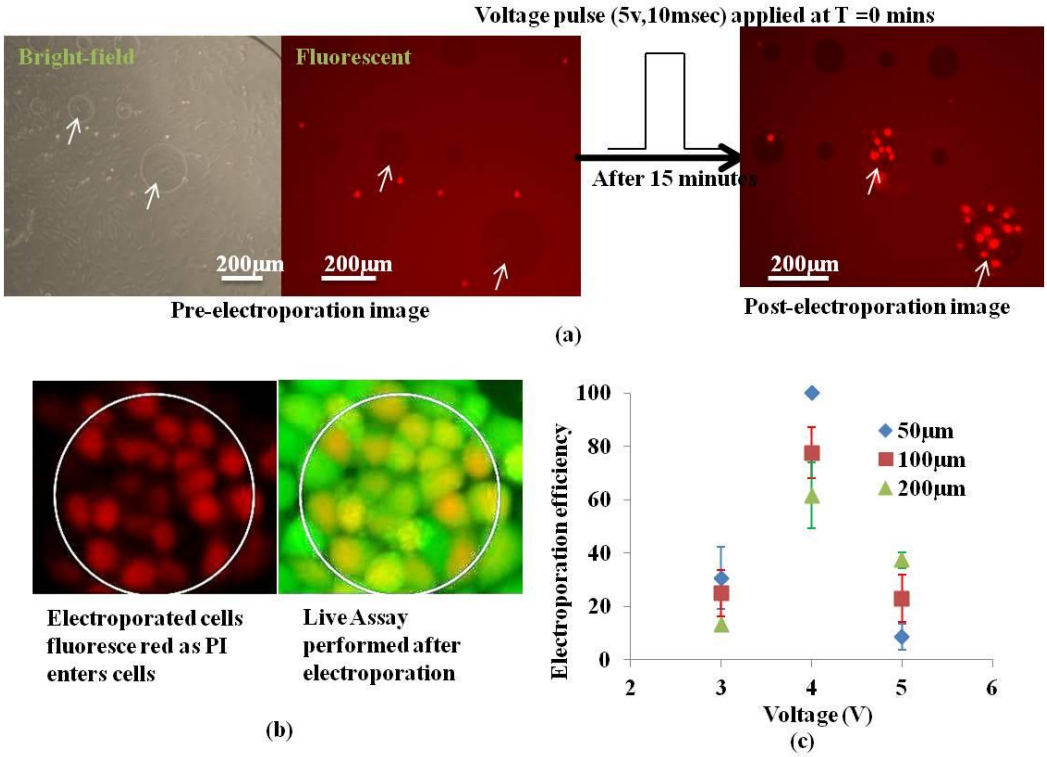

Figure 11. (a) Electroporation scheme. The white arrows point to electrodes targeted for electroporation. After application of electric pulse, cells on targeted electrodes fluoresce red due to uptake of PI. (b) A live assay performed after electroporation shows cell viability for a 4 V, 10 msec pulse. White circle marks the electrode boundary. (c) Electroporation efficiencies for the three electrode sizes at electroporation pulse amplitudes of 3, 4, and 5 V and fixed duration of 10 msec (N=3).

Here, the uptake of PI molecules, indicated by red fluorescence, was limited to cells on targeted electrodes. It was observed that region of electroporation was highly specific to surface area above the electrode. Post-electroporation, the viability of electroporated cells was determined by performing a live assay on the cells. Cells that were successfully electroporated and remained viable appear as stained by both PI (red fluorescence) and live assay (green fluorescence), as shown in Figure 11(b). However, cells that died due to electroporation were stained only by PI. To determine the optimal electroporation electric pulse parameters, anodic voltage pulses with amplitudes ranging from 3V to 10 V and pulse durations of 1 msec and 10 msec were evaluated for their electroporation efficiencies. The electroporation efficiency was estimated by dividing the number of cells that were electroporated and alive divided by the total number of cells on the electrode. The viability was estimated as the percentage of cells alive on the electrode. For the 100 μm electrode, the highest electroporation efficiency for the 1 msec and 10 msec duration pulses for PI were determined to be 90±9.4% and 77.7±9.7% (N=3) at 7 V and 4 V, respectively (Appendix B). At voltage amplitudes higher than 4 V for 10 msec pulse and 7 V for 1 msec pulse, although the percentage of total number of cells electroporated increased, the electroporation efficiencies decreased due to a decrease in cell viability (Appendix B). In all the experiments, a single anodic voltage pulse was applied for electroporation.

The anodic voltage pulse was used to facilitate the delivery of polar molecules such as siRNA and GFP plasmid(Golzio, Teissié, & Rols, 2002) .

3.3.2 Impact of electrode size on electroporation efficiency

In this study, MEAs with electrodes consisting of three different sizes of diameters (50μm, 100μm and 200μm) were patterned to demonstrate that the number of cells targeted for electroporation can be controlled by controlling the size of the electrode, as shown in Figure 10(b). However, it was observed that the optimal electroporation efficiencies for the three electrode sizes were dependent on the size of the electrodes. Figure 11(c) shows the plot for electroporation efficiencies for the three electrode sizes at three different voltage pulse amplitudes (3 V-5 V) and a pulse duration of 10 msec. As seen in Figure 11(c), at the optimal electroporation pulse (4 V and 10 msec), the electroporation efficiencies for 50 μm, 100 μm and 200 μm electrodes were found to be 100%, 77.7±9.7% and 61.7±12.3% (N=3), respectively. In order to understand the observed inversely proportional relationship between the size of the electrode and the electroporation efficiency, FEM simulations of electric field (EF) intensities for the three electrode sizes were performed in COMSOL v3.4. The simulation results showed that the distribution of EF intensity over the surface of the electrodes is non-uniform, with regions of high intensities along the edges of the electrode and low intensities at the center of the electrodes (Figure 12(a)).

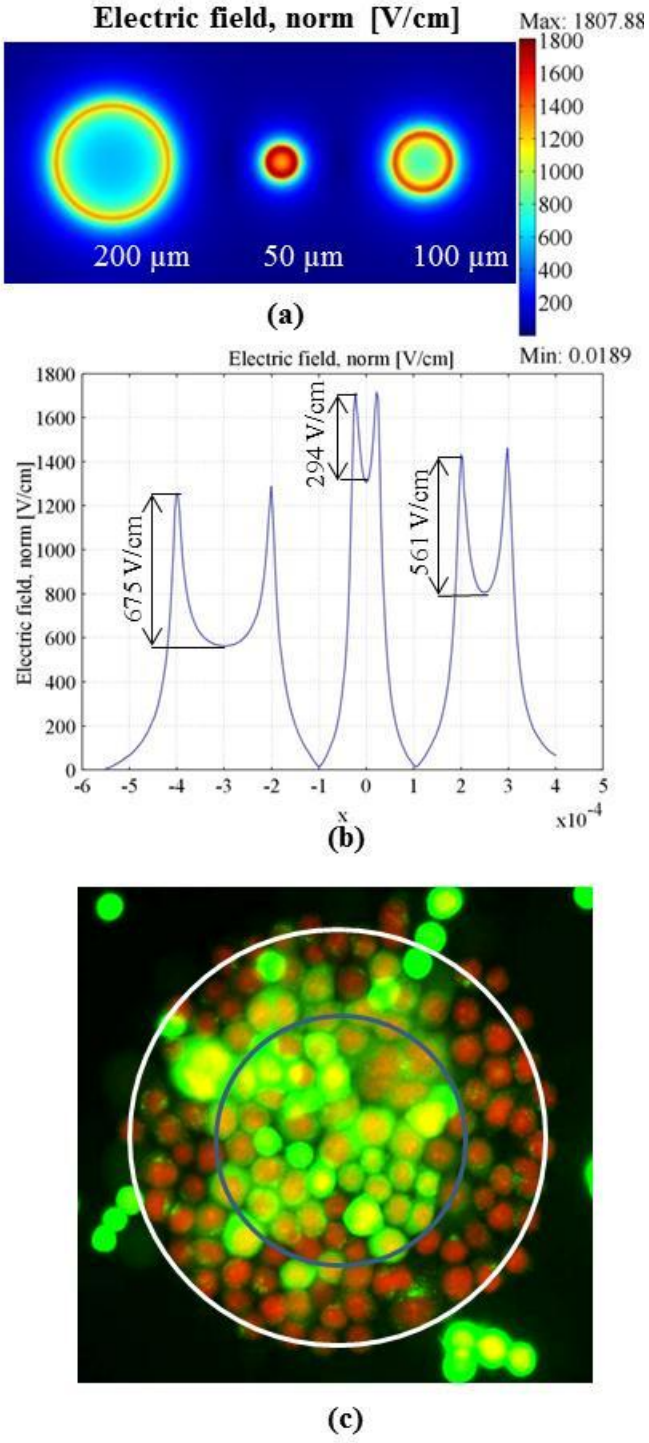

Figure 12. Electric field simulation for three electrode sizes. (a) Top view of the electric field intensity distribution over the surface of electrodes.

Simulation results are shown for three different electrode sizes (50, 100 and 200 μm in diameter). (b) Show a plot of the electric field intensity along the diameter of the electrodes. (c) An image of HeLa cells on 200 μm electrode after electroporation with a 5 V, 10 msec pulse, showing cell death at the edge of the electrode. The white circle marks the electrode boundary and the blue circle highlights the cells on the center of the electrode.

A plot of EF intensity along the diameter of the three electrodes (Figure 12(b)) shows that maximum change in EF intensity from the edge of the electrode to the center of the electrode was proportional to the size of the electrode. On the 200 μm electrode, the EF intensity at the edge of the electrode was more than two times as strong when compared to the center of the electrode. The above described FEM simulation results indicate that cells adhered on large diameter electrodes, such as 200 μm, experience a varying degree of electro-permeabilization depending on their location on the electrodes. The areas of high field intensities on the 200 μm electrodes (at the edge of the electrodes) lead to cell death, thereby negatively impacting the electroporation efficiency. Figure 12(c) shows the image of a 200 μm diameter electrode with HeLa cells after electroporation with a 5V, 10 msec pulse. It can be observed that cells at the edge of the electrodes are electroporated but dead, whereas the cells at the center of the electrodes are electroporated and alive, as predicted by the EF intensity simulation.

3.3.3 Site-specific gene delivery and silencing

To demonstrate the applicability of the ITO MEA for site-specific transfection, HeLa cells adherent on the ITO MEA were targeted for electroporation in the presence of GFP plasmid and Alexa 488 tagged scrambled sequence of siRNA (Alexa 488 – siRNA), separately, using an 8 V, 1 msec pulse. Figure 13(a) shows an image of HeLa cells on ITO MEA

expressing GFP, 24 hours after transfection with GFP plasmid, and Figure 13(b) shows the image of HeLa cells 4 hours after transfection with Alexa 488 – siRNA. Transfection efficiencies (TE) for the GFP plasmid and Alexa 488 – siRNA on a 100 μm electrode for an 8 V, 1 msec anodic pulse were found to be 55.1±14.8% and 25.6±10% (N=5), respectively (Figure 13(c)).

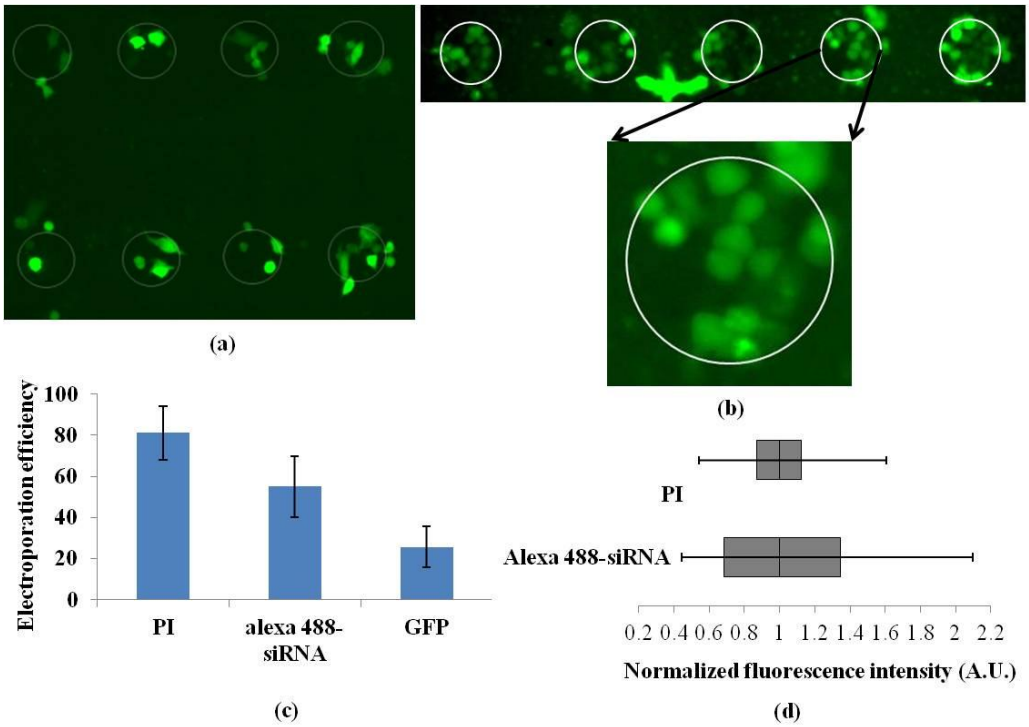

Figure 13. (a) Image shows GFP expression in HeLa cells on targeted electrodes 24 hours after transfection. (b) Image of HeLa cells on targeted electrodes transfected with Alexa 488-siRNA. (c) Comparison of transfection efficiency for three molecules with different sizes (PI, siRNA and GFP plasmids) (N=5) (d) A boxplot displaying the variability in the siRNA and PI intensity among different cells on one electrode. White circles mark the electrode boundary.

Here, the TE is defined as the percentage of cells transfected, with GFP or siRNA, and alive on a given electrode. The low TE for siRNA and GFP as compared to the PI molecules (Figure 13(c)) can be attributed to the size and charge of the molecules. In electroporation based delivery, the size of the probe molecule has been shown to be a strong determinant of the TE(He, Chang, & Lee, 2007) . Larger polar molecules, such as GFP and siRNA, require larger pores that need to remain open longer for electrophoretic migration into the cell cytoplasm.

Observation of transfection results of HeLa cells with Alexa 488 – siRNA indicated a variation in the level of fluorescence intensity among cells on a targeted electrode (Figure 13(b)), indicating a variability in the level of siRNA uptake amongst different cells on the same electrode. This variability in the level of transfection was quantified by determining the level of fluorescence (mean intensity) of each cell on an electrode, targeted for delivery of either Alexa 488 – siRNA or PI, and then plotting it as a box and whisker plot, as shown in Figure 13(d). The data was plotted for a sample size of 18 cells per electrode for both siRNA and PI. The median of the siRNA and PI fluorescence intensity were normalized to 1 for the purpose of comparison. The interquartile range (IQR) for the Alexa 488 – siRNA (IQR = 0.66) was found to be 2.54 times larger than PI (IQR = 0.26); this indicates that the variability in the level of transfection amongst cells was higher for siRNA than for PI. The average fluorescence intensity of the cells with Alexa 488 – siRNA in the 3rd quartile was 1.36 times more

than the average fluorescence intensity of the 1st quartile. The cells in the highest quadrant were 3.55 times more fluorescent than the cells in the lowest quadrant; this demonstrates that 25% of the total cells on the electrode had siRNA levels greater than 3 folds in comparison to the 25% of the cells with the lowest fluorescent intensity.

To evaluate the efficacy of gene silencing using the MEA based platform, siRNA against an endogenous gene, GAPDH, was delivered to targeted HeLa cells. Here, two controls were established on the same device, one with siRNA against GFP (control siRNA) and one with no electroporation. Twenty-four hours post transfection, an immunofluorescence assay was performed to assess the level of GAPDH. Figure 14(a) shows the results of GAPDH silencing in HeLa cells 24 hours after transfection with GAPDH siRNA. As seen in Figure 14(a), the level of GAPDH in the cells transfected with GAPDH siRNA is much lower in the cells transfected with control siRNA. Cells transfected with GAPDH siRNA showed a 52% reduction in GAPDH level (Figure 14(b)) and cells transfected with control siRNA showed a slight reduction (7.4%), albeit statistically insignificant, in GAPDH levels when compared to control cells, probably due to some cell death at electroporation. The viability at the 8 V, 1 msec pulse was found to be 83.4±7.9% (N=3).

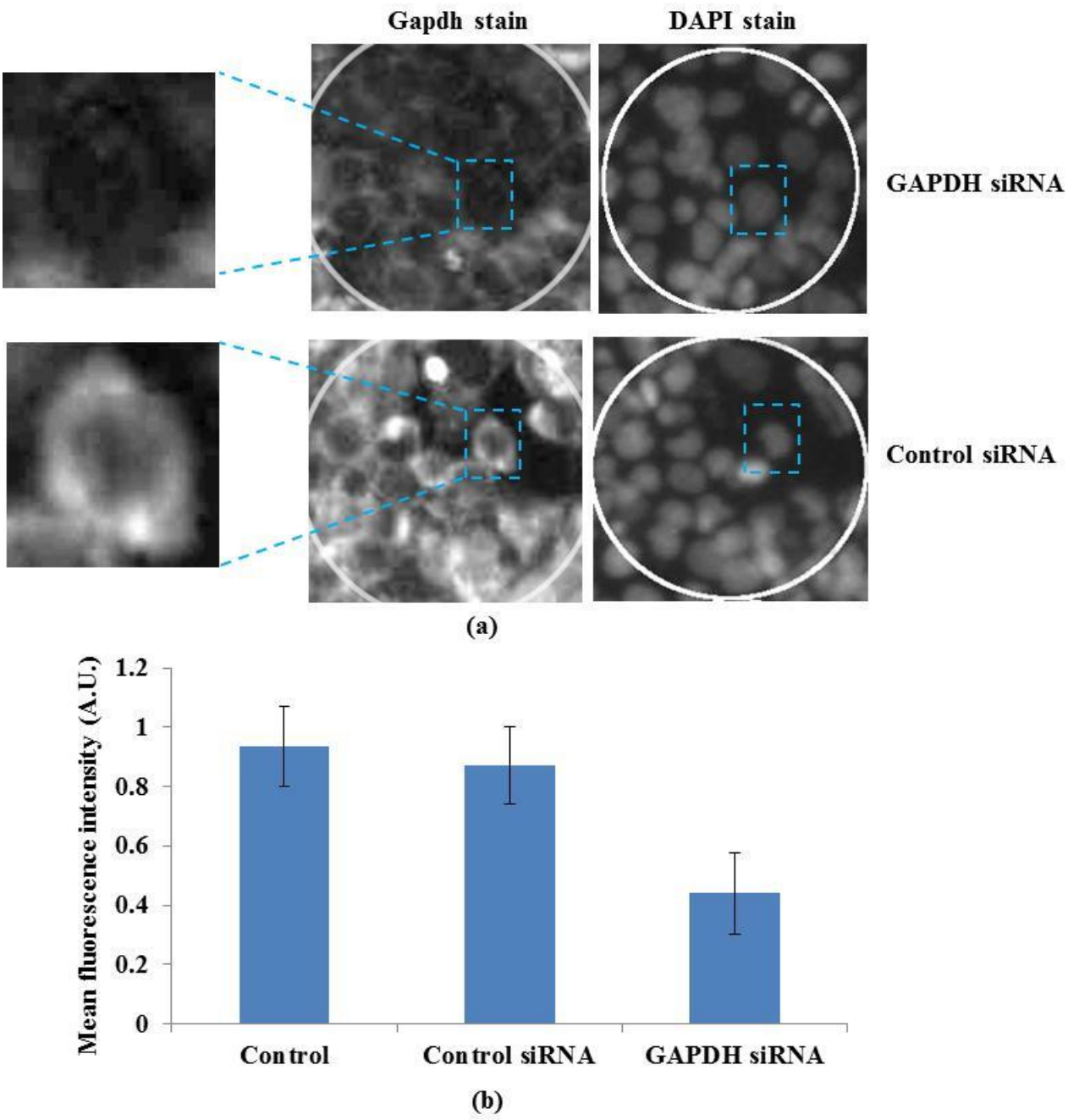

Figure 14. (a) Figure shows GAPDH immunostained image of HeLa cells on two electrodes targeted with GAPDH siRNA and control siRNA. Cell nuclei are shown by DAPI stain. White circles mark the electrode boundary. (b) Figure shows mean fluorescence intensity of GAPDH on

electrodes with control cells, cells targeted with control siRNA and GAPDH siRNA (N=6).

3.3.4 Actin disruption and reorganization post electroporation

To demonstrate the utility of MEA for assessment of sub-cellular phenotypes, the impact of microscale electroporation on F-actin filaments, a key cytoskeletal protein, was investigated. In this study, the MEA was used to specifically look at the disruption and reorganization of F-actin filaments in response to microscale electroporation in adherent HeLa cells. Experimentally, predetermined electrodes (100 μm) on a single MEA were targeted for electroporation at five different time points (8 hours, 4 hours, 2 hours, 1 hour and 5 min) prior to fixation and staining for F-actin. An electrode with no electroporation was established as a control. Electroporation was carried out by applying the optimal voltage pulse of 8 V and 1msec to the targeted electrodes in the presence of electroporation buffer. The capability of MEA to perform multiple independent experiments enabled temporal analysis of actin filaments disruption and its subsequent reorganization in response to electroporation, as shown in Figure 15. It was observed that up to 2 hours after electroporation, HeLa cells sustained a disruption in the structural composition of the actin filaments, characterized by the aggregation of actin filaments at the cell periphery and the dissolution of fine fibers traversing the cytoplasm (Figure 15). The microfilaments reorganized to their original state within 4 hours of electroporation (Figure 15). Interestingly, up to 5 minutes after electroporation (Figure 15), the actin filaments remained intact indicating

that the disruption of microfilaments in HeLa cells did not occur immediately after or during electroporation.

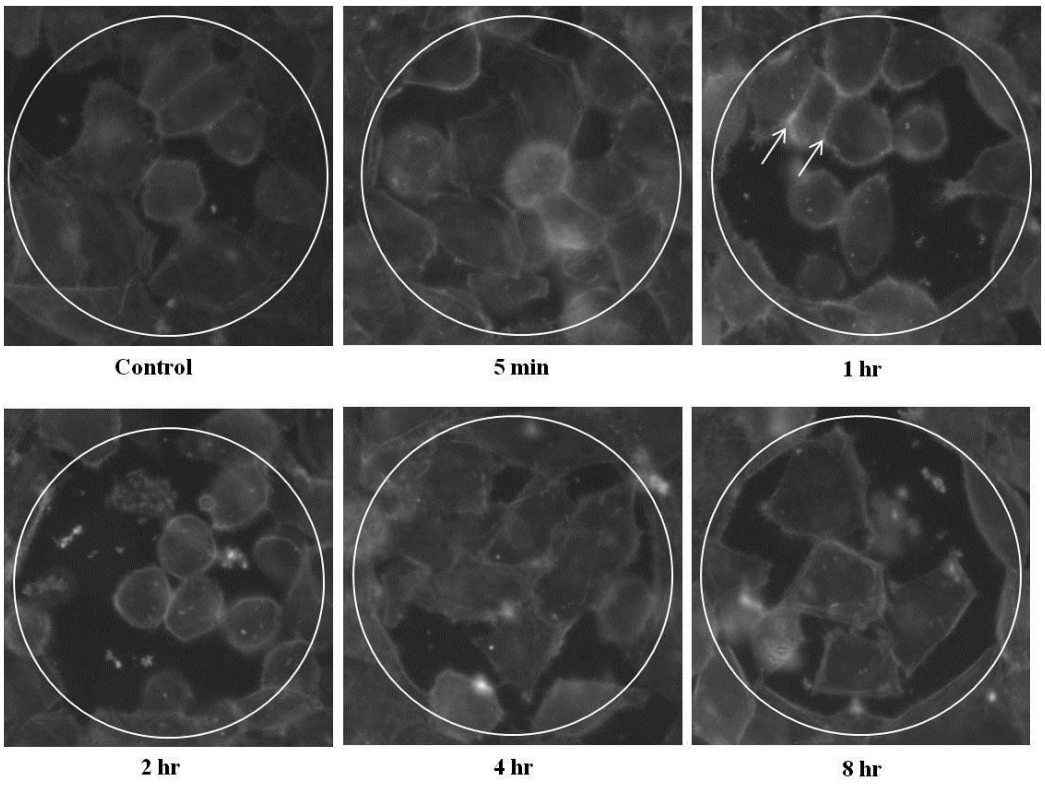

Figure 15. Disruption and subsequent reorganization of actin filaments in HeLa cells at different time points after electroporation. White circles mark the electrode boundaries.

3.4 Discussion and Conclusion

A major advantage of the MEA based system is the precise control over the region of electroporation, derived from the spatial arrangement of the electrodes in the MEA, which is highly desirable in high-throughput screening. The combined spatial and temporal control demonstrated by the MEA based system allowed multiple experiments to be performed on the same culture, thereby decreasing the culture-to-culture variability and increasing the experimental throughput. In addition, compatibility with imaging based assays is highly desirable in cell based experiments. Traditional MEAs are opaque in nature and hence are mostly compatible with only upright microscopes. In addition, the presence of a well mounted on MEA for containing the cell media severely restricts the working distance of an objective lens, making it difficult to image at high magnifications (>10X objectives). The optically transparent nature of the ITO MEA makes it compatible with both upright and inverted microscopes. The thickness of the glass substrate can potentially be reduced to 200μm, allowing magnifications higher than 400X and confocal microscopy. Alternatively, incorporation of microfluidics can potentially reduce the height of the well to under 1 mm, allowing higher magnifications using an upright microscope. In any scenario, the ITO MEA allows brightfield imaging of cells which enables morphological assessment of modified cells.

It is well known that electroporation of a cell occurs when the strength of the applied EF exceeds a certain threshold value (Gehl, 2003). Reversible electroporation is possible only for a narrow range of EF intensities above the threshold value; at EF intensities higher than the reversible range, cell death occurs due to severe irreversible damage to the cell membrane. FEM simulations of EF intensity have been previously used to predict regions of successful transfection and regions of cell death for various electrode shapes and configurations (W. C. Chang & Sretavan, 2009; Dong-yang, Cheng-xiang, Yan, & Chen-guo, 2008; H. Huang et al., 2010; Jain & Muthuswamy, 2007a; Jain & Muthuswamy, 2007b). In this study, the FEM simulation of the EF intensity distribution on the surface of the electrodes with three different sizes assisted in identification of potential regions of reversible and irreversible electroporation on the 200 μm electrode surface. The simulation results correlated well with the experimental observations (Figure 12(c)) in providing the explanation for the lower transfection efficiencies on the 200 μm electrode when compared to the 100 μm and 50 μm electrodes. The low electroporation efficiency of large diameter electrodes (>200 μm) is a major disadvantage in applications that require transfection of a large number of cells per single site. An alternative approach to overcome this limitation would be to use multiple smaller electrodes patterned close to each other, allowing electroporation of a large number of cells in a targeted region. In addition, for applications that require single cells targeting, electrodes in the order

of a few microns can be patterned. Furthermore, electrodes could be patterned to micron or sub-micron diameters to target specific regions of single cells (Hai & Spira, 2012).

The siRNA transfection experiments demonstrated the applicability of the ITO MEA for site-specific gene silencing. It was observed that a certain degree of variability existed in the level of transfection each cell experienced on targeted electrodes. The variability in the level of siRNA transfection among different cells on an electrode is a common limitation in the majority of the transfection techniques. However, the effect of variation in gene silencing can be minimized by averaging the gene silencing results over multiple electrodes. In particular to microscale electroporation, the possible causes for the variability in the siRNA uptake include intrinsic factors such as, the state of each cell, cell shape and/or extrinsic factors such as non-uniform distribution of electric field on the electrode. A strategy that can be employed to overcome the extrinsic factors includes optimizing the shape and size of the electrode to deliver a highly uniform electric field distribution over the target region(H. Huang et al., 2010). In addition, simulations and experimental studies investigating the interaction of cell shape and size with electric field are also necessary to fully understand and predict the level of membrane permeabilization experienced by each cell (Agarwal et al., 2007). This would enable development of adaptive systems that can realize controlled

permeabilization of each cell based on its shape, size and position in the electric field (R. Yang, Tarn, & Zhang, 2010).

In this study, the successful site-specific transfection of HeLa cells with GAPDH-siRNA was demonstrated, resulting in a significant reduction (52%) in the level of the GAPDH 24 hours after transfection in comparison to control cells (Figure 14(b)). Future research will aim to deliver different functional siRNA at different sites in the culture and sequential delivery of multiple siRNA to the same site. The level of gene silencing depends on various factors such as cell type, dosage of siRNA, turnover rate for the protein, and the efficacy and stability of the siRNA molecules in the cytoplasm. In gene silencing experiments, it is extremely desirable to maintain a precise control over the dosage of siRNA delivered to cells. In the case of microscale electroporation, strategies that can potentially be implemented to gain control over the dosage of siRNA include controlling the concentration of siRNA in the electroporation buffer and sequentially repeated electroporation at different time points. Such a strategy would require optimization of time points between subsequent electroporation steps to maintain highest possible cell viability.

In addition to the site-specific transfection, the applicability of the ITO MEA was also demonstrated in investigating the functional impact of electroporation on cells. For instance, in electroporation mediated cell transfection, the cytoskeleton of the cells is thought to play an active role

in the transfer of genetic payload through the cell membrane and into the cytoplasm (Kanthou et al., 2006; Rosazza, Escoffre, Zumbusch, & Rols, 2011; Teissie & ROLS, 1994). Electroporation has also been shown to have a reversible effect on the structural organization of the cytoskeleton microfilaments, which may in part be responsible for the observed interaction of the cytoskeleton with the genetic material (Kanthou et al., 2006). In order to achieve high transfection efficiencies, it is imperative to fully understand the involvement of cytoskeleton in gene transfer. In a study by Rosazza et al., the role played by actin filaments in the transfer of DNA plasmid molecules across the cell membrane was investigated (Rosazza, Escoffre, Zumbusch, & Rols, 2011). The study found that DNA molecules interacted with actin filament patches in the membrane 10 minutes after electroporation in chinese hamster ovary cells. This interaction was also found to assist the translocation of DNA molecules through the cell membrane. Thus, it is plausible that the disruption of actin filaments post electroporation mediates the transfer of DNA molecules to the cytoplasm; however, the underlying phenomenon of actin filaments disruption due to electroporation and its impact on cell functioning remains unknown. The actin experiments performed here served a dual purpose of establishing the applicability of the MEA for assessment of sub-cellular phenotypes and to perform preliminary experiments using the MEA towards understanding the impact of microscale electroporation on the cell cytoskeleton and the mechanism of

DNA transfer to the nucleus in adherent cells. The experiment results showed that actin filaments get disrupted post-electroporation and sustain the disruption for up to 2 hours before reorganization occurs.

In this study, a scalable ITO based MEA was fabricated for site-specific delivery of genetic material in adherent cells. Successful gene silencing and exogenous plasmid expression in targeted cells was demonstrated 24 hours after transfection. In addition, it was determined that electroporation efficiencies are influenced by the size of the electrodes, with small electrodes (≤ 100 μm) offering the highest efficiency. The technology presented here offers a cost-effective approach, which is highly suited for primary cells lines such as neurons, for high-throughput genetic studies.

CHAPTER 4

A NEURO-CHIP FOR SIMULTANEOUS DELIVERY OF NUCLEIC ACIDS AND ASSESSMENT OF FUNCTIONAL CHANGES IN TARGETED NEURONS IN CULTURE

4.1 Introduction

Genetic intervention techniques such as gene silencing (RNA interference) and gene expression (plasmid vectors) offer a powerful approach to determine function of genes that are implicated in neurological disorders, neuronal differentiation and regenerative medicine (Friedmann, 1994; Poole, Bashllari, Cochella, Flowers, & Hobert, 2011; Y. Yao, Wang, Varshney, & Wang, 2009). However, a major challenge in the above applications is the efficient delivery of siRNA molecules or plasmid vectors to spatially targeted neuronal populations (Krichevsky & Kosik, 2002; Whitehead, Langer, & Anderson, 2009). A majority of the current non-viral transfection methods such as chemical transfection (Lonez, Vandenbranden, & Ruysschaert, 2008; Park, Jeong, & Kim, 2006), bulk electroporation(Dityateva et al., 2003; McCall, Nicholson, Weidner, & Blesch, 2012; Prasanna & Panda, 1997), and nanoparticles assisted delivery (Bonoiu et al., 2011; Ghosh, Han, De, Kim, & Rotello, 2008), lack precise spatial control over delivery. Targeted delivery of genetic material is particularly desirable in a heterogeneous cell population, such as the nervous system, where delivery to non-targeted cell types can elicit

unwanted responses (Matthaei, 2007). In addition, site-specific transfection in network forming cells, such as neurons, enables investigation of cell-network interactions (L. Luo, Callaway, & Svoboda, 2008; Takahashi et al., 2011). Furthermore, high-throughput miniaturized genetic screening platforms can greatly benefit from precise spatio-temporal control over delivery of nucleic acids (Wheeler, Carpenter, & Sabatini, 2005). For example, the transfected cell microarrays technique developed by Ziauddin and Sabatini more than a decade ago, enabled site-specific transfection of cells in a culture in a microarray fashion allowing screening multiple genes in a single cell culture grown on a glass slide (Ziauddin & Sabatini, 2001). However, in addition to lack of temporal control over transfection, a major limitation with this technique is its reliance on chemical based transfection which offers low transfection efficiency in primary cell lines such as neurons. Since then advances in microfabrication techniques have led to development of several miniaturized platforms that utilize microscale electroporation as a method for transfection (Boukany et al., 2011; W. C. Chang & Sretavan, 2009; Hai & Spira, 2012; K. S. Huang, Lin, Su, & Fang, 2006; Y. Huang & Rubinsky, 2001; Inoue, Fujimoto, Ogino, & Iwata, 2008; Jain & Muthuswamy, 2007a; Jain & Muthuswamy, 2007b; Jain & Muthuswamy, 2008; Jain, Papas, Jadhav, McBride, & Saez, 2012; W. G. Lee, Demirci, & Khademhosseini, 2009; Y. C. Lin, Li, Fan, & Wu, 2003; Movahed & Li, 2011; Olbrich, Rebollar, Heitz, Frischauf, & Romanin, 2008; Stett et al.,

2003; Valero et al., 2008; Valley et al., 2009; Y. Xu, Yao, Wang, Xing, & Cheng, 2011). Microscale electroporation has been shown to offer high transfection efficiency in primary cell lines and it enables precise spatial and temporal control over transfection. In the above mentioned platforms, microscale electroporation is typically achieved by utilizing microelectrodes to generate localized electric field intensity patterns that allows spatially targeted electroporation of cell membranes of single cells and sub-cellular structures. Traditionally, microelectrode arrays have been used in neurophysiology for stimulation and measurement of electrical activity of cells (Stett et al., 2003). Electrical activity of neurons is one of the most widely preferred methods to assess neuronal function. Therefore, technology that integrates the ability to simultaneously deliver genetic material and measure electrical activity of precisely targeted neurons in a high-throughput fashion will enable the assessment of the impact of gene manipulation on the function of neurons in real time at the level of single cell and the entire network.

Based on the above premise, the use of patterned micro-electrode array (MEA) based platform for targeted transfection of primary neurons and NIH 3T3 cells in culture has been demonstrated (Jain & Muthuswamy, 2007a; Jain & Muthuswamy, 2007b; Jain & Muthuswamy, 2008). In the above approach, the MEA is used to induce electroporation in a targeted group of cells in a culture and simultaneously utilize the same electrodes to monitor electrical activity of single neurons. However, a

major limitation with traditional MEAs is the optically opaque nature of the electrodes and/or substrate that restricts imaging which is a crucial necessity for various biological assays, especially in high-throughput and high-content genetic studies (Wheeler, Carpenter, & Sabatini, 2005). In this study, the application of an optically transparent MEA for spatially and temporally controlled transfection of primary hippocampal neurons in a culture was demonstrated. Secondly, targeted transfection of genetic payloads of different sizes and molecular characteristics, such as GFP plasmids and fluorescently tagged siRNA molecules (Alexa 488-siRNA), was successfully demonstrated for the first time in a primary culture of hippocampal neurons. Additionally, the impact of electroporation itself on spontaneous electrical activity of neurons was assessed. Finally, this work reports for the first time delivery of GFP plasmids to neurons through electroporation of neuronal processes.

4.2 Materials and Methods

4.2.1 MEA fabrication

The neuro-chip was fabricated using standard microelectromechanical systems (MEMS) based process. The MEA was patterned in indium-tin oxide (ITO), a transparent conductive material, on a glass substrate. A thin layer of parylene was deposited on the MEA as an insulation layer. The parylene layer was selective etched using oxygen

plasma to expose the microelectrodes and the bond pads. The MEA consisted of 32 circular microelectrodes, each with a diameter of 100 μm. Figure 16(b) shows a picture of the neuro-chip with a well containing cell media placed on the MEA.

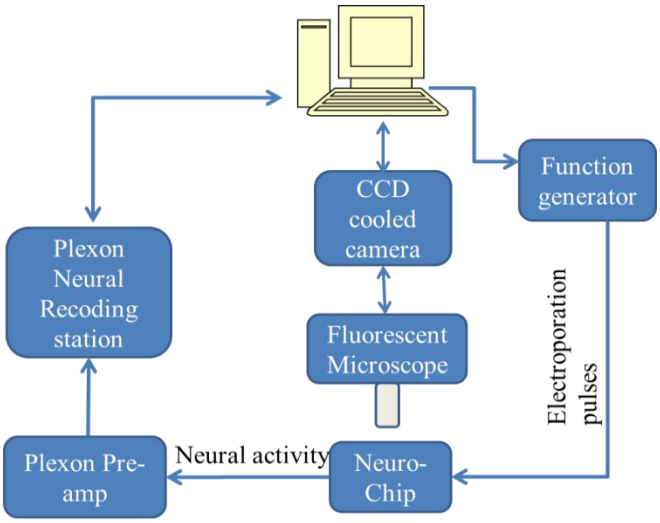

(a)

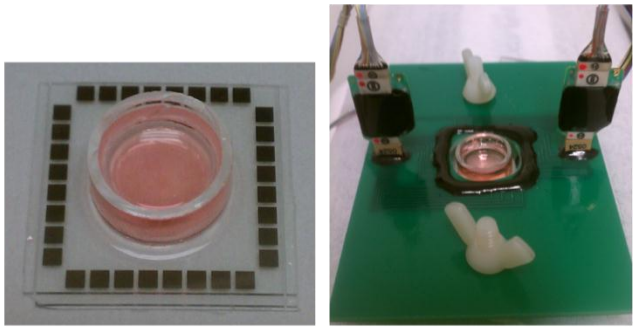

(b) (c)

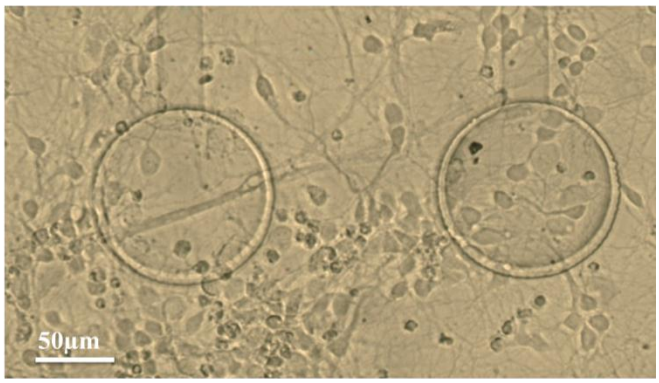

(d)

Figure 16. (a) Experimental setup. (b) Image of the MEA with well containing media. (c) Connector for neural recording. (d) 4 DIV culture of E18 hippocampal neurons on the ITO MEA.

4.2.2 Electrical characterization of the MEA

The electrical characterization of the microelectrodes was conducted using an electrochemical workstation (Model 660a, CH instruments, TX, USA). The electrical impedance spectroscopy (EIS) was carried out in the presence of phosphate buffered solution (PBS) with the microelectrodes as working electrodes and platinum wire as the reference and counter electrode. A frequency sweep of 100 Hz -100,000 Hz was performed for the EIS measurements. The integrity of the interconnect traces and the microelectrodes was determined by examining the EIS results. Electrodes with discontinuous traces and/or unexpectedly high impedances were excluded from the experiments.

4.2.3 MEA preparation and cell culture

The parylene insulation layer on the MEA is naturally hydrophobic in nature. In order to make the MEA surface hydrophilic, it was treated with oxygen plasma for 1 – 2 min. Afterwards, the MEAs were coated with poly-D-lysine (PDL) at a concentration of 100 μg/ml for a period of 12 h at room temperature in a sterilized flow hood to facilitate cell adhesion. Prior to cell seeding, the MEAs were treated with laminin (20 μg/ml) for 20 – 30 min. The E18 hippocampal neurons for culture on the MEA were obtained from Brainbits, LLC (Springfield, IL). On the day of cell seeding the E 18 hippocampal tissue was digested in 2 ml of 2 mg/ml sterilized papain (Sigma Aldrich, St. Louis, MO) in Hibernate-E without $CaCl_2$

(Brainbits. LLC, Springfield, IL) for 30 mins at 34°C. Post digestion, the tissue was washed and dissociated in Hibernate-E media by trituration (10X) using a standard 1000 µl pipet tip. Next, the cells were pelleted by spinning at 200 RCF for 4 mins. The cells were then raised to a concentration of 1000 – 3000 cells/µl in Nbactiv-1 media (Brainbits. LLC, IL), depending on the desired seeding concentration. A 25 – 30 µl drop of cells was then placed on the center of MEA and the cells were allowed to adhere for 2 h in a humidified incubator maintained at 37°C and 5 % CO_2. The cells were maintained in 600 µl of Nbactive-1 (Brainbits. LLC, IL) medium and half of the medium was changed every 2 – 3 days.

4.2.4 Electroporation setup and imaging

The microelectrodes were accessed for electrical stimulation by using a dual-inline-package (DIP) clip to connect the bond pads of the MEA with a function generator (2414A, Pragmatic. Inc., Geneva, OH). Prior to each electroporation experiment, the function generator was configured to output a single anodic square pulse with desired pulse amplitude and duration. Individual access to the microelectrodes was achieved by using an 8 switch demultiplexor board that connected to the output of the function generator. For the ground, a sterilized steel electrode was lowered into the MEA well and was positioned 1 mm above the surface of the MEA. Imaging of cells on the MEA was carried out using an inverted fluorescence microscope.

4.2.5 Experimental protocol

Figure 16(a) shows the experimental setup. The electroporation experiments were typically performed on a 4-5 day old neuronal culture. By this time the neurons were typically differentiated and the processes have formed (Figure 16(d)). On the day of the experiment, a 200 – 300 µl solution of probe molecule in electroporation buffer (#165-2677, Bio-rad, Hercules, CA) was prepared and maintained at 4°C. The three different probe molecules used in experiments were, propidium iodide, alexa-488 conjugated scrambled sequence siRNA (#1027992, Qiagen, Inc., Valencia, CA), and GFP plasmids; these molecules were prepared at 50 µg/ml, 2.5 µM, and 50 µg/ml respectively. Prior to the electroporation of cells, the media in the MEA well was replaced with the ice-cold electroporation buffer containing the probe molecule. Immediately afterwards, the MEA was connected with the function generator via the DIP clip and multiplexor board. Next, electric pulses for electroporation were applied to the desired microelectrodes. Upon completion of voltage pulse application, the MEA was transferred to the incubator. After a 10 min incubation period, the electroporation buffer in the MEA well was replaced with pre-warmed and CO_2 equilibrated media. For PI experiments, a live assay was performed on the cells 2 – 4 h after electroporation to determine the viability of cells. In the case of PI and alexa-488 conjugated siRNA experiments fluorescent imaging was done 4 h after electroporation and in

the case of GFP transfection, cells were imaged 24 h after electroporation. The electroporation efficiency was calculated as the percentage fraction of total number of viable cells loaded with PI. The transfection efficiency for alexa-488-siRNA and GFP was calculated as the percentage fraction of the total number of cells displaying uptake of siRNA or expressing GFP.

4.2.6 Neuronal recordings

A custom made connector with spring loaded pins (Figure 16(c)) was used to connect the MEA with a data acquisition system (MAP system, Plexon, Inc., Dallas, TX) for measuring the electrical activity of neurons. The MEA was maintained in the incubator during recording sessions. Recording sessions were performed in 10 min intervals. The spike data was analyzed in Offline sorter v2.8.8 (Plexon, Inc., Dallas, TX) and Neuroexplorer (Plexon, Inc., Dallas, TX). Typically, neural activity was observed after 7 days of culture or days in vitro (DIV).

4.3 Results

4.3.1 Optimal electroporation parameters

The EP parameters were optimized as previously described (Patel & Muthuswamy, 2012). Briefly, to determine the highest transfection efficiency, a series of experiments were conducted to optimize the electroporation voltage pulse amplitude and pulse width. In all the

experiments, a single anodic square wave pulse was applied to the microelectrodes to achieve electroporation. To quantitatively assess the transfection efficiencies, different electroporation pulse amplitudes, with a constant pulse width of 1 msec, were applied to different microelectrodes in the presence of PI, a cell impermeable nuclei stain. Successfully electroporated neurons were detected by red fluorescence due to the staining of nucleic material by PI. Approximately 2-4 h post electroporation, a calcein based live assay was conducted to determine the viability of neurons. A picture of the entire MEA with a 4 DIV culture of E18 hippocampal neurons post electroporation is shown in Figure 17(a). The image on the left shows PI stained neurons on microelectrodes that were stimulated with square wave anodic pulses of 6 V, 7 V, 8 V, 9 V, and 10 V amplitude and the image on the right displays the result of a live assay performed 4 h post electroporation. A close-up image of microelectrodes stimulated with 7 V and 10 V pulse is shown in Figure 17(b).

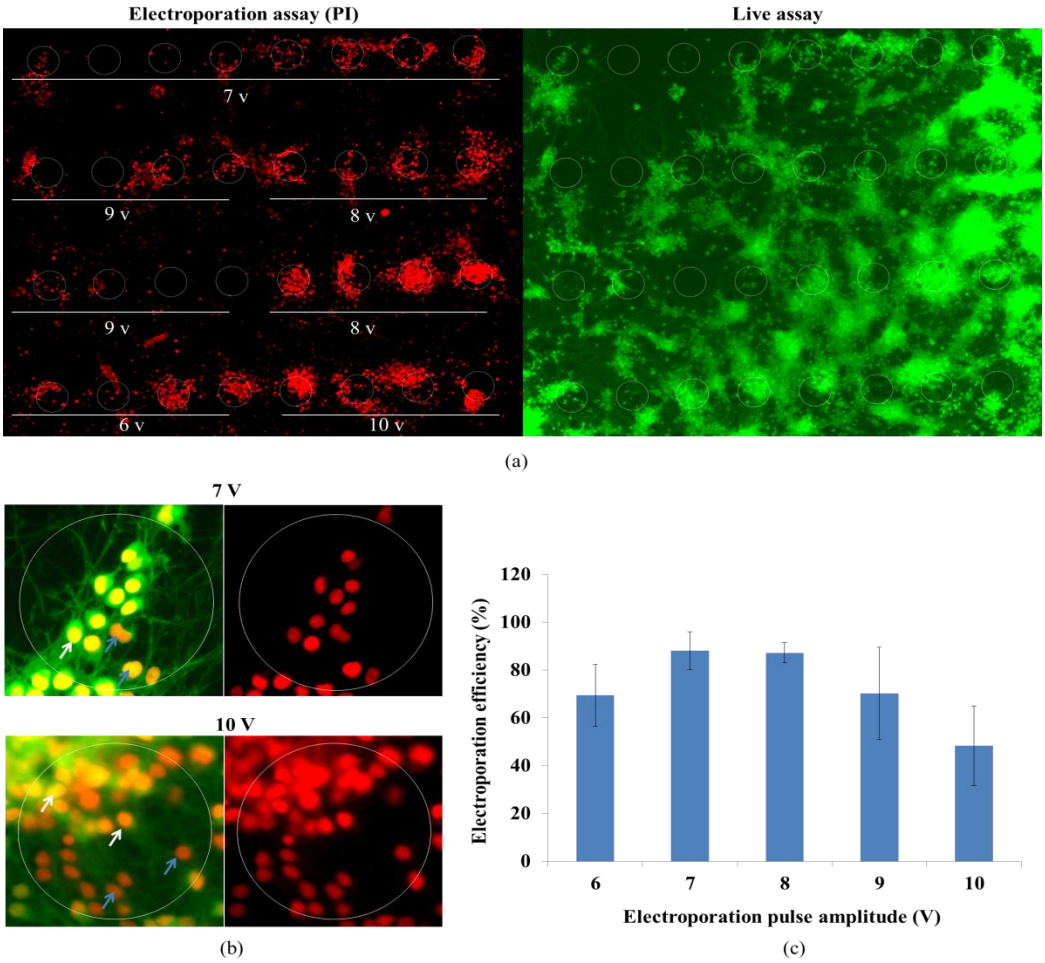

Figure 17. Optimization of electroporation (EP) parameters for hippocampal neurons : (a) Shown in left image is targeted delivery of PI to neurons on a 4x8 microelectrode array (MEA) stimulated with1 msec anodic square pulse of amplitudes 6 V, 7 V, 8 V, 9 V and 10 V; the right image shows the result of live assay performed on the same neurons after electroporation. (b) Close-up images of two electrodes stimulated with 7 V and 10 V, 1 msec anodic pulses. The white arrows indicate representative neurons that are alive and loaded with PI. The blue arrows point to

neurons that are dead. The image on the left is superimposed image of live assay and PI. The image on the right shows PI. The white circles indicate the boundary of the 100 μm diameter microelectrodes. (c) Electroporation efficiencies at different EP voltage pulse amplitudes (n=4).

As seen in Figure 17(b) majority of the cells on 7 V stimulated microelectrode stained both red and green indicating high electroporation efficiency in viable neurons. In contrast, neurons on the 10 V stimulated microelectrode displayed average viability of 48.3±16.6% (N=4) resulting in low electroporation efficiency. A plot of electroporation efficiencies as a function of voltage pulse amplitude is shown in Figure 17(c). Electroporation efficiencies were found to be lower when pulse voltage amplitudes were less than or equal to 6 V due to smaller number of electroporated cells. Similarly, electroporation efficiencies were lower at voltage pulse amplitudes higher than 8 V but due to increased cell death. The highest electroporation efficiencies for neurons of 88.2±7.9 % and 87.3±4.2% were observed consistently at pulse amplitudes of 7 V and 8 V respectively.

4.3.2 Site-Specific transfection of GFP plasmid vectors and siRNA molecules

GFP plasmid vectors and Alexa-Fluo-488 conjugated scrambled sequence of siRNA were transfected into neurons on targeted microelectrodes to evaluate the applicability of the ITO based neuro-chip for site-specific transfection in neuronal cultures. The transfection experiments were accomplished using the optimal 8 V, 1 msec anodic pulse. The expression of GFP in neurons on top of three microelectrodes

that were targeted for transfection with GFP plasmids is shown in Figure 18(a).

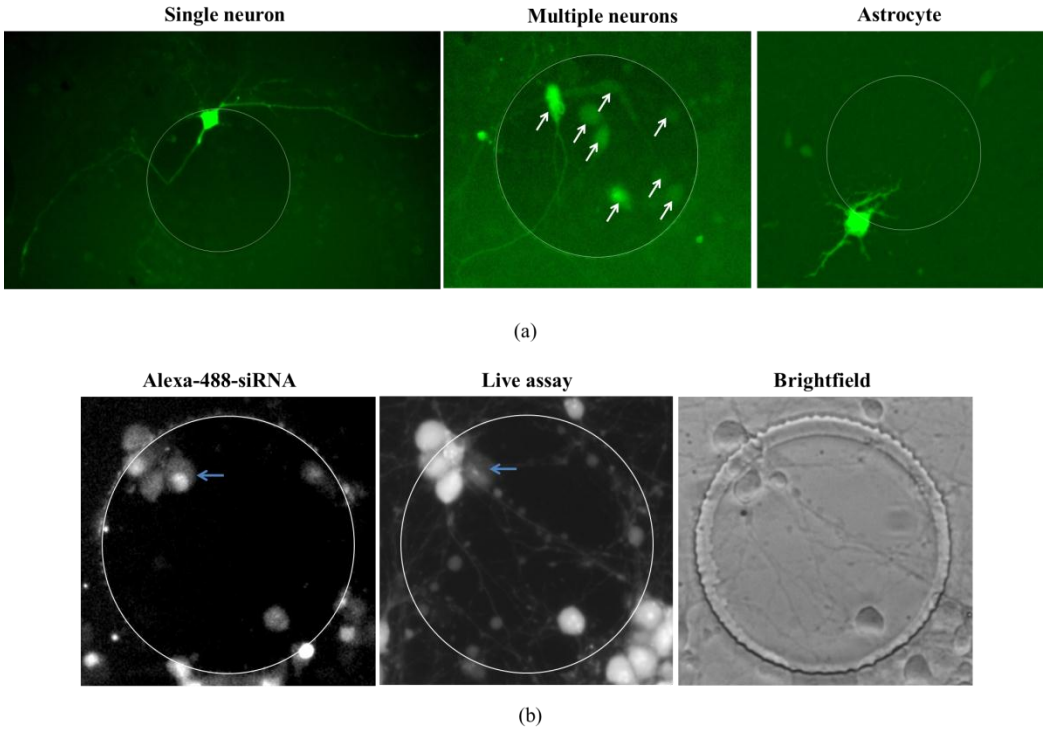

Figure 18. Site-specific transfection of hippocampal neurons. (a) The images shows expression of GFP 24 h after neurons were transfected with GFP plasmid vectors at 4 DIV. The white arrows point to the neurons expressing GFP. The black arrow points to an astrocyte transfected with GFP plasmid. (b) The image on the left shows neurons transfected with Alexa-488-siRNA; the image on its right shows the result of live assay performed after imaging the siRNAs. The blue arrow points to a dead cells. In all of the above cases a 8 V, 1 msec anodic pulse was applied to microelectrodes for electroporation.

The GFP expression images were taken 24 h post transfection. The transfection efficiency for GFP plasmids was observed to be highly variable, as seen in Figure 18(a), with some microelectrodes displaying no more than 1 neuron transfected and some microelectrodes displaying 34 % of neurons transfected in the same culture. In addition, the level of GFP expression amongst transfected cells on the same electrode was also found to be variable. GFP transfection was observed both in neurons as well as astrocytes (Figure 18(a)). Shown in Figure 18(b) is the result of Alexa-Fluor-488 conjugated siRNA transfection in neurons on top of two microelectrodes. The transfection of Alexa-Fluor-488 conjugated siRNA into targeted neurons caused their somas to fluoresce green. A dead assay was performed 4 h post-electroporation to determine viability of cells. The average transfection efficiency for siRNA molecules was determined to be greater than 60%.

4.3.3 Transfection through neuronal processes

In the analysis of the transfection assay results, the possibility of transfection occurring through neuronal processes adhered on top of targeted microelectrodes was discovered. Figure 19(a) shows brightfield, PI fluorescence and live assay images of a 4 DIV culture of hippocampal neurons on an electrode stimulated with 7 V, 1 msec pulse.

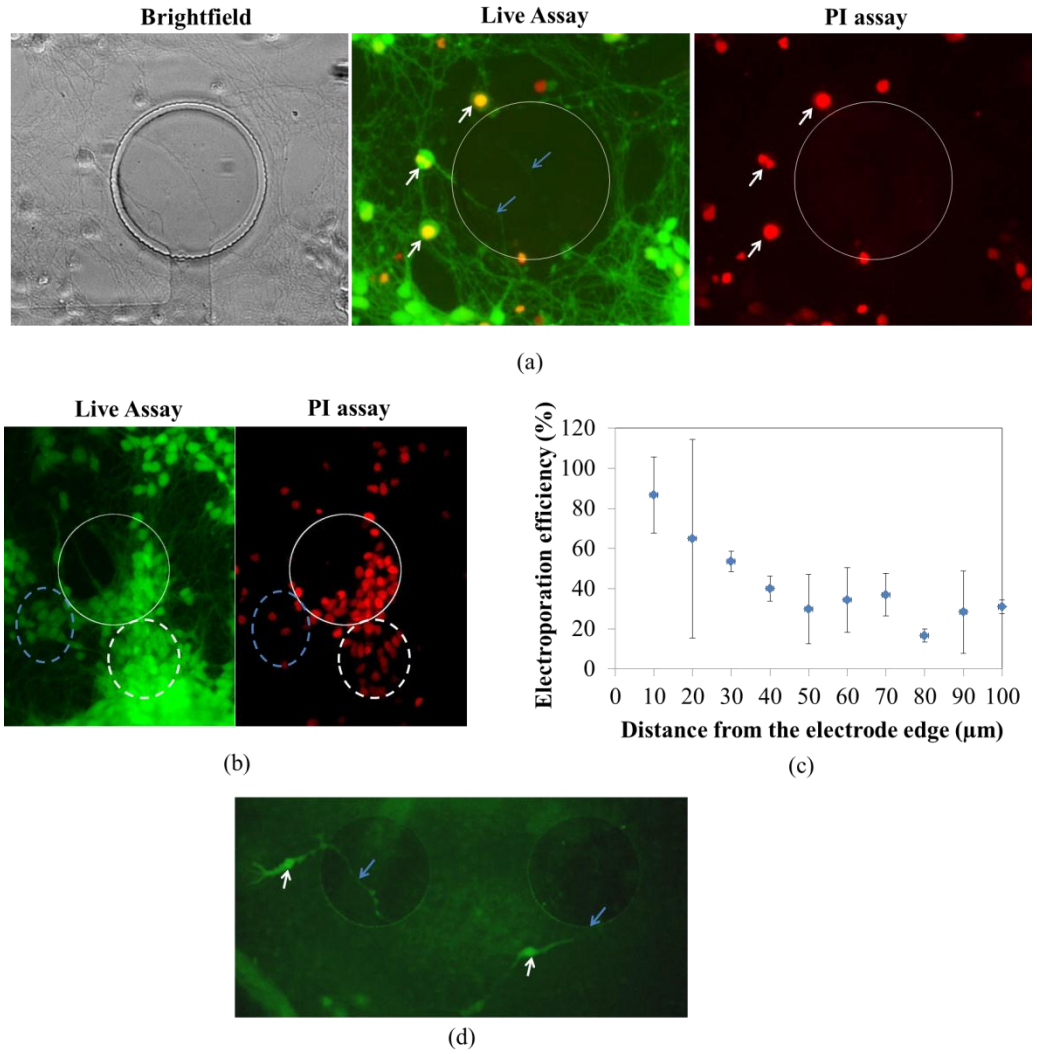

Figure 19. Transfection of neurons through localized electroporation of neural processes. (a) The figures here show neurons with cell bodies outside the electrode region but with axons on the electrode pulsed with a 7 V, 1 msec pulse display uptake of PI, indicating electroporation of axons. The blue arrows point to the neural processes on the electrodes. The white arrows point to the neurons outside the electrodes that fluoresce red due to the uptake of PI. (b) At the same distance away from the electrode,

different regions show different number of neurons with PI. The white circle (in broken lines) is showing a region next to the microelectrode where majority of the total neurons display an uptake of PI whereas the blue circle (in broken lines) is showing a region next to the microelectrode where only a few of the total viable neurons display an uptake of PI. (c) A plot of electroporation efficiency in the neighboring region of the microelectrode as a function of distance from the edge of the microelectrode. (d) The figure displays the result of GFP transfection of neurons through process. The blue arrows show the processes of transfected neurons and the white arrows show the somas of the transfected neurons.

It can be observed that the three neurons indicated by the blue arrows (Figure 19(a)) are viable and present outside the region of the targeted electrode. However, contrary to expectation the three neurons were found to be successfully electroporated, as indicated by red fluorescence of nuclei due to the PI uptake, upon stimulation of the electrode. Interestingly, the processes of the electroporated neurons can be clearly seen on top of the targeted microelectrodes (shown by white arrows). This indicates the possibility of electroporation induced transfection occurring at the level of subcellular structures for the same EP pulse parameters that lead to electroporation of cell bodies. In Figure 19(b) the PI electroporation assay of an electrode stimulated with 7 V, 1 msec pulse shows that electroporation of neurons was observed up to as far as 150 μm from the edge of the stimulated microelectrodes. The plot in Figure 19(c) displays the transfection probability of a neuron as a function of its distance from the edge of the microelectrode (up to 100 μm from the edge of the electrode) using 7 V, 1 msec voltage pulses. The average probability of neuron being electroporated dropped below 50 % at a distance of 25 μm from the edge of the microelectrode and remained as high as 30 % upto a distance of 100 μm from the edge of the microelectrode. An alternative explanation for the electroporation of neurons outside the region of targeted microelectrodes is the presence of strong fringe electric field intensities away from the edge of the electrode.

In order to assess the presence and impact of fringe electric field intensities beyond the boundaries of the electrode, electroporation of HeLa cells cultured on the MEA was performed. HeLa cells were used because they covered the MEA surface completely upon reaching confluency thereby enabling an accurate assessment of electroporation efficiency away from the edge of the microelectrode. In addition, HeLa cells lacked processes, thus any electroporation observed outside the electrode region can be attributed to the presence of fringe electric field intensities beyond the electrode boundaries. Appendix B shows the transfection assay of HeLa cells on an electrode stimulated with 8 V, 1 msec EP pulse. It can be clearly seen that electroporation was strictly confined to a region of 10 μm beyond the edge of the electrode. This strongly suggests the uptake of PI by neurons beyond 10 μm from the edge of the microelectrodes is most likely due to electroporation of the processes of those neurons on the stimulated microelectrode; the electroporation of the dendrites or axons allow the entry of PI molecules and is transported to the cell bodies where it stains the nucleic material. Transfection of neuronal processes was also observed for large molecules such as GFP plasmids indicating a possibility of transfection of neurons through the electroporation of axons, as seen in Figure 19(d); the two cells indicated by the blue arrows with axons running on neighboring microelectrodes (indicated by white arrows) both displayed an expression of GFP 24 h after transfection with GFP plasmids.

4.3.4 Neuronal recordings

EIS results for ITO microelectrodes on the neuro-chip are shown in Figure 20(a) for a frequency sweep of 100 Hz to 100000 Hz. The impedance of 100 μm microelectrodes at 1 kHz was in the range of 379.1 ±14.0 kohm (N=4). Although, the impedance of ITO microelectrodes is comparatively higher than typical gold or iridium oxide coated microelectrodes, it is acceptable for measuring neural activity in vitro. The phase plots for the 100 μm ITO microelectrodes show in Figure 20(a) indicates that the phase is capacitive in nature for frequencies of the expected neural signal spectra. An example of unit activity recorded from a 10 DIV hippocampal culture is show in Figure 20(b).

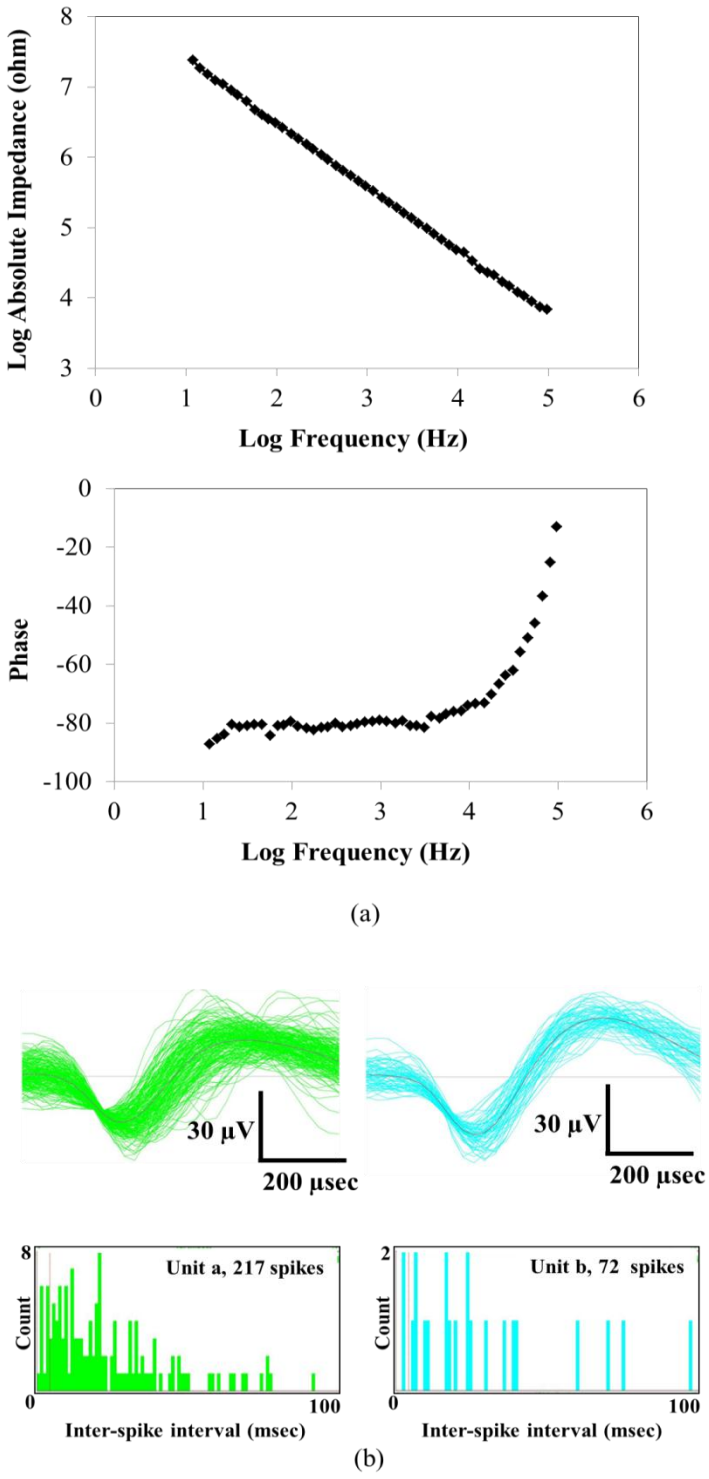

Figure 20. Electrochemical impedance spectroscopy (EIS) characterization of electrodes and sample unit activity (a) The top figure

shows the impedance of the microelectrodes versus frequency and the bottom figure shows the phase versus frequency. (b) The top figure shows the typical unit activity from a 10 DIV hippocampal culture from one electrode. The bottom figures show the corresponding ISI for the units.

The neuronal cultures on the MEA were fully differentiated by 4 DIV and the electrical activity could be recorded by 7 DIV. To validate the applicability of the neuro-chip for functional assessment of neurons, the effect of electroporation on neural activity was evaluated. To accomplish this, two 10 min recording sessions were performed for 16 microelectrodes, one 15 min prior to and one 15 min post-electroporation; an 8 V, 1 msec anodic voltage pulse was applied to all the 16 microelectrodes to achieve electroporation. The experiment was carried out on a 10 DIV E18 hippocampal culture. In this experiment, the goal was to determine the impact of one voltage pulse used for electroporation on the electrical excitability of neurons. Figure 21(a) shows the mean firing rate (spikes/min) per channel (microelectrode) for 10 min recording sessions prior to and post-electroporation; data is shown only for the 7 channels that displayed neuronal activity. The temporal profile of the electrical activity for the 10 min recording sessions is shown in Figure 21(b) for channels 10, 11, 12 and 14. Neurons in channels 10 and 14 displayed a statistically significant decrease in the electrical activity of neurons post electroporation, while neurons in channels 11 and 12 showed a statistically significant increase in the firing rate. Remaining channels showed no statistically significant change in their electrical activity. Data outside the 95% confidence interval was considered to be statistically significant.

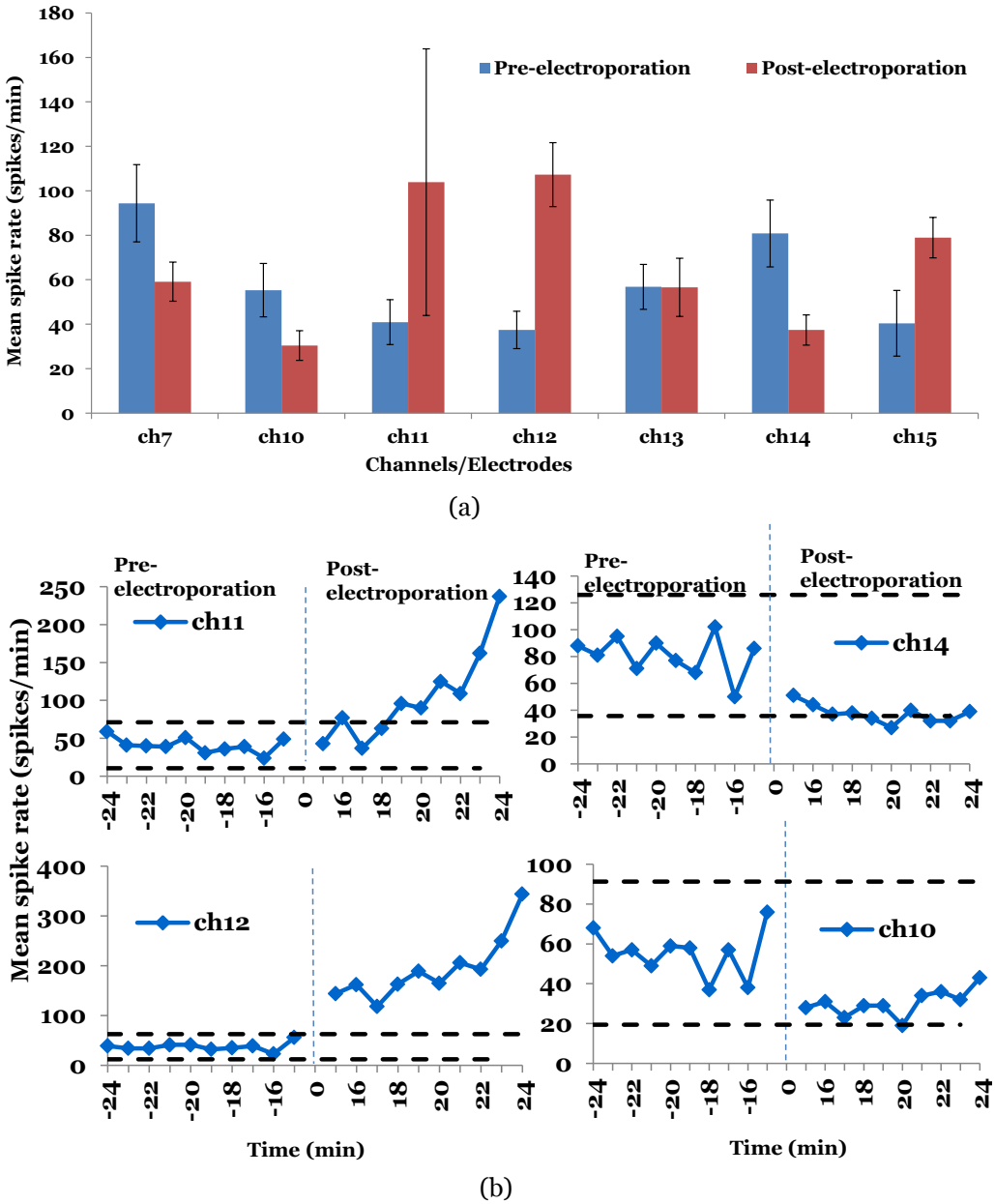

Figure 21. Neural activity before and after electroporation. (a) The figure shows the average spike rate over a period of ten minutes before and after electroporation. (b) The figures show the temporal profile of mean spike rate from 4 channels (10, 11, 12, and 14) before and after electroporation. The black dashed lines represent the 95% confidence interval.

4.4 Discussion and Conclusion

In this study, the aim was to demonstrate the use of an optically transparent neuro-chip for precisely targeted transfection in primary neurons and simultaneous functional assessment of neuronal electrophysiology. Towards this end, an MEA was fabricated with microelectrodes and leads patterned in ITO on a glass substrate. The electroporation pulse parameters were first optimized in E18 hippocampal neurons using the PI/live cell assay (Patel & Muthuswamy, 2012). Second, the optimal pulse parameters were used to deliver GFP plasmid vectors and fluorescently tagged siRNA molecules into targeted neurons in a 4 DIV culture on the MEA. Third, neurons can be transfected with plasmid vectors through localized electroporation of neuronal processes was reported. Finally, the utility of the neuro-chip for measuring electrical activity of targeted neurons was demonstrated.

The development of the ITO based neuro-chip was motivated by the need for a high-throughput gene function assessment platform for neuronal studies. A major challenge with neuronal studies is consistent and efficient transfection of neurons. The neuro-chip overcomes this limitation by utilizing microscale electroporation for achieving transfection; microscale electroporation has been shown to deliver high transfection efficiency in hard-to-transfect cells lines such as neurons both in vivo and in vitro (W. G. Lee, Demirci, & Khademhosseini, 2009). A critical step in electroporation based transfection is the optimization of the

electroporation parameters for each cell type. The use of PI/live electroporation assay provided a quick and cost effective way to determine the optimal electroporation pulse parameters. High electroporation efficiencies were observed over a range of electroporation pulse amplitudes (7 V to 9 V) indicating a robust and consistent electroporation, that is not highly sensitive to small changes in voltage amplitude. The optimal electroporation parameters determined here were for 4-7 DIV neuronal cultures. It remains unknown if the optimal electroporation parameters change with the age of the culture. The electroporation efficiency can possibly be further enhanced by investigating effect of several other factors such as the constitution and conductivity of the electroporation buffer, number of pulses and the polarity of pulse (Hui, 1995). A potential issue could arise from the fact that the amplitude of the optimal electroporation pulse, 8 V, lies beyond the water window of the ITO electrodes in cell culture media (-1.2 to +1.2 V). Electrode potentials beyond water window can lead to hydrolysis of water and formation of bubbles and reactive ionic species at the electrode-media interface that can potentially cause irreversible cell damage or death over a period of time. However, no bubble formation was visually observed at the electrode-media interface probably due to the fact that only a short duration of a single stimulation pulse was applied to the electrodes. Further, results of the cell viability assay indicated high level of survivability among neurons post-electroporation confirming that the potentially adverse consequences

of the voltage pulse amplitude exceeding the water window are minimal in these experiments. The above mentioned concerns can be potentially serious when multiple long duration voltage pulses with amplitudes exceeding the water window are applied to the microelectrodes.

The successful delivery of GFP plasmid and its expression in targeted neurons was critical in establishing the functionality of nucleic acids inside the neurons after delivery. The transfection efficiency per electrode for GFP was found to be highly variable. However, in all the cases, the transfection efficiency per electrode for the GFP is higher than or comparable to current chemical transfection based methods. In addition, given the consistency seen in transfection of GFP plasmid per electrode, it is possible to increase the overall transfection efficiency in the entire culture by increasing the number of transfection sites (microelectrodes) in the culture. The variability in the transfection efficiency of smaller molecules such as siRNA and PI was much lower when compared to GFP molecules suggesting that the larger size of the GFP plasmids might be directly responsible for the variability in the transfection of GFP plasmids. Small molecules such as PI and siRNA can diffuse rapidly through the pores formed in the membrane upon electroporation; however, larger molecules such as GFP plasmids have been reported to be internalized into the cells through membrane interaction at the sites of pore formation post electroporation (Paganin-Gioanni et al., 2011).

The investigation of the role played by axons in intracellular transport and transmission of action potentials is of crucial significance in neuroscience research. In a previous study, Chang and Sretavan fabricated microelectrodes with vertical sidewalls that enabled localized delivery of EGTA to axons by electroporation (W. C. Chang & Sretavan, 2009). In a similar observation, electroporation of neuronal processes present on the surface of the stimulated microelectrodes was demonstrated. The localized electroporation of neuronal processes led to the entry and transport of the probe molecules (PI and GFP plasmids) to the cell bodies that were present well outside the edge of the stimulated microelectrodes. This is the first report of transfection of neurons with genetic constructs through localized electroporation of axons. However, in gene-silencing experiments, transfection of neurons away from the targeted site of electroporation can potentially lead to confounding results. The loss in site-specificity due to the transfection of neurons through the electroporation of its processes can potentially be minimized by reducing the size of the microelectrodes. Microelectrodes with diameters as small as 10 μm, comparable to the dimensions of neuronal cell bodies, can be fabricated using standard photolithography. It is likely that siRNA molecules can also be transfected through neuronal processes. The entry of siRNA through the neuronal processes was hard to detect due to low fluorescence intensity of siRNA molecules. This can partly be resolved in future experiments by using better imaging equipment such as confocal

microscopy. The prospect of siRNA delivery through processes offers a new way to silence genes locally in targeted neuronal processes which is highly desirable in studies investigating the role of genes that are locally translated in the axons and dendrites (Hengst, Cox, Macosko, & Jaffrey, 2006).

The data for neuronal recording pre- and post-electroporation indicated that neurons at different electrodes displayed a varying response to electroporation (Figure 21(a)). Neuronal cultures consist of different excitatory and inhibitory neuronal cell types that form complex networks. It is likely that differing response seen at different channels was dependent on the type and location of targeted neurons within the network. In the experiments, it was difficult to determine any immediate consistent effect of electroporation on the neural activity as the culture was maintained in electroporation buffer for 10 min after electroporation. However, the MEA based system is ideally suited for gene-silencing experiments where long term recordings are desired from neurons at different transfection sites. RNAi is one of the most powerful gene silencing techniques and is being rapidly adopted in genetic screens and as a potential therapeutic tool in neurological disorders (Boudreau & Davidson, 2010; Krichevsky & Kosik, 2002; Mohr, Bakal, & Perrimon, 2010). The ITO based MEA offers a novel approach for developing high-throughput and high-content neuronal studies. A key requirement of such a technology is its compatibility with phenotype detection assays. The neuro-chip described in this study, in

addition to the site-specific transfection of siRNA molecules, enables simultaneous assessment of a) neuronal morphology, b) specific proteins using fluorescent immunohistochemistry and c) electrical activity of single neurons and neuronal networks. The key challenges faced by the technology describe here towards realizing a high-throughput platform are the ability to deliver of multiple siRNA molecules and control over the dosage of delivery. Currently, the siRNA molecules are manually added to the wells prior to transfection. This will pose a major challenge in high-throughput studies where hundreds of different siRNAs are to be transfected at different sites in the culture. This can potentially be overcome by incorporating mircofluidics with the MEA that would allow either serial or localized delivery of siRNA molecules. In another approach, different siRNAs can be spotted on the predetermined microelectrodes prior to cell seeding and the siRNAs then can be transferred into the cells sitting on the microelectrodes by reverse electroporation (Jain, Papas, Jadhav, McBride, & Saez, 2012; Yamauchi, Kato, & Iwata, 2004). In siRNA studies, one of the key factors that determine the level of target gene silencing is the number of siRNA molecules delivered to cells. The different turnover rates of different proteins require varying amounts of siRNA to achieve the same level of silencing. Additionally, a precise control over the level of gene silencing is highly desirable in gene interaction studies. The dosage of siRNA delivered to cells can be controlled to a certain extent by controlling the

concentration of the siRNA molecules in the electroporation buffer. Further control over siRNA dosage can potentially be established by either applying multiple pulses or performing repeated transfections. In either scenario, the time duration between multiple pulses and repeated transfections will have to be optimized to minimize cell death.

CHAPTER 5

NANOCHANNELS TO ENHANCE CONSISTENCY OF TRANSFECTION EFFICIENCY

5.1 Introduction

Postmitotic cells, such as differentiated neurons, remain amongst the hardest cells to transfect. GFP transfection of neurons using microscale electroporation, as reported in chapter 4, displayed variable transfection efficiency. Transfection efficiencies per electrode in one MEA varied from 34% to 0%. Highly consistent and efficient transfection of genetic constructs is crucial in many neuronal cell biology experiments. Nanochannel based electroporation as demonstrated by Boukany et al. (2011) offers a promising approach for achieving highly efficient and consistent transfection (the work was demonstrated in chinese hamster ovary cells). In addition, the technique provides a precise control over the dosage of biomolecules delivered to cells, which is important in various genetic studies and therapeutic applications. In the above approach reported by Boukany et al. (2011), a setup comprising of two microchannels connected by a nanochannel (90 nm in diameter) (Figure 22) is used for nanoscale electroporation of cells.

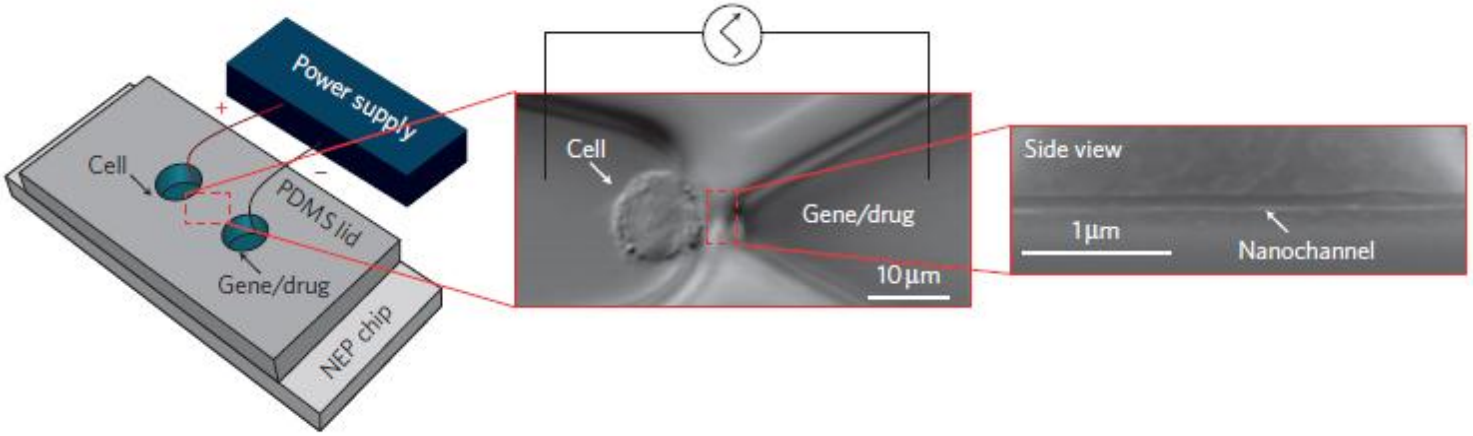

Figure 22. Schematic and image of the nanochannel electroporation. Image adapted by permission from : Nature Publishing group: Nature Nanotechnology (Boukany et al., 2011), copyright (2011)

A single cell is positioned at the opening of the nanochannel in one of the microchannels. The other microchannel is filled with electroporation buffer containing biomolecules for transfection. An electric pulse is then applied by two wires placed in the microchannels causing transfection. High-intensity electric field generated at the end of the nanochannel electroporate a localized area on the membrane and biomolecules in the nanochannel are directly injected into the cell under the influence of the electric field. Major advantages of nanochannel based technique include, a) high cell viability due to electroporation of small area of the membrane, b) direct entry of the plasmids and siRNA into the cytoplasm from the nanochannel that lead to gene expression within 4 hours of transfection, and c) control over dosage by manipulating the pulse width and number. However, a major area of improvement in the technique developed by Boukany et al. (2011) is the experimental throughput; currently, the technique only allows electroporation of one cell at a time and requires manual manipulation of the cell next to the channel. In another approach, Fei et al. (2007) demonstrated electroporation of cells trapped between two membranes (Fei et al., 2007). However, both of the above mentioned techniques are not compatible with situ experiments in adherent cell cultures.

This study investigated the use of nano-porous alumina membrane in tandem with MEA for achieving site-specific nanochannel based electroporation in adherent cells (Figure 23). It is hypothesized that the

integration of the MEA with nanochannels will provide a high-throughput method for transfecting cells with efficiency and consistency offered by nanochannel electroporation. The nano-sized pores (200 nm) in the alumina membrane act as nano-channels (Figure 23(a)) that can potentially electroporate small area of cell membrane. This study aims to demonstrate proof-of-concept of the integrated approach by electroporating HeLa cells cultured on alumina membrane with an MEA placed underneath the alumina membrane (Figure 23(a)).

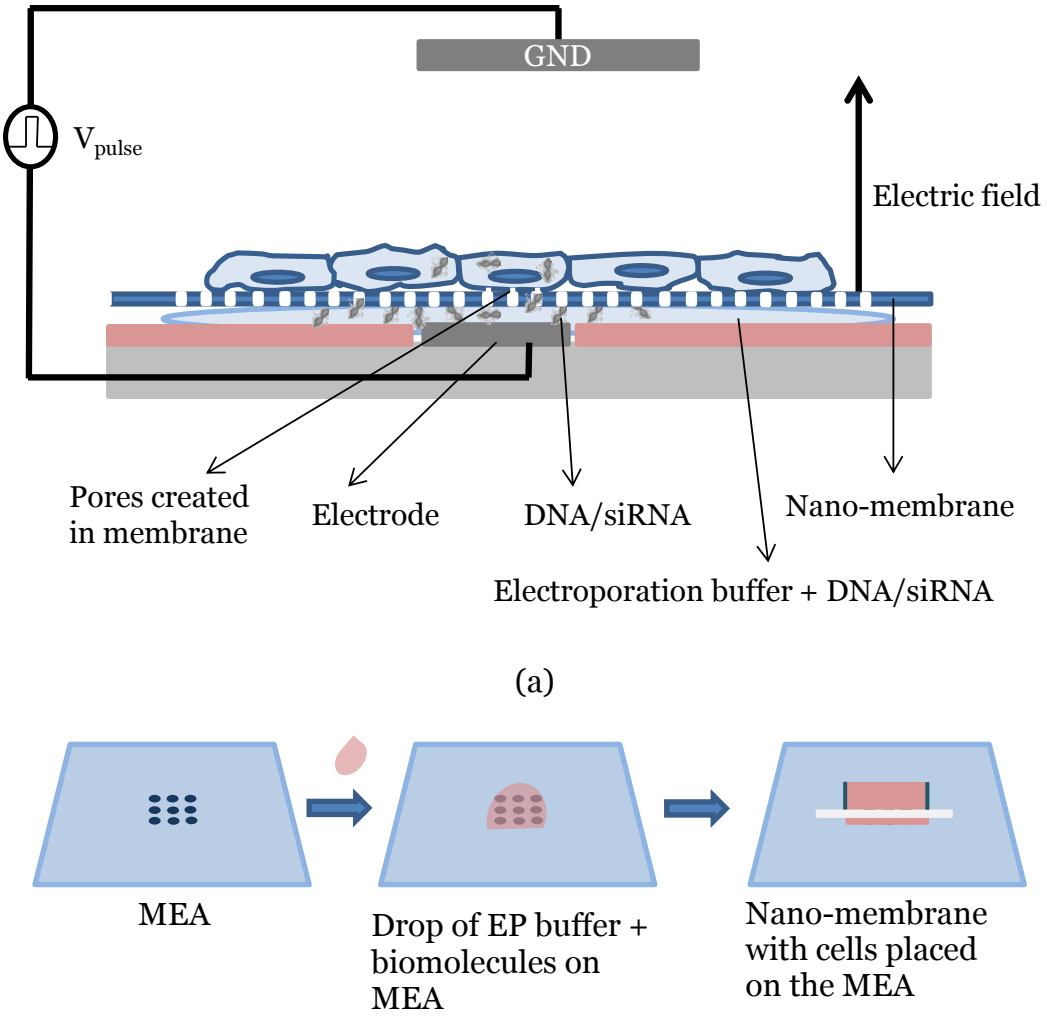

Figure 23. Schematic of electroporation scheme integrating the MEA with a nano-porous membrane. (a) A schematic of cell culture onalumina membrane with nanopores. The MEA placed under the nanoporous membrane generate the electric field for electroporation. (b) A schematic showing the steps for electroporation.

5.2 Materials and methods

5.2.1 Cell culture on nanoporous membranes

Alumina membranes used in this study were purchased from Whatman Ltd. (Anodisc 13). The membranes were 60 μm thick and the pores in the membrane were 200 nm in diameter. Small glass wells with 1 cm diameter were bonded on the alumina membranes to contain the cell media. 24-48 hours prior to electroporation experiments, HeLa cells were seeded on the alumina membranes in 200 μL of cell media. The cell cultures were stored in 37°C humidified incubator.

5.2.2 Electrical characterization

The electrical characterization of the microelectrodes was conducted using an electrochemical workstation (Model 660a, CH instruments, TX, USA). The electrical impedance spectroscopy (EIS) was carried out for a frequency sweep of 100 Hz -100,000 Hz. Cyclic voltammetry (CV) was conducted for -1.5 V to 1.5 V. For the EIS and CV experiments, a 30 μL drop of phosphate buffered solution was placed on the MEA. Following which, an alumina membrane with a glass well, containing PBS, was placed on the MEA, sandwiching the drop of PBS on MEA. A platinum wire was placed in the glass well with PBS acted as a reference and counter electrode.

5.2.3 Electric field simulations

FEM simulations of electric field were carried out in COMSOL v3.5. For the FEM simulations, a 2D model representing an electrode with nanomembrane on it was created. The pores in the membrane act as individual nano-channels with 200 nm diameter width and 60 μm length. The model was solved using finite element analysis, as described in chapter 3, to simulate the electric field intensity distribution at the end of the nanochannel.

5.2.4 Electroporation and imaging

Prior to electroporation experiment, 300 μL of 30 μg/ml PI solution in ice cold electroporation buffer and 300 μL of 4 μM calcien AM solution in PBS was prepared. Immediately before electroporation, a 30 μL drop of electroporation buffer with PI was placed on the MEA (Figure 23 (b)). Subsequently, the alumina membrane with HeLa cell culture was placed on top of the MEA; sandwiching the drop of electroporation buffer with PI between the MEA and the alumina membrane. The MEA and the alumina assembly was then placed in the incubator for five minutes to allow diffusion of PI into the nanochannels. Thereafter, the media in the well on the alumina membrane was replaced with electroporation buffer with PI. Single square anodic pulses with duration of 1 msec were applied to the microelectrodes for electroporation with a ground electrode placed in the well. After the pulse application, the MEA assembly was immediately

placed in the incubator. The cells were allowed to incubate for 10 mins before replacing the electroporation buffer in the well with media to provide time for the cell membrane resealing.

A live assay was performed 2 hours after the electroporation experiments to assess the viability of the cells. Images were captured and analyzed in image j.

5.3 Results

5.3.1 Electrical characterization

EIS and CV were performed to assess the changes in the electrode-electrolyte interface in the presence of the alumina membrane. Figure 24 shows the plot of EIS and CV results for the MEA with and without the alumina membrane. As seen in Figure 24, the shape of CV remained unaltered by the presence of the nanoporous membrane. In addition, the impedance measurements of the electrode-electrolyte interface also indicated no significant change.

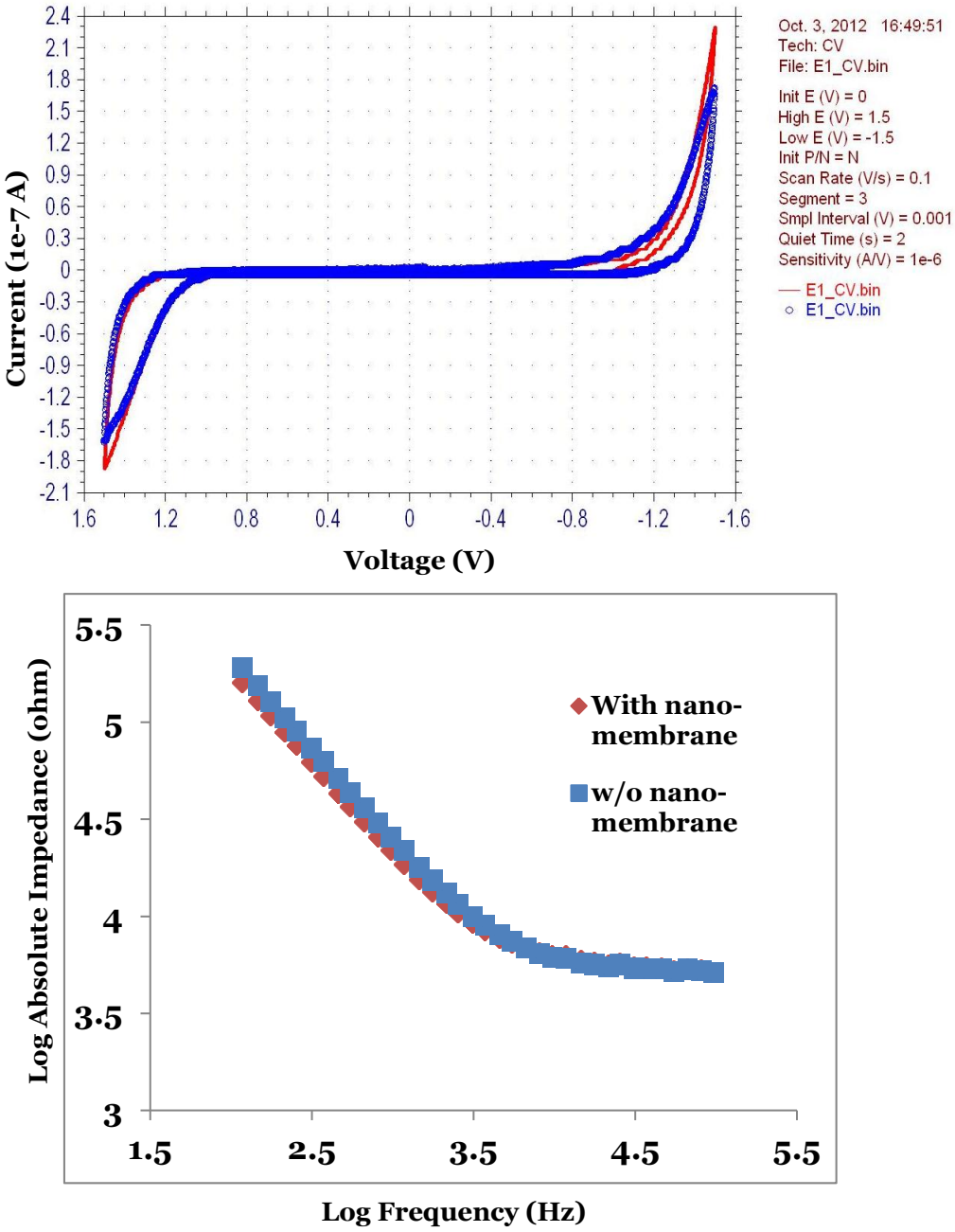

Figure24. CV (a) and EIS (b) with the nanoporous membrane on the MEA.

5.3.2 Electric field simulation

The simulation of the electric field intensity at the end of the nanochannel showed presence of very high fields at the corners of the nanochannels (Figure 25), similar to FE simulation of microelectrodes (chapter 3). At the center of the nanochannels the electric field intensities decreased by more than 2.5 times. Simulation of electric field intensity for four neighboring nanochannels showed electric field interactions between neighboring nanochannels. The electric field intensities at the surface of the nanoporous membrane remained similar to single channel simulation with high intensities at the corners of the nanochannels and low at the center at of nanochannels. However, at height of 500 nm above the surface of the nanochannels, the interaction of electric field between neighboring channels led to a more uniform distribution of the electric field. It is likely that cells experience electroporation on the membrane facing the nanochannels as well as on the side of the membrane facing the ground electrode.

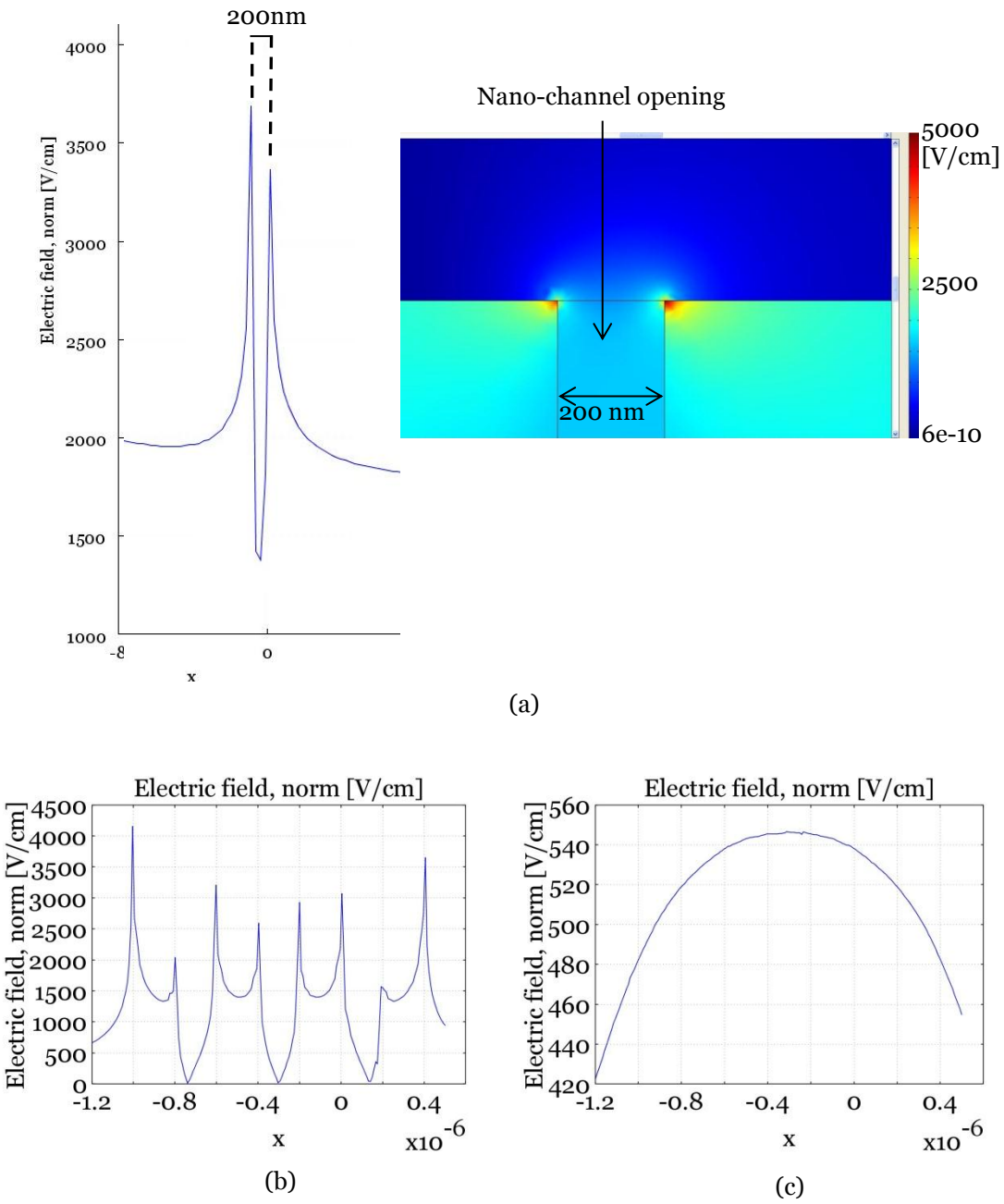

Figure 25. Simulation of electric field intensities for the nanochannels. (a) Electric field intensity at the opening of the 200 nm channel at 10 V. (b) Left is shown electric field simulation for four 200nm channels (spacing of 200nm) at the opening of the opening. Right shows the electric field simulation at a height of 500 nm above the channel opening.

5.3.3 Electroporation

HeLa cells cultured on the nanoporous membranes were electroporated in the presence of PI at different pulse amplitudes (15 V – 50 V) with fixed pulse duration of 10 msec to evaluate electroporation efficiency and viability. Figure 26 shows image of cells on nanoporous membranes after electroporation. Successfully electroporated cells stained red due to entry of PI and live assay stained cells green. At high voltage electroporation pulses (50 V) cell fusion was a common observation (Figure 26). Total percent of cells electroporated and cell viabilities at electroporation pulses of 15, 20 and 25 V is shown in Figure 27.

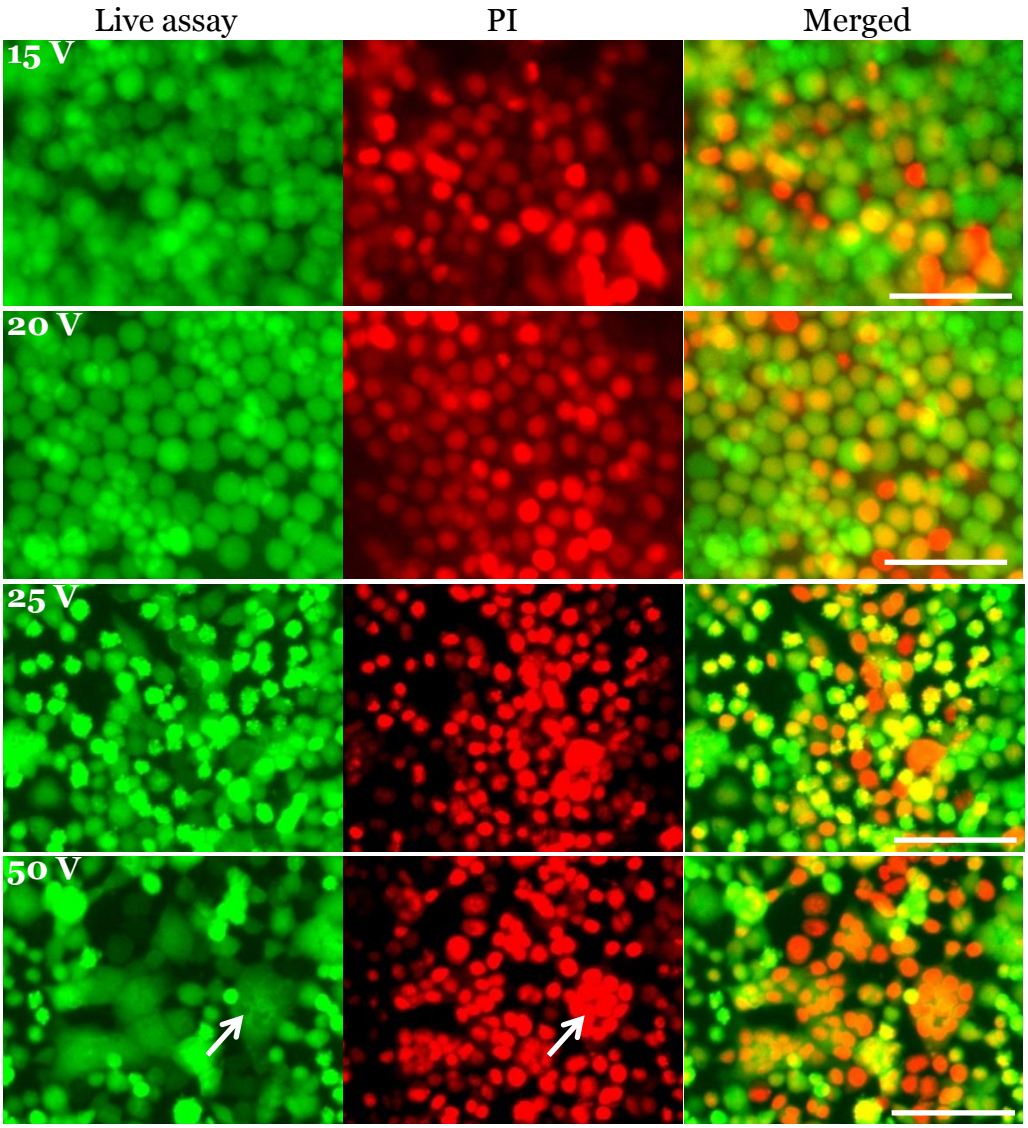

Figure 26. Electroporation and viability results for electroporation pulse of amplitudes 15, 20, 25 and 50 V (10 msec) on the nanoporous membrane. The white arrow points to cell fusion observed at the 50 V pulse. The scale bars are 100 μm.

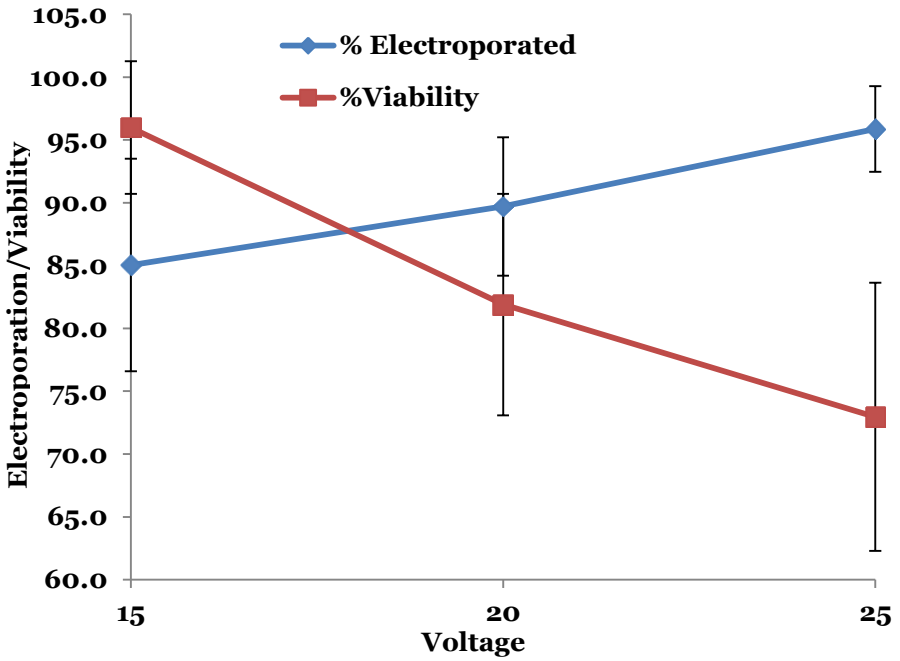

Figure 27. Percentage of cell Electroporated and viability plot for 15, 20 and 25 V electric pulses with a fixed width of 10 msec.

5.4 Discussion and conclusion

This study demonstrated successful targeted electroporation of cells cultured on a nanoporous membrane by manipulating electric field intensities associated with MEA placed under the membrane. The nano sized pores in the alumina membranes act as nanochannels and allowed electroporation of the cell adhered on the membrane. It is likely that the number of sites on cell membrane that get electroporated depends on the density of nanopores present in alumina membrane, which might influence cell viability; high density of nanopores might cause irreversible damage to the cell membrane upon electroporation. The electroporation parameters need to be further optimized for both electric pulse amplitude and duration to realize the highest transfection efficiency in neurons and to determine if alumina membrane based method offers significant enhancement in transfection efficiency in comparison to microscale electroporation. It also remains to be tested if the dosage of genetic constructs delivered to cells using the alumina membrane method can be controlled by pulse amplitude and duration, as demonstrated by Boukany et al. (2011) in nanochannel electroporation.

The EIS and CV measurements indicate that it is possible to record electrical activity of neurons cultured on the nanoporous membranes through an MEA placed under the membrane, however, this remains to be experimentally tested. Since the alumina membrane is likely to be separated from the ITO electrodes by at least few hundred microns (Figure

23(a)) cells might suffer less damage from electrolysis that takes place at the electrode-electrolyte interface for the duration of the electric pulse. Further development and validation of this technology may provide a novel approach for achieving highly efficient transfection with precise dosage control in primary neuronal cultures.

CHAPTER 6

CONCLUSION AND FUTURE WORK

6.1 Spatially and temporally controlled transfection in a secondary cell line

This work in this dissertation reports the fabrication of a fully transparent MEA for targeted transfection in adherent primary and secondary cell lines using microscale electroporation. The ITO based MEA with parylene insulation provided a transparent and biocompatible substrate for cell growth. A critical requirement of technologies that enable gene manipulation is to be able to assess the resulting phenotype. The compatibility of the ITO based MEA with standard imaging equipment was crucial in bio-imaging assays. In the current state, cells on the MEA can be imaged at a maximum magnification of 400X (40X objective). In applications that desire higher magnification, for detailed analysis of sub-cellular phenotypes, the thickness of the glass substrate can be further reduced to less than 200 μm using microfabrication techniques.

The technology developed here allowed rapid optimization of electroporation parameters which were used for delivery of siRNA and GFP. The optimization of electroporation parameters is often a time-consuming and tedious process and the parameters need to be separately optimized for each cell type. The protocol developed in this work provides detailed steps for using any custom-made or commercially available MEA for site-specific transfection in cells and is independent of the cell type.

The protocol was described for use in a typical lab, equipped for cell culture, without the need of any specialized equipment. The strength of the microarray based approach lies in the ability to perform multiple experiments on the same culture, as demonstrated in this work, thereby increasing the experimental throughput and decreasing culture-to-culture variability. Another advantage of using MEA for microscale electroporation is the ability to create different patterns and sizes of electrodes which directly control the target area and target locations in the culture. However, the electroporation experiments with electrodes of three different sizes and finite element simulation of the associated electric field showed that the electroporation efficiency decreases with increase in electrode size (>100 μm in diameter) due to the non-uniform electric field distribution on large diameter electrodes. This knowledge is extremely useful in developing future platforms for applications that may require large populations of cells to be transfected per site. In such a scenario, multiple small electrodes could be patterned close to each other allowing transfection of larger population of cells within a culture.

In this work, successful delivery payloads of different sizes (PI, siRNA and plasmid vector) to precisely targeted locations in a HeLa cell culture using microscale electroporation was demonstrated. The use of microscale electroporation resulted in efficient and consistent gene silencing and gene expression in targeted cells. In addition, the platform developed in this study also allowed for in-situ assessment of the response

of cells to microscale electroporation. The temporal analysis of actin disruption and reorganization in response to electroporation demonstrate the applicability of this technology in assessment of sub-cellular phenotypes. The ITO based MEA described in this study is a readily scalable platform and further development of this technology will provide a cost-effective high-throughput approach for genetic screens.

6.2 Targeted transfection and simultaneous electrophysiological assessment in primary neurons

A major obstacle in genetic studies involving primary neurons has been the difficulty to efficiently transfect them. In this study, the use of MEA for targeted delivery of genetic payloads of different sizes and characteristics (PI, siRNA and GFP) to hippocampal neurons in culture has been demonstrated for the first time. In addition, the patterned microelectrodes were used to measure spontaneous electrical activity of neurons in response to electroporation. The technology described in this study offers a powerful tool for investigating cell-cell interactions. Delivery of genetic constructs to targeted neurons in a network would allow functional electrophysiological assessment of the impact of gene manipulation on targeted neurons and the entire network behavior in real time. In addition, this study demonstrated successful delivery of GFP plasmid vectors through microscale electroporation of neuronal processes. This opens the possibility of delivering genetic construct to neurons with

remotely located cell bodies by localized electroporation of axons (currently done by viral vectors). In addition, delivery of siRNA directly to axons would enable localized inhibition of genes involved in synapse formation, axonal growth and transport.

6.3 Nanochannels based high-throughput transfection

A major limitation with neuronal studies in low and inconsistent transfection efficiencies associated with majority of the current transfection methods. In this study, the use of nanoporous membrane in tandem with MEA to achieve nanochannel electroporation in adherent cells was evaluated. Nanochannel electroporation has been demonstrated to offer highly consistent and efficient transfection with precise dosage control (Boukany et al., 2011). In this study, HeLa cells cultured on a nanomembrane were electroporated to demonstrate the proof-of-concept. In addition, the electrical characterization of the results of the nano-membrane and MEA assembly suggest the possibility of measuring the electrical activity of neurons. Further development and validation of this technology may provide a novel approach for achieving highly efficient transfection with precise dosage control in primary neuronal cultures.

6.4 Limitations

An extremely important element of the genetic screens is the development of appropriate phenotypical assays. The technology

described in this work allows electrophysiological assessment of neurons in real time along with the assessment of neuronal morphology and protein levels using fluorescent immunohistochemistry. However, it presents a major challenge in the extraction of modified cells for further extensive analysis of gene expression levels with techniques such as PCR, DNA microarrays and western blotting. One of the approaches to overcome this limitation is to fabricate customized stencils that would allow selective trypsinization and extraction of cells only from the electrodes. Another approach would be to implement in situ PCR for detection of specific RNA transcript levels (Bagasra, 2007).

In this work, successful delivery of functional siRNA to targeted HeLa cells has been demonstrated. However, a variable with very limited control was the dosage of the siRNA delivered to cells. siRNAs achieve only a partial knock down of the target gene and the level of knock down is a function of the concentration of the siRNA in the cells (D. H. Kim & Rossi, 2008) . Thus, in siRNA based studies, it is extremely desirable to maintain a precise control over the dosage of siRNA delivered to cells. There are several strategies that could be employed to overcome this limitation. For instance, the use of nanochannel for electroporation has previously demonstrated precise control over dosage of siRNA delivered to cells (Boukany et al., 2011), which has been one of the motivations behind us investigating the use of nanochannel template in site-specific transfection. Another approach includes repeated electroporation of cells at different

time points to increase the siRNA concentration levels in the cells, which would also enable subsequent delivery of different siRNAs. A key variable here that would need optimization is the time between subsequent electroporations for maximizing viability.

Another limitation with the current MEA based system is the large amount of siRNA needed for transfection (400 µl of 1µM siRNA), which is very high compared to conventional chemical transfection based approaches and thus limits the cost effectiveness of the system (Patel & Muthuswamy, 2012). This can partly be overcome by incorporating mircofluidics with the MEA based system to decrease the total volume of siRNA electroporation solution to less than a few microliters, as described in the following sections. Additionally, the microfluidics can enable serial delivery of different siRNA molecules; thereby greatly enhancing the throughput of the MEA based technology. Alternatively, siRNA molecules can be spotted on the microelectrodes prior to cell seeding, after which the siRNA molecules can be transfected into cells by reverse electroporation (Jain, Papas, Jadhav, McBride, & Saez, 2012; Yamauchi, Kato, & Iwata, 2004).

6.5 Future directions

RNAi offers a powerful method for elucidating gene function in a high-throughput fashion; especially in a post genome sequencing era that has led to the discovery of hundreds of thousands of genes with unknown function. The technique of RNAi offers a unified approach for both

discovering therapeutic genetic targets and as a therapeutic agent. In the recent years, siRNA have been the focus of many clinical studies (Burnett, Rossi, & Tiemann, 2011). In this study, a scalable technology for localized transfection in primary neurons is presented. The technology developed in this work can be extended in two parallel directions with the ultimate motivation of providing a therapeutic strategy for CNS disorders. These two directions are discussed in the following sub-sections.

6.5.1 High-throughput and high content screening in vitro

An example of the design of a scaled-up version of the nanochannel based MEA system for high-throughput screening (HTS) is shown in Figure 28. In this approach, microwells can be patterned on the nanochannel template to restrict neuronal populations in microwells. MEAs patterned beneath each well would allow independent transfection of neurons within each well. Microfluidic channels can be patterned in between the nanochannel template and MEAs for individual delivery of genetic reagents to each well in nanoliter volumes. The advantages of such a system would be the cost-effectiveness and the consistent delivery of genetic constructs to neurons. In addition, the MEA present in each well can be used for measuring the electrical activity of neurons.

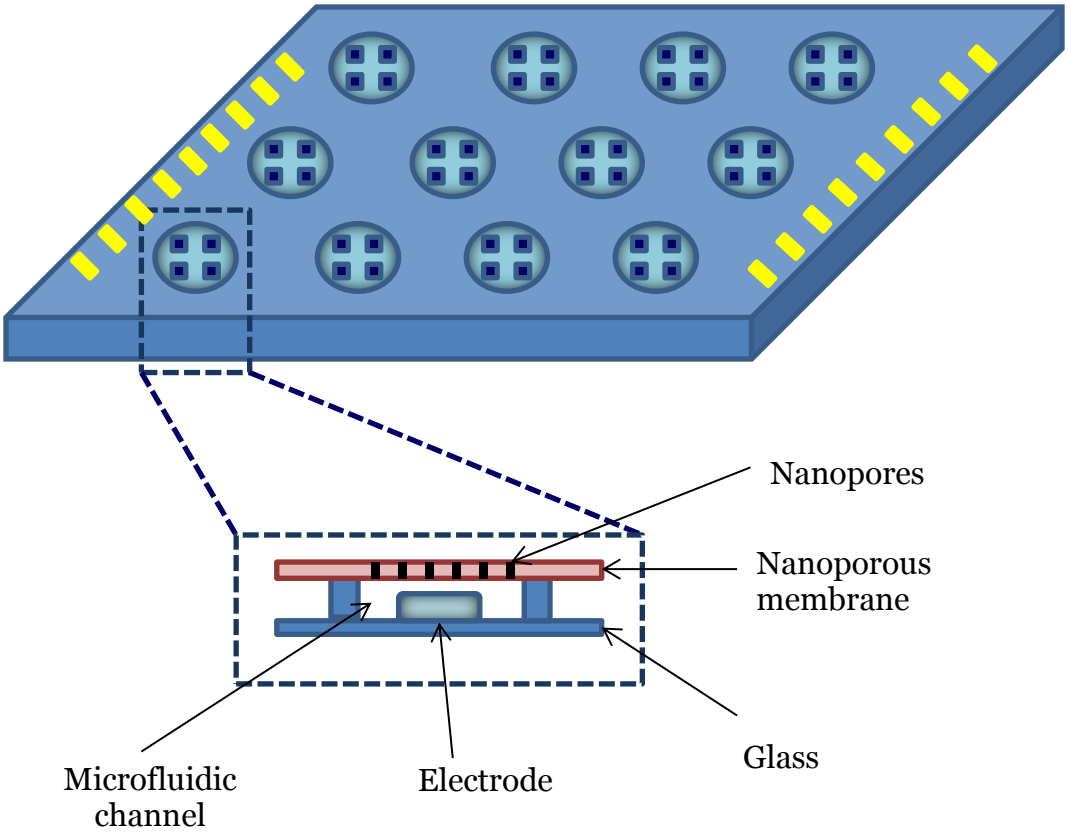

Figure 28. The above schematic describes a hypothesized nanochannel electroporation based biochip for HTS.

The key steps for the design of high-throughput screens (HTS) include a) clear definition of the goal of the screen, b) selection of appropriate phenotypical assays, c) a clearly defined metric for assessment and scoring of phenotypes, d) a well-defined criteria for selection of hits and e) secondary validation screens to identify the biologically significant hits (Boutros & Ahringer, 2008). A major limitation with the current HTS for neuronal studies has been the lack of ability to measure the electrical activity of neurons in a high-throughput fashion in real time, which is an important phenotypical assay in neuronal studies. MEA based systems offer unique advantage of simultaneous multiple phenotype assessment in neurons including electrophysiological assessment, thereby greatly enhancing identification of key players and relationships in signaling pathways in neurons. Another significant area for advancement in HTS is high content screening, as it generates data rich in information. For example, in axonal outgrowth studies, GFP expressing primary neurons can be screened against a library of siRNA molecules to identify genes involved in axonal outgrowth (Sepp et al., 2008). In such a study, GFP expressing primary neurons harvested from embryonic Day 18 rat could be grown in microwells of a high-throughput MEA based system (Figure 28). Subsequently, the MEA present within each well could be used for electroporating neurons in different wells with different siRNA, followed by monitoring of the electrical activity of neurons. The process of the axonal growth of neurons in different microwells can then be captured in

real time by fluorescent imaging as the neurons mature, fully differentiate and become electrically active. The obtained images and electrical activity data can then be analyzed and quantified with automated scripts to identify genes involved in axonal outgrowth. A major advantage of MEA based systems here would be the ability to draw connections between the genes involved in axonal growth and the molecular pathways underlying the onset of electrical activity in maturing neurons and synapse formation in a high-throughput and cost-effective manner.

6.5.2 Localized transfection in the brain

Neural circuitry in the brain is very complex in nature with each neuron making approximately 5,000 to 200,000 connections with other neurons. There are more than 10,000 types of neurons, which are spaced very close to each other. Neurons that are near each other may be involved in completely different circuits and have completely different functions. Any technique that aims to intervene at the neural circuit or individual neuron level needs to have precise spatial control over delivery(L. Luo, Callaway, & Svoboda, 2008) . The target area generally may be in micrometers; hence an accurate system with a precise delivery mechanism is absolutely essential. A potential direction of future work would involve translation of the work described herein to in vivo. Such a technique would allow precise localized silencing and expression in the brain; thereby enabling

investigation of neural circuit function and evaluation of therapeutic strategies.

A neural probe can be fabricated using a standard MEMS process. Figure 29 shows the example of a hypothetical neural probe for targeted transfection in CNS. A microfluidic channel fabricated in the probe would allow delivery of genetic reagents in the targeted area. Subsequently, electric fields associated with the microelectrodes, which are patterned on the neural probe, can be manipulated to electroporate desired regions in the brain.

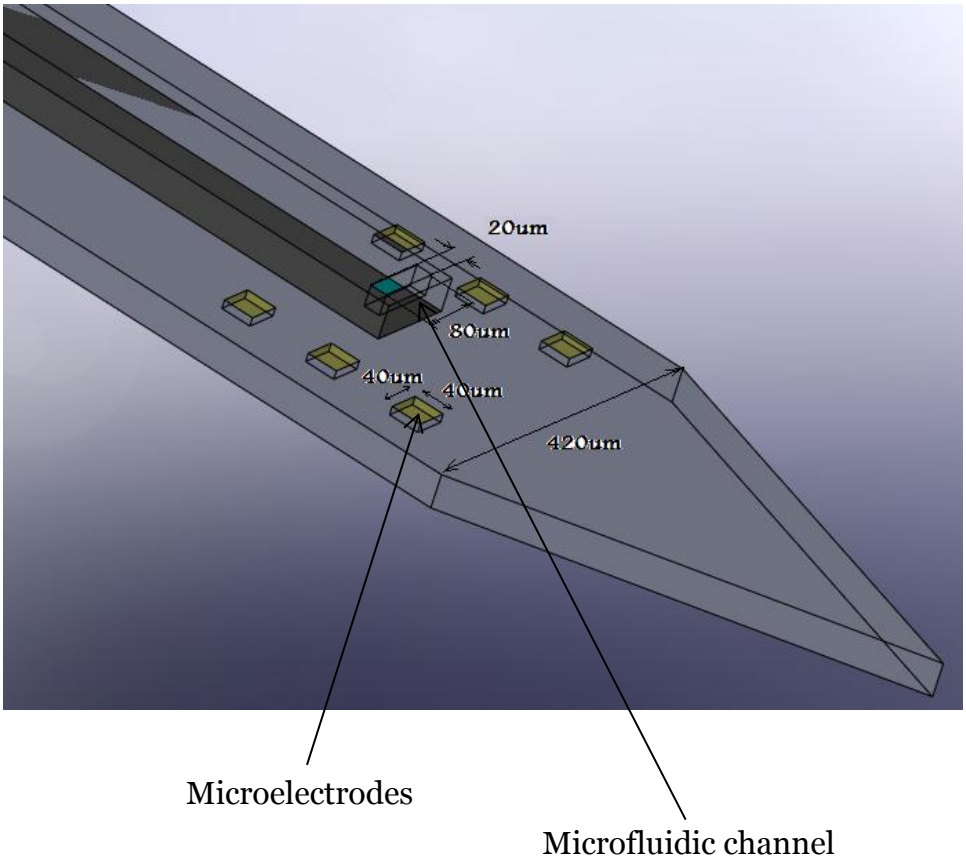

Figure 29. The above figure shows a hypothesized neural probe for targeted electroporation in the brain. The microelectrodes would generate the electric field necessary for electroporation and the microfluidic channel would deliver the biomolecules for transfection.

REFERENCES

Åberg, M. A. I., Ryttsén, F., Hellgren, G., Lindell, K., Rosengren, L. E., MacLennan, A. J., . . . Eriksson, P. S. (2001). Selective introduction of antisense oligonucleotides into single adult CNS progenitor cells using electroporation demonstrates the requirement of STAT3 activation for CNTF-induced gliogenesis. *Molecular and Cellular Neuroscience, 17*(3), 426-443.

Abidor, I., Arakelyan, V., Chernomordik, L., Chizmadzhev, Y. A., Pastushenko, V., & Tarasevich, M. (1979). Electric breakdown of bilayer lipid membranes: I. the main experimental facts and their qualitative discussion. *Journal of Electroanalytical Chemistry and Interfacial Electrochemistry, 104*, 37-52.

Agarwal, A., Zudans, I., Weber, E. A., Olofsson, J., Orwar, O., & Weber, S. G. (2007). Effect of cell size and shape on single-cell electroporation. *Analytical Chemistry, 79*(10), 3589-3596.

Akaneya, Y., Jiang, B., & Tsumoto, T. (2005). RNAi-induced gene silencing by local electroporation in targeting brain region. *Journal of Neurophysiology, 93*(1), 594.

Al-Dosari, M. S., & Gao, X. (2009). Nonviral gene delivery: Principle, limitations, and recent progress. *The AAPS Journal, 11*(4), 671-681.

Bagasra, O. (2007). Protocols for the in situ PCR-amplification and detection of mRNA and DNA sequences. *Nature Protocols, 2*(11), 2782-2795.

Bernhardt, J., & Pauly, H. (1973). On the generation of potential differences across the membranes of ellipsoidal cells in an alternating electrical field. *Radiation and Environmental Biophysics, 10*(1), 89-98.

Bonoiu, A. C., Bergey, E. J., Ding, H., Hu, R., Kumar, R., Yong, K. T., . . . Bhattacharjee, A. (2011). Gold nanorod–siRNA induces efficient in vivo gene silencing in the rat hippocampus. *Nanomedicine, 6*(4), 617-630.

Boudreau, R. L., & Davidson, B. L. (2010). RNAi therapeutics for CNS disorders. *Brain Research,*

Boudreau, R. L., McBride, J. L., Martins, I., Shen, S., Xing, Y., Carter, B. J., & Davidson, B. L. (2009). Nonallele-specific silencing of mutant and wild-type huntingtin demonstrates therapeutic efficacy in huntington's disease mice. *Molecular Therapy, 17*(6), 1053-1063.

Boukany, P. E., Morss, A., Liao, W., Henslee, B., Jung, H. C., Zhang, X., . . . Li, L. (2011). Nanochannel electroporation delivers precise amounts of biomolecules into living cells. *Nature Nanotechnology, 6*(11), 747-754.

Boutros, M., & Ahringer, J. (2008). The art and design of genetic screens: RNA interference. *Nature Reviews Genetics, 9*(7), 554-566.

Brummelkamp, T. R., Bernards, R., & Agami, R. (2002). A system for stable expression of short interfering RNAs in mammalian cells. *Science, 296*(5567), 550.

Buerli, T., Pellegrino, C., Baer, K., Lardi-Studler, B., Chudotvorova, I., Fritschy, J. M., . . . Fuhrer, C. (2007). Efficient transfection of DNA or shRNA vectors into neurons using magnetofection. *Nature Protocols, 2*(12), 3090-3101.

Bumcrot, D., Manoharan, M., Koteliansky, V., & Sah, D. W. Y. (2006). RNAi therapeutics: A potential new class of pharmaceutical drugs. *Nature Chemical Biology, 2*(12), 711-719.

Burnett, J. C., Rossi, J. J., & Tiemann, K. (2011). Current progress of siRNA/shRNA therapeutics in clinical trials. *Biotechnology Journal, 6*(9), 1130-1146.

Caplen, N. J., Parrish, S., Imani, F., Fire, A., & Morgan, R. A. (2001). Specific inhibition of gene expression by small double-stranded RNAs in invertebrate and vertebrate systems. *Proceedings of the National Academy of Sciences, 98*(17), 9742.

Chang, W. C., & Sretavan, D. W. (2009). Single cell and neural process experimentation using laterally applied electrical fields between pairs

of closely apposed microelectrodes with vertical sidewalls. *Biosensors and Bioelectronics, 24*(12), 3600-3607.

Chu, G., Hayakawa, H., & Berg, P. (1987). Electroporation for the efficient transfection of mammalian cells with DNA. *Nucleic Acids Research, 15*(3), 1311.

Citron, M., Westaway, D., Xia, W., Carlson, G., Diehl, T., Levesque, G., . . . Davis, A. (1997). Mutant presenilins of alzheimer's disease increase production of 42-residue amyloid β-protein in both transfected cells and transgenic mice. *Nature Medicine, 3*(1), 67-72.

Dauer, W., & Przedborski, S. (2003). Parkinson's disease: Mechanisms and models. *Neuron, 39*(6), 889-909.

Davidson, B. L., & Breakefield, X. O. (2003). Viral vectors for gene delivery to the nervous system. *Nature Reviews Neuroscience, 4*(5), 353-364.

Dityateva, G., Hammond, M., Thiel, C., Ruonala, M. O., Delling, M., Siebenkotten, G., . . . Dityatev, A. (2003). Rapid and efficient electroporation-based gene transfer into primary dissociated neurons. *Journal of Neuroscience Methods, 130*(1), 65-73.

Dong-yang, Z., Cheng-xiang, L., Yan, M., & Chen-guo, Y. (2008). The optimal design of electrod array using electroporation based on the finite element. *High Voltage Engineering and Application, 2008. ICHVE 2008. International Conference On,* 773-776.

During, M. J., & Ashenden, L. M. A. (1998). Towards gene therapy for the central nervous system. *Molecular Medicine Today, 4*(11), 485-493.

During, M. J., & Leone, P. (1997). Targets for gene therapy of parkinson's disease: Growth factors, signal transduction, and promoters. *Experimental Neurology, 144*(1), 74-81.

Elbashir, S. M., Harborth, J., Lendeckel, W., Yalcin, A., Weber, K., & Tuschl, T. (2001). Duplexes of 21-nucleotide RNAs mediate RNA interference in cultured mammalian cells. *Nature, 411*(6836), 494-498.

Endoh, M., Koibuchi, N., Sato, M., Morishita, R., Kanzaki, T., Murata, Y., & Kaneda, Y. (2002). Fetal gene transfer by intrauterine injection with microbubble-enhanced ultrasound. *Molecular Therapy, 5*(5), 501-508.

Escoffre, J. M., Portet, T., Wasungu, L., Teissié, J., Dean, D., & Rols, M. P. (2009). What is (still not) known of the mechanism by which electroporation mediates gene transfer and expression in cells and tissues. *Molecular Biotechnology, 41*(3), 286-295.

Fei, Z., Wang, S., Xie, Y., Henslee, B. E., Koh, C. G., & Lee, L. J. (2007). Gene transfection of mammalian cells using membrane sandwich electroporation. *Analytical Chemistry, 79*(15), 5719-5722.

Felgner, P. L., Gadek, T. R., Holm, M., Roman, R., Chan, H. W., Wenz, M., . . . Danielsen, M. (1987). Lipofection: A highly efficient, lipid-mediated DNA-transfection procedure. *Proceedings of the National Academy of Sciences, 84*(21), 7413.

Fire, A., Xu, S. Q., Montgomery, M. K., Kostas, S. A., Driver, S. E., & Mello, C. C. (1998). Potent and specific genetic interference by double-stranded RNA in caenorhabditis elegans. *Nature, 391*(6669), 806-811.

Friedmann, T. (1994). Gene therapy for neurological disorders. *Trends in Genetics, 10*(6), 210-214.

Gabriel, B., & Teissie, J. (1997). Direct observation in the millisecond time range of fluorescent molecule asymmetrical interaction with the electropermeabilized cell membrane. *Biophysical Journal, 73*(5), 2630-2637.

Gao, Y., Liu, X. L., & Li, X. R. (2011). Research progress on siRNA delivery with nonviral carriers. *International Journal of Nanomedicine, 6*, 1017.

Gehl, J. (2003). Electroporation: Theory and methods, perspectives for drug delivery, gene therapy and research. *Acta Physiologica Scandinavica, 177*(4), 437-447.

Ghosh, P., Han, G., De, M., Kim, C. K., & Rotello, V. M. (2008). Gold nanoparticles in delivery applications. *Advanced Drug Delivery Reviews, 60*(11), 1307-1315.

Golzio, M., Teissié, J., & Rols, M. P. (2002). Direct visualization at the single-cell level of electrically mediated gene delivery. *Proceedings of the National Academy of Sciences, 99*(3), 1292-1297.

Gupta, A. K., & Curtis, A. S. G. (2004). Lactoferrin and ceruloplasmin derivatized superparamagnetic iron oxide nanoparticles for targeting cell surface receptors. *Biomaterials, 25*(15), 3029-3040.

Haas, K., Sin, W. C., Javaherian, A., Li, Z., & Cline, H. T. (2001). Single-cell electroporationfor gene transfer in vivo. *Neuron, 29*(3), 583-591.

Hai, A., & Spira, M. E. (2012). On-chip electroporation, membrane repair dynamics and transient in-cell recordings by arrays of gold mushroom-shaped microelectrodes. *Lab Chip,*

He, H., Chang, D. C., & Lee, Y. K. (2007). Using a micro electroporation chip to determine the optimal physical parameters in the uptake of biomolecules in HeLa cells. *Bioelectrochemistry, 70*(2), 363-368.

Hengst, U., Cox, L. J., Macosko, E. Z., & Jaffrey, S. R. (2006). Functional and selective RNA interference in developing axons and growth cones. *The Journal of Neuroscience, 26*(21), 5727-5732.

Hibino, M., Shigemori, M., Itoh, H., Nagayama, K., & Kinosita, K. (1991). Membrane conductance of an electroporated cell analyzed by submicrosecond imaging of transmembrane potential. *Biophysical Journal, 59*(1), 209-220.

Huang, H., Wei, Z., Huang, Y., Zhao, D., Zheng, L., Cai, T., . . . Zhou, Z. (2010). An efficient and high-throughput electroporation microchip applicable for siRNA delivery. *Lab Chip, 11*(1), 163-172.

Huang, K. S., Lin, Y. C., Su, C. C., & Fang, C. S. (2006). Enhancement of an electroporation system for gene delivery using electrophoresis with a planar electrode. *Lab Chip, 7*(1), 86-92.

Huang, Y., & Rubinsky, B. (2001). Microfabricated electroporation chip for single cell membrane permeabilization. *Sensors & Actuators: A.Physical, 89*(3), 242-249.

Hui, S. W. (1995). Effects of pulse length and strength on electroporation efficiency. *Methods Mol.Biol, 48*, 29-40.

Inoue, Y., Fujimoto, H., Ogino, T., & Iwata, H. (2008). Site-specific gene transfer with high efficiency onto a carbon nanotube-loaded electrode. *Journal of the Royal Society Interface, 5*(25), 909-918.

Ishibashi, T., Takoh, K., Kaji, H., Abe, T., & Nishizawa, M. (2007). A porous membrane-based culture substrate for localized in situ electroporation of adherent mammalian cells. *Sensors and Actuators B: Chemical, 128*(1), 5-11.

Jackson, A. L., & Linsley, P. S. (2010). Recognizing and avoiding siRNA off-target effects for target identification and therapeutic application. *Nature Reviews Drug Discovery, 9*(1), 57-67.

Jain, T. (2007). *Biochip for Spatial-Temporal Electroporation of Exogenous Molecules into Secondary Cell Lines and Primary Neurons,*

Jain, T., McBride, R., Head, S., & Saez, E. (2009). Highly parallel introduction of nucleic acids into mammalian cells grown in microwell arrays. *Lab on a Chip, 9*(24), 3557-3566.

Jain, T., & Muthuswamy, J. (2007a). Bio-chip for spatially controlled transfection of nucleic acid payloads into cells in a culture. *Lab on a Chip, 7*(8), 1004-1011.

Jain, T., & Muthuswamy, J. (2007b). Microsystem for transfection of exogenous molecules with spatio-temporal control into adherent cells. *Biosensors and Bioelectronics, 22*(6), 863-870.

Jain, T., & Muthuswamy, J. (2008). Microelectrode array (MEA) platform for targeted neuronal transfection and recording. *Biomedical Engineering, IEEE Transactions On, 55*(2), 827-832.

Jain, T., Papas, A., Jadhav, A., McBride, R., & Saez, E. (2012). In situ electroporation of surface-bound siRNAs in microwell arrays. *Lab Chip, 12*(5), 939-947.

Jiang, M., Instrell, R., Saunders, B., Berven, H., & Howell, M. (2011). Tales from an academic RNAi screening facility; FAQs. *Briefings in Functional Genomics, 10*(4), 227-237.

Jordan, M., Schallhorn, A., & Wurm, F. M. (1996). Transfecting mammalian cells: Optimization of critical parameters affecting calcium-phosphate precipitate formation. *Nucleic Acids Research, 24*(4), 596-601.

Kanthou, C., Kranjc, S., Sersa, G., Tozer, G., Zupanic, A., & Cemazar, M. (2006). The endothelial cytoskeleton as a target of electroporation-based therapies. *Molecular Cancer Therapeutics, 5*(12), 3145-3152.

Kim, D. H., & Rossi, J. J. (2008). RNAi mechanisms and applications. *BioTechniques, 44*(5), 613.

Kitamura, K., Judkewitz, B., Kano, M., Denk, W., & Häusser, M. (2007). Targeted patch-clamp recordings and single-cell electroporation of unlabeled neurons in vivo. *Nature Methods, 5*(1), 61-67.

Krassen, H., Pliquett, U., & Neumann, E. (2007). Nonlinear current-voltage relationship of the plasma membrane of single CHO cells. *Bioelectrochemistry, 70*(1), 71-77.

Krichevsky, A. M., & Kosik, K. S. (2002). RNAi functions in cultured mammalian neurons. *Proceedings of the National Academy of Sciences, 99*(18), 11926.

Lee, N. S., Dohjima, T., Bauer, G., Li, H., Li, M. J., Ehsani, A., . . . Rossi, J. (2002). Expression of small interfering RNAs targeted against HIV-1 rev transcripts in human cells. *Nature Biotechnology, 20*(5), 500-505.

Lee, W. G., Demirci, U., & Khademhosseini, A. (2009). Microscale electroporation: Challenges and perspectives for clinical applications. *Integr.Biol., 1*(3), 242-251.

Li, S. (2004). Electroporation gene therapy: New developments in vivo and in vitro. *Current Gene Therapy, 4*(3), 309-316.

Li, S. D., & Huang, L. (2006). Targeted delivery of antisense oligodeoxynucleotide and small interference RNA into lung cancer cells. *Molecular Pharmaceutics, 3*(5), 579-588.

Li, Z., Wei, Z., Li, X., Du, Q., & Liang, Z. (2011). Efficient and high-throughput electroporation chips. *Solid-State Sensors, Actuators and Microsystems Conference (TRANSDUCERS), 2011 16th International,* 1825-1828.

Lin, Y. C., Jen, C. M., Huang, M. Y., Wu, C. Y., & Lin, X. Z. (2001). Electroporation microchips for continuous gene transfection. *Sensors and Actuators B: Chemical, 79*(2-3), 137-143.

Lin, Y. C., Li, M., Fan, C. S., & Wu, L. W. (2003). A microchip for electroporation of primary endothelial cells. *Sensors and Actuators A: Physical, 108*(1-3), 12-19.

Lonez, C., Vandenbranden, M., & Ruysschaert, J. M. (2008). Cationic liposomal lipids: From gene carriers to cell signaling. *Progress in Lipid Research, 47*(5), 340-347.

Luo, L., Callaway, E. M., & Svoboda, K. (2008). Genetic dissection of neural circuits. *Neuron, 57*(5), 634-660.

Luo, Y., Bolon, B., Kahn, S., Bennett, B. D., Babu-Khan, S., Denis, P., . . . Gong, Y. (2001). Mice deficient in BACE1, the alzheimer's β-secretase, have normal phenotype and abolished β-amyloid generation. *Nature Neuroscience, 4*(3), 231-232.

Mahato, R. I., Cheng, K., & Guntaka, R. V. (2005). Modulation of gene expression by antisense and antigene oligodeoxynucleotides and small interfering RNA. *Expert Opinion on Drug Delivery, 2*(1), 3-28.

Manto, M. U. (2005). The wide spectrum of spinocerebellar ataxias (SCAs). *The Cerebellum, 4*(1), 2-6.

Matsuda, T., & Cepko, C. L. (2004). Electroporation and RNA interference in the rodent retina in vivo and in vitro. *Proceedings of the National Academy of Sciences, 101*(1), 16-22.

Matsumoto, Y., Itaka, K., Yamasoba, T., & Kataoka, K. (2009). Intranuclear fluorescence resonance energy transfer analysis of plasmid DNA decondensation from nonviral gene carriers. *The Journal of Gene Medicine, 11*(7), 615-623.

Matthaei, K. I. (2007). Genetically manipulated mice: A powerful tool with unsuspected caveats. *The Journal of Physiology, 582*(2), 481-488.

McCall, J., Nicholson, L. S., Weidner, N., & Blesch, A. (2012). Optimization of adult sensory neuron electroporation to study mechanisms of neurite growth. *Frontiers in Molecular Neuroscience, 5*

Mehrle, W., Hampp, R., & Zimmermann, U. (1989). Electric pulse induced membrane permeabilisation. spatial orientation and kinetics of solute efflux in freely suspended and dielectrophoretically aligned plant mesophyll protoplasts. *Biochimica Et Biophysica Acta (BBA)-Biomembranes, 978*(2), 267-275.

Miller, D. L., Pislaru, S. V., & Greenleaf, J. F. (2002). Sonoporation: Mechanical DNA delivery by ultrasonic cavitation. *Somatic Cell and Molecular Genetics, 27*(1), 115-134.

Miyagishi, M., & Taira, K. (2002). U6 promoter–driven siRNAs with four uridine 3′ overhangs efficiently suppress targeted gene expression in mammalian cells. *Nature Biotechnology, 20*(5), 497-500.

Mohr, S., Bakal, C., & Perrimon, N. (2010). Genomic screening with RNAi: Results and challenges. *Annual Review of Biochemistry, 79*, 37-64.

Movahed, S., & Li, D. (2011). Microfluidics cell electroporation. *Microfluidics and Nanofluidics, 10*(4), 703-734.

Naldini, L. (2001). Viral vectors for gene therapy: The art of turning infectious agents into vehicles of therapeutics. *Nature Medicine, 7*(1), 33.

Nawarathna, D., Unal, K., & Wickramasinghe, H. K. (2008). Localized electroporation and molecular delivery into single living cells by atomic force microscopy. *Applied Physics Letters, 93*, 153111.

Neumann, E. (1992). Membrane electroporation and direct gene transfer. *Bioelectrochemistry and Bioenergetics, 28*(1), 247-267.

Neumann, E., Schaefer-Ridder, M., Wang, Y., & Hofschneider, P. (1982). Gene transfer into mouse lyoma cells by electroporation in high electric fields. *The EMBO Journal, 1*(7), 841.

Neumann, E., Tönsing, K., Kakorin, S., Budde, P., & Frey, J. (1998). Mechanism of electroporative dye uptake by mouse B cells. *Biophysical Journal, 74*(1), 98-108.

Nevian, T., & Helmchen, F. (2007). Calcium indicator loading of neurons using single-cell electroporation. *Pflügers Archiv European Journal of Physiology, 454*(4), 675-688.

Nolkrantz, K., Farre, C., Brederlau, A., Karlsson, R. I. D., Brennan, C., Eriksson, P. S., . . . Orwar, O. (2001). Electroporation of single cells and tissues with an electrolyte-filled capillary. *Analytical Chemistry, 73*(18), 4469-4477.

Olbrich, M., Rebollar, E., Heitz, J., Frischauf, I., & Romanin, C. (2008). Electroporation chip for adherent cells on photochemically modified polymer surfaces. *Applied Physics Letters, 92*(1), 013901-013901-3.

Olofsson, J., Nolkrantz, K., Ryttsén, F., Lambie, B. A., Weber, S. G., & Orwar, O. (2003). Single-cell electroporation. *Current Opinion in Biotechnology, 14*(1), 29-34.

Pacary, E., Haas, M. A., Wildner, H., Azzarelli, R., Bell, D. M., Abrous, D. N., & Guillemot, F. (2012). Visualization and genetic manipulation of dendrites and spines in the mouse cerebral cortex and hippocampus

using in utero electroporation. *Journal of Visualized Experiments : JoVE, (65). pii: 4163. doi*(65), 10.3791/4163. doi: 10.3791/4163; 10.3791/4163

Paganin-Gioanni, A., Bellard, E., Escoffre, J., Rols, M., Teissié, J., & Golzio, M. (2011). Direct visualization at the single-cell level of siRNA electrotransfer into cancer cells. *Proceedings of the National Academy of Sciences, 108*(26), 10443.

Pan, P. Y., Cai, Q., Lin, L., Lu, P. H., Duan, S., & Sheng, Z. H. (2005). SNAP-29-mediated modulation of synaptic transmission in cultured hippocampal neurons. *Journal of Biological Chemistry, 280*(27), 25769.

Park, T. G., Jeong, J. H., & Kim, S. W. (2006). Current status of polymeric gene delivery systems. *Advanced Drug Delivery Reviews, 58*(4), 467-486.

Patel, C., & Muthuswamy, J. (2012). High efficiency, site-specific transfection of adherent cells with siRNA using microelectrode arrays (MEA). *J. Vis. Exp.,* doi: 10.3791/4415

Paul, C. P., Good, P. D., Winer, I., & Engelke, D. R. (2002). Effective expression of small interfering RNA in human cells. *Nature Biotechnology, 20*(5), 505-508.

Pepperkok, R., & Ellenberg, J. (2006). High-throughput fluorescence microscopy for systems biology. *Nature Reviews Molecular Cell Biology, 7*(9), 690-696.

Pérez-Martínez, F. C., Guerra, J., Posadas, I., & Ceña, V. (2011). Barriers to non-viral vector-mediated gene delivery in the nervous system. *Pharmaceutical Research, 28*(8), 1843-1858.

Poole, R. J., Bashllari, E., Cochella, L., Flowers, E. B., & Hobert, O. (2011). A genome-wide RNAi screen for factors involved in neuronal specification in caenorhabditis elegans. *PLoS Genetics, 7*(6), e1002109.

Prasanna, G. L., & Panda, T. (1997). Electroporation: Basic principles, practical considerations and applications in molecular biology. *Bioprocess and Biosystems Engineering, 16*(5), 261-264.

Raptis, L. H., Brownell, H. L., Liu, S. K. W., Firth, K. L., MacKenzie, L. W., Stiles, C. D., & Alberta, J. A. (1995). Applications of electroporation of adherent cellsIn situ, on a partly conductive slide. *Molecular Biotechnology, 4*(2), 129-138.

Rogaeva, E., Meng, Y., Lee, J. H., Gu, Y., Kawarai, T., Zou, F., . . . Hasegawa, H. (2007). The neuronal sortilin-related receptor SORL1 is genetically associated with alzheimer disease. *Nature Genetics, 39*(2), 168-177.

Rols, M. P., & Teissié, J. (1990). Electropermeabilization of mammalian cells. quantitative analysis of the phenomenon. *Biophysical Journal, 58*(5), 1089-1098.

Rosazza, C., Escoffre, J. M., Zumbusch, A., & Rols, M. P. (2011). The actin cytoskeleton has an active role in the electrotransfer of plasmid DNA in mammalian cells. *Molecular Therapy, 19*(5), 913-921.

Ryttsén, F., Farre, C., Brennan, C., Weber, S. G., Nolkrantz, K., Jardemark, K., . . . Orwar, O. (2000). Characterization of single-cell electroporation by using patch-clamp and fluorescence microscopy. *Biophysical Journal, 79*(4), 1993-2001.

Sapru, M. K., Yates, J. W., Hogan, S., Jiang, L., Halter, J., & Bohn, M. C. (2006). Silencing of human [alpha]-synuclein in vitro and in rat brain using lentiviral-mediated RNAi. *Experimental Neurology, 198*(2), 382-390.

Scherer, F., Anton, M., Schillinger, U., Henke, J., Bergemann, C., Kruger, A., . . . Plank, C. (2002). Magnetofection: Enhancing and targeting gene delivery by magnetic force in vitro and in vivo. *Gene Therapy, 9*(2), 102-109.

Schillinger, U., Brill, T., Rudolph, C., Huth, S., Gersting, S., Krötz, F., . . . Plank, C. (2005). Advances in magnetofection—magnetically guided

nucleic acid delivery. *Journal of Magnetism and Magnetic Materials, 293*(1), 501-508.

Schwister, K., & Deuticke, B. (1985). Formation and properties of aqueous leaks induced in human erythrocytes by electrical breakdown. *Biochimica Et Biophysica Acta (BBA)-Biomembranes, 816*(2), 332-348.

Sepp, K. J., Hong, P., Lizarraga, S. B., Liu, J. S., Mejia, L. A., Walsh, C. A., & Perrimon, N. (2008). Identification of neural outgrowth genes using genome-wide RNAi. *PLoS Genetics, 4*(7), e1000111.

Singer, O., Marr, R. A., Rockenstein, E., Crews, L., Coufal, N. G., Gage, F. H., . . . Masliah, E. (2005). Targeting BACE1 with siRNAs ameliorates alzheimer disease neuropathology in a transgenic model. *Nature Neuroscience, 8*(10), 1343-1349.

Stett, A., Egert, U., Guenther, E., Hofmann, F., Meyer, T., Nisch, W., & Haemmerle, H. (2003). Biological application of microelectrode arrays in drug discovery and basic research. *Analytical and Bioanalytical Chemistry, 377*(3), 486-495.

Strittmatter, W. J., & Roses, A. D. (1995). Apolipoprotein E and alzheimer disease. *Proceedings of the National Academy of Sciences of the United States of America, 92*(11), 4725.

Takahashi, H., Sakurai, T., Sakai, H., Bakkum, D. J., Suzurikawa, J., & Kanzaki, R. (2011). Light-addressed single-neuron stimulation in dissociatedneuronal cultures with sparse expression of ChR2. *Biosystems,*

Tanaka, M., Yanagawa, Y., & Hirashima, N. (2009). Transfer of small interfering RNA by single-cell electroporation in cerebellar cell cultures. *Journal of Neuroscience Methods, 178*(1), 80-86.

Teissie, J., & ROLS, M. P. (1994). Manipulation of cell cytoskeleton affects the lifetime of cell membrane electropermeabilization. *Annals of the New York Academy of Sciences, 720*(1), 98-110.

Teissié, J., & Rols, M. P. (1993). An experimental evaluation of the critical potential difference inducing cell membrane electropermeabilization. *Biophysical Journal, 65*(1), 409-413.

ter Haar, G. (2007). Therapeutic applications of ultrasound. *Progress in Biophysics and Molecular Biology, 93*(1), 111-129.

Tsunoda, S., Mazda, O., Oda, Y., Iida, Y., Akabame, S., Kishida, T., . . . Imanishi, J. (2005). Sonoporation using microbubble BR14 promotes pDNA/siRNA transduction to murine heart. *Biochemical and Biophysical Research Communications, 336*(1), 118-127.

Valero, A., Post, J., Van Nieuwkasteele, J., Ter Braak, P., Kruijer, W., & Van Den Berg, A. (2008). Gene transfer and protein dynamics in stem cells using single cell electroporation in a microfluidic device. *Lab Chip, 8*(1), 62-67.

Valley, J. K., Neale, S., Hsu, H. Y., Ohta, A. T., Jamshidi, A., & Wu, M. C. (2009). Parallel single-cell light-induced electroporation and dielectrophoretic manipulation. *Lab Chip, 9*(12), 1714-1720.

Vanhecke, D., & Janitz, M. (2005). Functional genomics using high-throughput RNA interference. *Drug Discovery Today, 10*(3), 205-212.

Walther, W., & Stein, U. (2000). Viral vectors for gene transfer: A review of their use in the treatment of human diseases. *Drugs, 60*(2), 249-271.

Washbourne, P., & McAllister, A. K. (2002). Techniques for gene transfer into neurons. *Current Opinion in Neurobiology, 12*(5), 566-573.

Wasungu, L., & Hoekstra, D. (2006). Cationic lipids, lipoplexes and intracellular delivery of genes. *Journal of Controlled Release, 116*(2), 255-264.

Weaver, J. C. (2000). Electroporation of cells and tissues. *Plasma Science, IEEE Transactions On, 28*(1), 24-33.

Weaver, J. C. (2003). Electroporation of biological membranes from multicellular to nano scales. *Dielectrics and Electrical Insulation, IEEE Transactions On, 10*(5), 754-768.

Wheeler, D. B., Carpenter, A. E., & Sabatini, D. M. (2005a). Cell microarrays and RNA interference chip away at gene function. *Nature Genetics, 37*, S25-S30.

Whitehead, K. A., Langer, R., & Anderson, D. G. (2009). Knocking down barriers: Advances in siRNA delivery. *Nature Reviews Drug Discovery, 8*(2), 129-138.

Xia, H., Mao, Q., Eliason, S. L., Harper, S. Q., Martins, I. H., Orr, H. T., . . . Davidson, B. L. (2004). RNAi suppresses polyglutamine-induced neurodegeneration in a model of spinocerebellar ataxia. *Nature Medicine, 10*(8), 816-820.

Xia, H., Mao, Q., Paulson, H. L., & Davidson, B. L. (2002). siRNA-mediated gene silencing in vitro and in vivo. *Nature Biotechnology, 20*(10), 1006-1010.

Xie, C., Lin, Z., Hanson, L., Cui, Y., & Cui, B. (2012). Intracellular recording of action potentials by nanopillar electroporation. *Nature Nanotechnology, 7*(3), 185-190.

Xu, Y., Yao, H., Wang, L., Xing, W., & Cheng, J. (2011). The construction of an individually addressable cell array for selective patterning and electroporation. *Lab Chip, 11*(14), 2417-2423.

Xu, Z. P., Zeng, Q. H., Lu, G. Q., & Yu, A. B. (2006). Inorganic nanoparticles as carriers for efficient cellular delivery. *Chemical Engineering Science, 61*(3), 1027-1040.

Yamauchi, F., Kato, K., & Iwata, H. (2004). Spatially and temporally controlled gene transfer by electroporation into adherent cells on plasmid DNA-loaded electrodes. *Nucleic Acids Research, 32*(22), e187.

Yamauchi, F., Kato, K., & Iwata, H. (2005). Layer-by-layer assembly of poly (ethyleneimine) and plasmid DNA onto transparent indium– tin oxide electrodes for temporally and spatially specific gene transfer. *Langmuir, 21*(18), 8360-8367.

Yang, R., Tarn, T. J., & Zhang, M. (2010). Data-driven feedforward control for electroporation mediated gene delivery in gene therapy. *Control Systems Technology, IEEE Transactions On, 18*(4), 935-943.

Yao, Y., Wang, C., Varshney, R. R., & Wang, D. A. (2009). Antisense makes sense in engineered regenerative medicine. *Pharmaceutical Research, 26*(2), 263-275.

Zhan, Y., Wang, J., Bao, N., & Lu, C. (2009). Electroporation of cells in microfluidic droplets. *Analytical Chemistry, 81*(5), 2027-2031.

Ziauddin, J., & Sabatini, D. M. (2001). Microarrays of cells expressing defined cDNAs. *Nature, 411*(6833), 107-110.

Zimmermann, U., Pilwat, G., & Riemann, F. (1974). Dielectric breakdown of cell membranes. *Biophysical Journal, 14*(11), 881-899.

APPENDIX A

FABRICATION PROCESS

Below: Complete photolithography process for the biochip fabrication

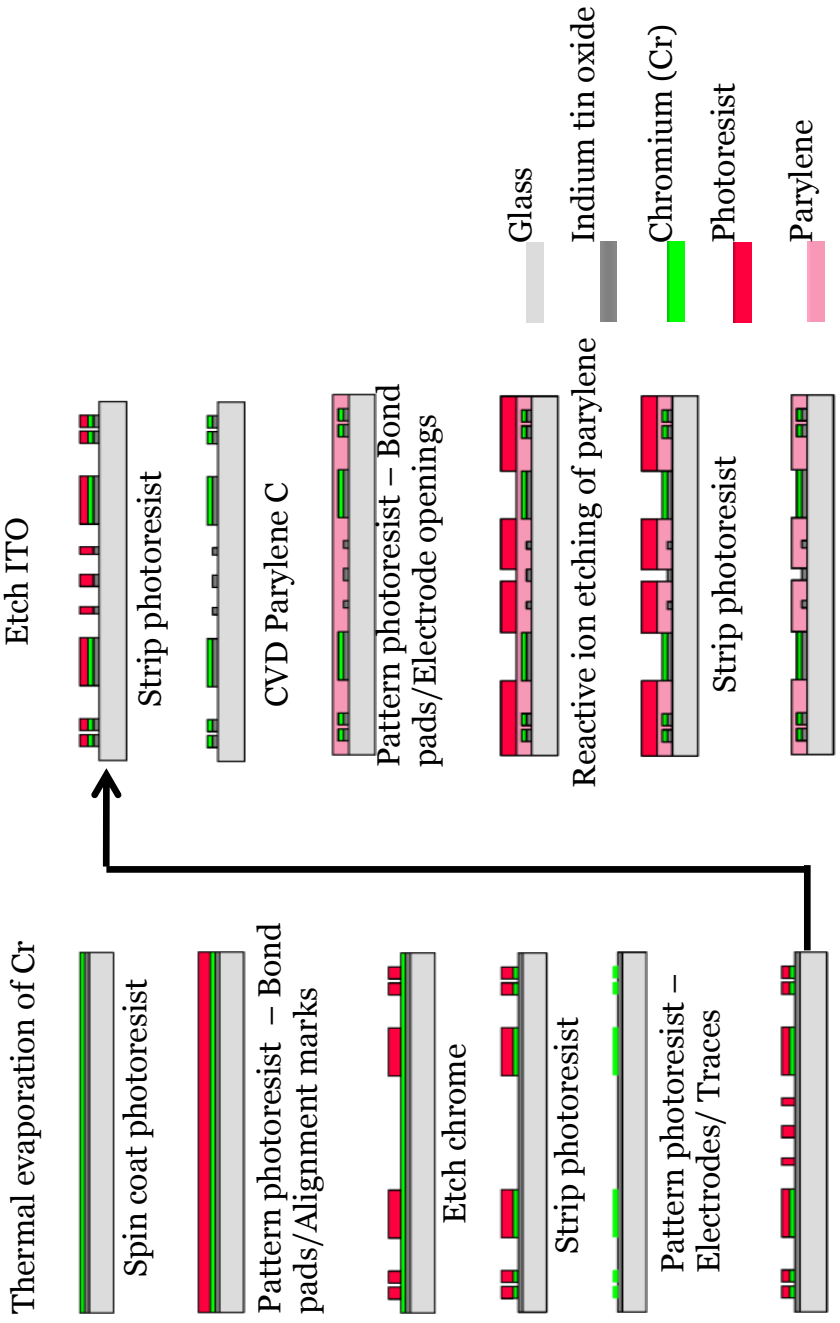

APPENDIX B

EP PARAMETER OPTIMIZATION

Below: Electroporaiton pulse voltage optimization HeLa cell for 1 msec duration pulse.

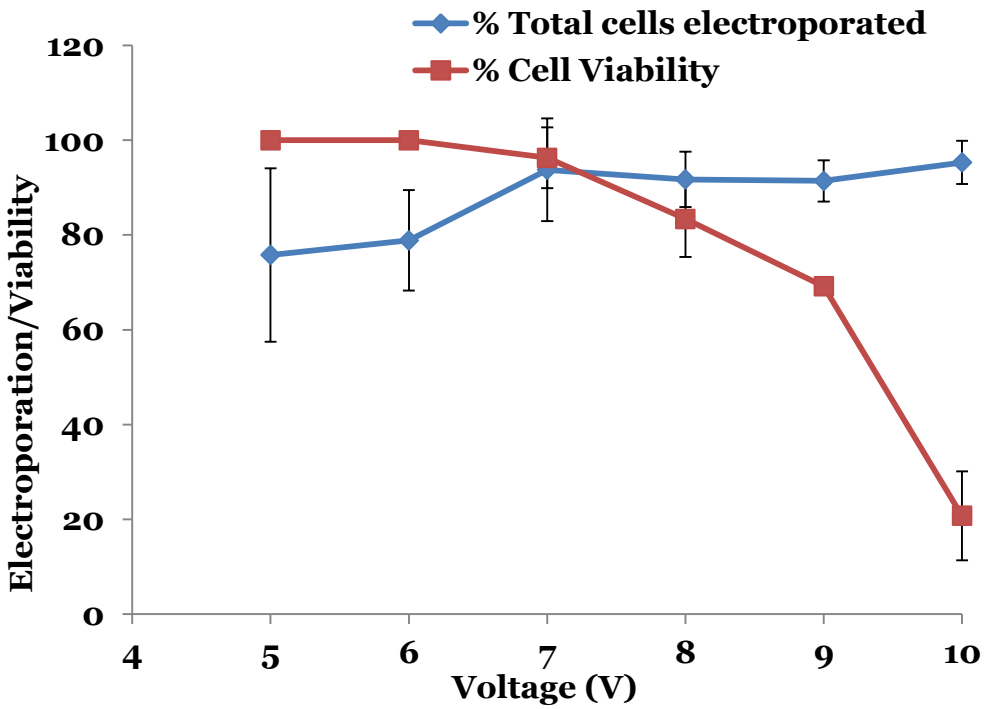

Below: Site-specific delivery of PI to HeLa cells for an 8 V, 1 msec pulse on a 100 μm diameter electrode. The image on the left shows the cells on the electrode fluorescing red due to the uptake of PI. The image on the right is a superimposed image of PI and live assay. The white circle marks the boundary of the electrode.

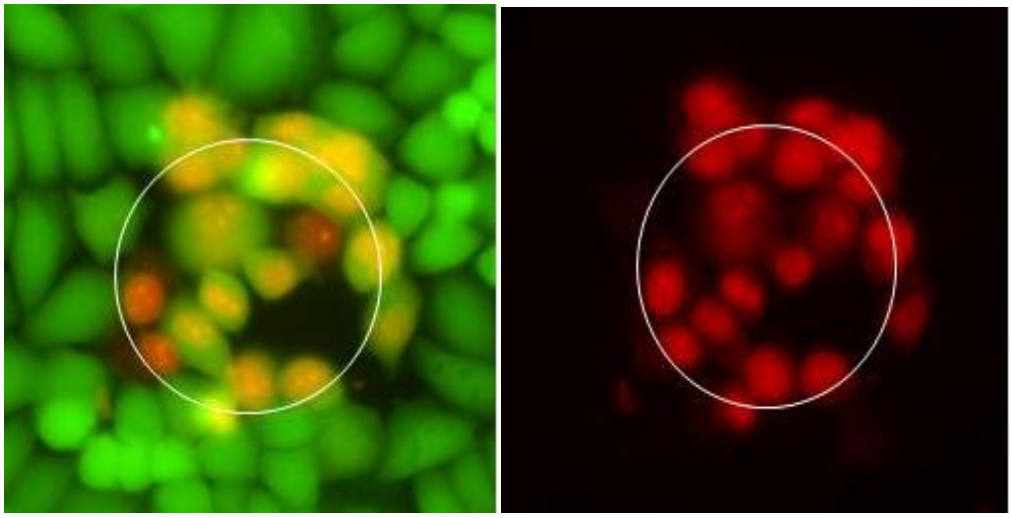

APPENDIX C

NEURAL ACTIVITY AFTER GLUTAMATE STIMULATION

Below: Neural activity recording before and after glutamate addition. Neural activity was recorded for 10 mins before and after addition of glutamate to cells. Neural recording from 23 channels with activity was sorted to identify individual units in each channel. The data shows an increase in the number of units in 14 out 23 channels.

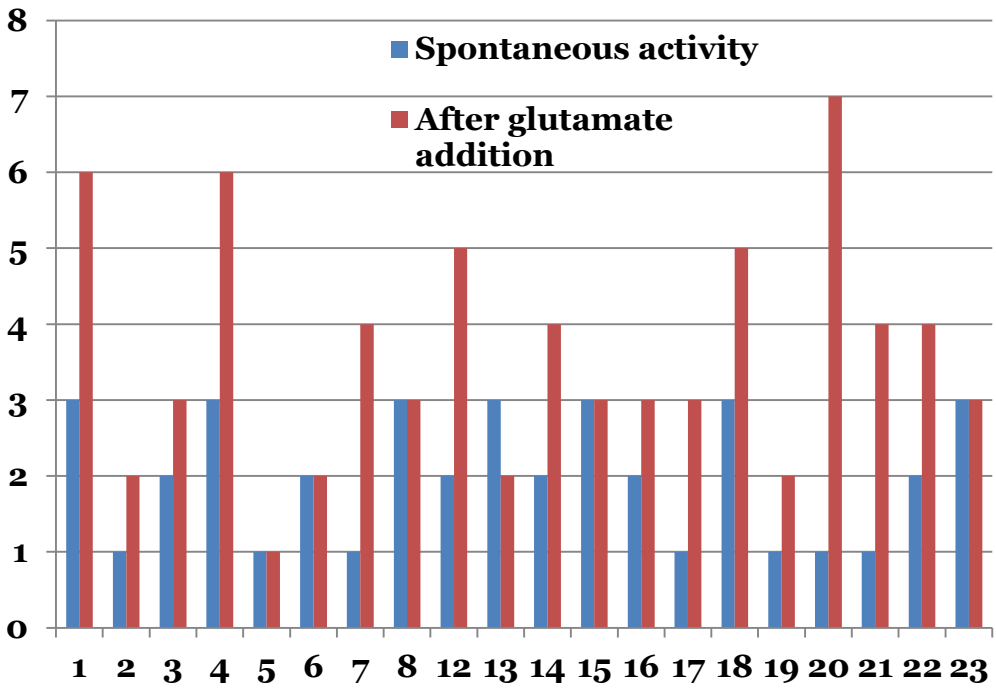

APPENDIX D

COPYRIGHT LICENSES

Below: License for Figure 1

Supplier Elsevier Limited
The Boulevard,Langford Lane
Kidlington,Oxford,OX5 1GB,UK
Registered Company
Number
1982084
Customer name Chetan Patel
Customer address 501 E Tyler Mall, ECG 334
Tempe, AZ 85287-9709
License number 3022350442843
License date Nov 05, 2012
Licensed content publisher Elsevier
Licensed content
publication
Molecular Medicine Today
Licensed content title Towards gene therapy for the central nervous system
Licensed content author Matthew J During,Liana-Marie A Ashenden
Licensed content date 1 November 1998
Licensed content volume
number
4
Licensed content issue
number
11
Number of pages 9
Start Page 485
End Page 493
Type of Use reuse in a thesis/dissertation
Portion figures/tables/illustrations
Number of
figures/tables/illustrations
1

Below: License for Figure 2

License Number 3022351392811
License date Nov 05, 2012
Licensed content publisher Nature Publishing Group
Licensed content publication
Nature Chemical Biology
Licensed content title RNAi therapeutics: a potential new class of pharmaceutical drugs
Licensed content author David Bumcrot, Muthiah Manoharan, Victor Koteliansky and Dinah
W Y Sah
Licensed content date Dec 1, 2006
Volume number 2
Issue number 12
Type of Use reuse in a thesis/dissertation
Requestor type academic/educational
Format print and electronic
Portion figures/tables/illustrations
Number of figures/tables/illustrations
1
High-res required no
Figures Figure 1: Cellular mechanism of RNA interference.
Author of this NPG article no
Your reference number
Title of your thesis / dissertation
Microscale electroporation for transfection of genetic constructs into adherent secondary cells and primary neurons in culture
Expected completion date Dec 2012

Below: License for Figure 3

License Number 3022361133117
License date Nov 05, 2012
Licensed content publisher Nature Publishing Group
Licensed content publication
Nature Medicine
Licensed content title Viral vectors for gene therapy: the art of turning infectious agents into vehicles of therapeutics
Licensed content author Mark A. Kay, Joseph C Glorioso, Luigi Naldini
Licensed content date Jan 1, 2001
Volume number 7
Issue number 1
Type of Use reuse in a thesis/dissertation
Requestor type academic/educational
Format print and electronic
Portion figures/tables/illustrations
Number of figures/tables/illustrations
1
Figures Figure 2
Author of this NPG article no
Your reference number
Title of your thesis / dissertation
Microscale electroporation for transfection of genetic constructs into adherent secondary cells and primary neurons in culture
Expected completion date Dec 2012
Estimated size (number of pages)
100
Total 0.00 USD
Terms and Conditions

Below: License for Figure 4

Supplier Elsevier Limited
The Boulevard,Langford Lane
Kidlington,Oxford,OX5 1GB,UK
Registered Company
Number
1982084
Customer name Chetan Patel
Customer address 501 E Tyler Mall, ECG 334
Tempe, AZ 85287-9709
License number 3022371453800
License date Nov 05, 2012
Licensed content publisher Elsevier
Licensed content
publication
Journal of Magnetism and Magnetic Materials
Licensed content title Advances in magnetofection—magnetically guided
nucleic acid
delivery
Licensed content author Ulrike Schillinger,Thomas Brill,Carsten
Rudolph,Stephanie
Huth,Sören Gersting,Florian Krötz,Johannes
Hirschberger,Christian Bergemann,Christian Plank
Licensed content date May 2005
Licensed content volume
number
293
Licensed content issue
number
1
Number of pages 8
Start Page 501
End Page 508
Type of Use reuse in a thesis/dissertation
Intended publisher of new
work
other
Portion figures/tables/illustrations

Below: License for Figure 6

License Number 3022390679888
License date Nov 05, 2012
Licensed content publisher John Wiley and Sons
Licensed content publication
Acta Physiologica
Book title
Licensed content author J. Gehl
Licensed content date Mar 21, 2003
Start page 437
End page 447
Type of use Dissertation/Thesis
Requestor type University/Academic
Format Print and electronic
Portion Figure/table
Number of figures/tables 1
Number of extracts
Original Wiley figure/table number(s)
Figure 1
Will you be translating? No
Order reference number
Total 0.00 USD

Below: License for Figure 7

License Number 3022391215264
License date Nov 05, 2012
Licensed content publisher Springer
Licensed content publication
Molecular Biotechnology
Licensed content title What is (Still not) Known of the Mechanism by Which
Electroporation Mediates Gene Transfer and Expression in Cells and Tissues
Licensed content author Jean-Michel Escoffre
Licensed content date Jan 1, 2008
Volume number 41
Issue number 3
Type of Use Thesis/Dissertation
Portion Figures
Author of this Springer article
No
Order reference number
Title of your thesis / dissertation
Microscale electroporation for transfection of genetic constructs into adherent secondary cells and primary neurons in culture
Expected completion date Dec 2012
Estimated size(pages) 100
Total 0.00 USD

Below: License for Figure 8

All payments must be made in full to CCC. For payment instructions, please see
information listed at the bottom of this form.
License Number 3022391215264
License date Nov 05, 2012
Licensed content publisher Springer
Licensed content
publication
Molecular Biotechnology
Licensed content title What is (Still not) Known of the Mechanism by Which
Electroporation Mediates Gene Transfer and Expression in Cells and Tissues
Licensed content author Jean-Michel Escoffre
Licensed content date Jan 1, 2008
Volume number 41
Issue number 3
Type of Use Thesis/Dissertation
Portion Figures
Author of this Springer
article
No
Order reference number
Title of your thesis /
dissertation
Microscale electroporation for transfection of genetic constructs into adherent secondary cells and primary neurons in culture
Expected completion date Dec 2012
Estimated size(pages) 100
Total 0.00 USD
Terms and Conditions
Introduction
The publisher for this copyrighted

Below: License for Figure 22

License Number 3023361325364
License date Nov 06, 2012
Licensed content publisher Nature Publishing Group
Licensed content publication
Nature Nanotechnology
Licensed content title Nanochannel electroporation delivers precise amounts of biomolecules into living cells
Licensed content author Pouyan E. Boukany, Andrew Morss, Wei-ching Liao, Brian Henslee, HyunChul Jung, Xulang Zhang
Licensed content date Oct 16, 2011
Volume number 6
Issue number 11
Type of Use reuse in a thesis/dissertation
Requestor type academic/educational
Format print and electronic
Portion figures/tables/illustrations
Number of figures/tables/illustrations
1
High-res required no
Figures Figure 1
Author of this NPG article no
Your reference number
Title of your thesis / dissertation
Microscale electroporation for transfection of genetic constructs into adherent secondary cells and primary neurons in culture
Expected completion date Dec 2012
Estimated size (number of pages)
100
Total 0.00 USD